

BIOPHYSICAL AND BIOCHEMICAL CHARACTERIZATION OF A REC DOMAIN:

UNFOLDED TO FOLDED TRANSITION OF EL_LOVR.

APPROVED BY SUPERVISORY COMMITTEE

PhD advisor _____
Kevin H. Gardner, PhD

Committee Chair _____
David Hendrixson, PhD

Committee Member _____
Vanessa Sperandio, PhD

Committee Member _____
Jose Rizo Rey, PhD

Dedication

To my parents Victor Ocasio and Rosaly Ramirez.

For teaching me the important lessons in life.

To Angelica Barrero-Tobon, my best friend and partner.

For being the person that changed my life.

ACKNOWLEDGEMENTS

First of all, I would like to thank my advisor Dr. Kevin H. Gardner. He gave me the opportunity to join the lab and work with photosensors. He always had patience teaching me the basics of NMR spectroscopy and how to apply this to answer problems in microbiology. I am grateful for having him as my mentor and thanks to him, my passion for science has only become stronger. Additionally, I would also give thanks to Dr. Fernando Corrêa. His knowledge on NMR spectroscopy and assistance in the structure determination of EL_LovR and numerous NMR experiments has been invaluable. Special thanks go to Sean Crosson and Aretha Feibig from the university of Chicago, for providing many reagents, *C. crescentus* strains and training me on how to perform the stress assays. I would also give thanks to the past and current members of the Gardner lab, for their valuable advice and discussions.

I would like to thank the biophysics department staff and faculty, Jo Appleton, Linda Akau, Darlene Reynolds, Dr. Qiong Wu for their assistance during my stay at UT Southwestern. Additionally, my committee members, Dr. David Hendrixson, Dr. Vanessa Sperandio, and Dr. Jose Rizo-Rey for their support, encouragement and advice during my graduate career.

Finally, I would like to thank my family and friends, especially my mother and father Rosaly Ramirez and Victor Ocasio, who gave me the strength to keep pushing the boundaries. My fiancée, Angelica Barrero-Tobon, who has made me a better person and scientist. I am grateful to have her in my life.

BIOPHYSICAL AND BIOCHEMICAL CHARACTERIZATION OF A REC DOMAIN:
UNFOLDED TO FOLDED TRANSITION OF EL_LOVR.

by

VICTOR J. OCASIO

DISSERTATION/THESIS

Presented to the Faculty of the Graduate School of Biomedical Sciences

The University of Texas Southwestern Medical Center at Dallas

In Partial Fulfillment of the Requirements

For the Degree of

DOCTOR OF PHILOSOPHY

The University of Texas Southwestern Medical Center

Dallas, Texas

December 2014

Copyright

by

Victor J. Ocasio, 2014

All Rights Reserved

ABSTRACT

BIOPHYSICAL AND BIOCHEMICAL CHARACTERIZATION OF A REC DOMAIN:

UNFOLDED TO FOLDED TRANSITION OF EL_LOVR.

Victor J. Ocasio

The University of Texas Southwestern Medical Center, 2014

Supervising Professor: Kevin H. Gardner, PhD

Prokaryotes frequently use two component systems to couple environmental stimuli to adaptive responses. These pathways use histidine kinases to detect environmental cues, harnessing these to control phosphorylation of the receiver domain of the response regulator, which convert this signal into a physiological response. Knowledge of how phosphorylation shifts receiver domains between their inactive and active states is limited, chiefly assembled from several prototypical receiver domains that switch between two similar and well-folded structures. However, it remains unclear how general these observations apply to other receiver domains, particularly for full-length proteins. Here we present a blue light-regulated two-component system from the marine α -proteobacterium *Erythrobacter litoralis* HTCC2594. The sensor domain of the 3 histidine kinases found in *E. litoralis* contain a LOV

(Light-Oxygen-Voltage) domain, part of the widely used PAS (Per-ARNT-Sim) family of environmental sensors. Interestingly, one of the histidine kinases (EL362) contains a naturally occurring glycine to arginine mutation in the LOV domain that prevents chromophore binding, resulting in a “blind” histidine kinase. Reverting the arginine to a glycine residue allows blue light to trigger the autophosphorylation of EL362 and subsequent phosphotransfer towards the cognate response regulator EL_LovR. This arrangement of RRs is reminiscent of similar systems used in other bacterial general stress responses, most of which have been characterized entirely with genetic methods. Notably, EL_LovR is a single domain response regulator proposed to play a critical role in shutting off such systems via a potent phosphatase activity. Size exclusion chromatography, light scattering and NMR experiments show that phosphorylation and Mg(II) transitions EL_LovR between unfolded and folded monomeric states. Parallel functional assays show that EL_LovR has a fast dephosphorylation rate, consistent with its proposed function as a phosphate sink. Taken together, our findings provide evidence that EL_LovR undergoes drastic conformational changes that have not been seen in other response regulators, likely with effects on its autophosphatase activity. In conclusion, our work expands the kinds of conformational changes and regulation used by receiver domains, critical components of bacterial signaling systems.

TABLE OF CONTENTS

PRIOR PUBLICATIONS & PRESENTATIONS.....	xii
Chapter 1 General introduction.....	1
1.1 Two-component signal transduction.....	1
1.2 Histidine kinases	4
1.2.1 Sensor domains	6
1.2.1.1 PAS domains are modular environmental sensors.....	9
1.2.1.2 LOV domains, a subfamily of PAS domains, which sense blue light and redox .	12
1.2.1.3 LOV domain photocycle.....	13
1.2.2 Kinase domain	13
1.2.2.1 Kinase domain structure and signaling mechanism.....	18
1.3 Response regulators	23
1.3.1 Receiver domain structure	25
1.3.2 Response regulator activation	26
1.3.3 Effector domain diversity	32
1.3.4 Atypical response regulators.....	34
1.4 Blue light regulated two-component systems.....	35
1.5 Relevance of two-component systems.....	37
Chapter 2 Experimental procedures.....	39

2.1 General growth conditions and strain construction	39
2.2 Cloning, expression and purification of LOV-HK and response regulator proteins	40
2.3 Visible absorption spectroscopy	41
2.4 Autophosphorylation Assays	42
2.5 Phosphotransfer profiling.....	43
2.6 Phosphotransfer kinetic measurements.....	43
2.7 Phosphatase assay	44
2.8 Size exclusion chromatography and multiple angle laser light scattering.....	45
2.9 NMR solution structure determination and relaxation experiments.....	46
2.10 Limited proteolysis and Mass Spectrometry analysis.....	47
2.11 Titration with MgCl ₂ and BeF ₃ ⁻	48
2.12 β-galactosidase assays	48
Chapter 3 Enzymatic analysis of LOV-HK in <i>Erythrobacter litoralis</i> HTCC2594	52
Abstract.....	52
3.1 Introduction.....	53
3.2 Results.....	55
3.2.1 Characterization of light-dependent enzymatic activity	55
3.2.2 LOV domain stabilizes dimeric conformation.....	59
3.2.3 Light regulated two-component signaling: Identification of target response regulators and influence of light stimulus on phosphotransfer	62

3.2.4 EL368 controls a transduction cascade involving an sigma/anti-sigma interaction system	67
3.2.5 EL_LovR forms a two-component system with a “blind” LOV histidine kinase: Non-flavin binding protein has impaired kinase activity.....	71
3.3 Discussion	78
3.4 Conclusion	84
Chapter 4 Ligand induced folding in a TCS receiver domain	86
Abstract.....	86
4.1 Introduction.....	87
4.2 Results.....	91
4.2.1 EL_LovR undergoes significant changes in global shape upon Mg ²⁺ binding and phosphorylation.....	91
4.2.2 EL_LovR becomes increasingly folded in activating conditions	95
4.2.3 Solution structure of EL_LovR.....	103
4.2.4 Conserved residues involved in Mg ⁺² binding have a key role in structural changes of EL_LovR.....	106
4.2.5 EL_LovR has a short-lived phosphorylated state	108
4.3 Discussion.....	111
Chapter 5 Functional analysis of EL_LovR: Using <i>C. crescentus</i> as a model	116
5.1 Introduction.....	116

5.2 Results.....	120
5.2.1 Functional analysis of <i>E. litoralis</i> light regulated TCS.....	120
5.2.2 EL368 and EL_LovR have specific phosphatase activity to EL_PhyR	121
5.2.3 EL_PhyR can restore SigT dependent transcription to wild type levels	122
5.2.4 EL368/EL_LovR/EL_PhyR results in hyper-activation of sigT dependent transcription	128
5.3 Discussion.....	128
5.4 Conclusion	132
Chapter 6 Conclusions	133
REFERENCES	139

PRIOR PUBLICATIONS & PRESENTATIONS

PUBLICATIONS:

- Correa, F., Ko, W. H., Ocasio, V., Bogomolni, R. A., and Gardner, K. H. (2013) Blue Light Regulated Two-Component Systems: Enzymatic and Functional Analyses of Light-Oxygen-Voltage (LOV)-Histidine Kinases and Downstream Response Regulators. *Biochemistry* **52**, 4656-4666.
- Ocasio, V., Correa, F., Gardner, K.H. (2014) Activation-induced folding of a receiver domain (submitted)

PRESENTATIONS AND POSTERS:

Poster Presentations:

- Ocasio, V., Corrêa, F., Gardner, K.H. (August 2014) Phosphorylation-induced folding of a bacterial signaling protein. *International Conference on Magnetic Resonance in Biological Systems, Dallas, TX*
- Ocasio, V., Corrêa, F., Gardner, K.H. (July 2013) Phosphorylation-induced folding of a bacterial signaling protein. *Gordon Research Conference “Microbial Adhesion and Signal Transduction”, Newport, RI*
- Ocasio, V., Corrêa, F., Gardner, K.H. (April 2012) Phosphorylation-induced protein folding: a novel mechanism for response regulator activation. *Biomolecular Structure, Dynamics and Function, Memphis, TN*
- Ocasio, V., Corrêa, F., Gardner, K.H. (October 2011) Light Regulated two-component signal transduction. *Society for Advancement of Chicanos and Native American in Science, San Jose, CA*
- Ocasio, V., Corrêa, F., Gardner, K.H. (May 2011) Light Regulated two-component signal transduction. *American Society for Microbiology, New Orleans, LA*

LIST OF TABLES

Table 2.1 <i>C. crescentus</i> and <i>E. coli</i> strains used in this study	50
Table 3.1 Predicted response regulators in <i>Erythrobacter litoralis</i> HTCC2594	64
Table 4.1 Statistics for EL_LovR solution structure determination.	105

LIST OF FIGURES

Figure 1.1 Two component signal transduction.....	2
Figure 1.2 Schematic representation of histidine kinases with different sensor domain organization.....	5
Figure 1.3 Classification of histidine kinases.	7
Figure 1.4 Ribbon diagram of PDC domain of PhoQ (43-190) (PDB code: 3BQA).	8
Figure 1.5 2.0 Å crystal structure of <i>N. crassa</i> VIVID shown in ribbon diagram.....	11
Figure 1.6 Diversity of output domains attached to LOV domain.	14
Figure 1.7 The LOV domain photocycle.	15
Figure 1.8 2.8 Å crystal structure of the kinase core of <i>Thermotoga maritima</i> HK853.....	16
Figure 1.9 HK activation models.....	20
Figure 1.10 Crystal structure of KinB bound to the Sda inhibitor.....	22
Figure 1.11 Full-length structure of the hybrid histidine kinase YF1 and the cytoplasmic portion of VicK from <i>Streptococcus mutans</i>	24
Figure 1.12 Structure of CheY in inactive and active conformations.....	27
Figure 1.13 Structure of the REC domain of NtrC and Spo0F.....	29
Figure 1.14 Classification of RRs by their output domain.	33
Figure 3.1 Light enhances the phosphorylation activity of EL368.....	57
Figure 3.2 EL368 undergoes a reversible photocycle.....	58
Figure 3.3 Dimeric solution structure of EL368 is stabilized by elements located N-terminal if	

the LOV domain.	60
Figure 3.4 Predicted secondary structure of EL368.....	61
Figure 3.5 Phosphotransfer profiling of EL368.....	65
Figure 3.6 Phosphotransfer profiling of the EL346 HK.	66
Figure 3.7 Influence of light on the EL368 phosphorylation of the EL_PhyR substrate.	68
Figure 3.8 EL_PhyR binds to an anti- σ factor upon activation.	69
Figure 3.9 Presence of EL_LovR induces phosphate loss of EL_PhyR.....	72
Figure 3.10 EL362 forms a two-component system with its downstream cognate response regulator, EL_LovR.	74
Figure 3.11 EL368 and EL362 have a high degree of sequence identity.	75
Figure 3.12 The EL362 LOV domain contains an unconserved arginine residue in the I β strand.	76
Figure 3.13 Biochemical characterization of EL362: a blind LOV-HK protein.	77
Figure 3.14 Decoding light two-component specificity.	81
Figure 3.15 Comparison of <i>Caulobacter crecentus</i> and <i>Erythrobacter litoralis</i> stress-responsive two component systems with LOV-HK proteins.....	85
Figure 4.1 Crystal structure of CheY bound to magnesium.	88
Figure 4.2 EL_LovR undergoes global conformational changes upon phosphorylation.	93
Figure 4.3 EL_LovR~P undergoes phosphorylation-dependent conformational changes to become more resistant to trypsin digestion.....	96
Figure 4.4 EL_LovR progressively becomes more folded with binding to Mg ²⁺ and BeF ₃ ⁻	97

Figure 4.5 NOESY experiment show the lack of long distance NOEs of Apo-EL_LovR compared to EL_LovR + Mg ²⁺ + BeF ₃ ⁻	99
Figure 4.6 Ligand binding to EL_LovR induces the formation of stable secondary structure...	100
Figure 4.7 C-terminal region of EL_LovR (α4/β5/α5) exhibit conformational exchange.	102
Figure 4.8 NMR solution structure of EL_LovR + Mg ²⁺ + BeF ₃ ⁻	104
Figure 4.9 Structural effects of point mutations to the acidic Mg ²⁺ -binding residues of EL_LovR.	107
Figure 4.10 Mutation of conserved D13/D56 to alanine allows EL_LovR to fold in the absence of phosphate and Mg ²⁺	109
Figure 4.11 EL_LovR~P is short-lived <i>in vitro</i>	110
Figure 5.1 <i>C. crescentus</i> and <i>E. litoralis</i> TCS components	118
Figure 5.2 Sequence alignments of EL_PhyR and PhyR.	119
Figure 5.3 Overexpression of EL368/EL_LovR in <i>C. crescentus</i> results in wild type levels of SigT activity.....	123
Figure 5.4 The presence of CC_LovR or EL_LovR failed to induce phosphate loss of PhyR. .	124
Figure 5.5 EL_PhyR can form a complex with NepR upon phosphorylation.....	126
Figure 5.6 EL_PhyR expression under control of a vanillate-inducible promoter is able to restore SigT activity to wild type levels.	127
Figure 5.7 Overexpression of EL_368, EL_lovR, EL_phyR results in hyper activation of SigT activity.....	129

LIST OF ABBREVIATIONS

CA, catalytic and ATP binding domain

DHp, dimerization and histidine phosphotransfer domain

FAD, flavin adenine dinucleotide

FMN, flavin mononucleotide

HK, histidine kinase

LOV, Light-Oxygen-Voltage domain

MALS, multi-angle laser light scattering

NMR, nuclear magnetic resonance

PAS, Period-ARNT-Single Minded domain

REC, receiver domain

RR, response regulator

SDRR, single domain response regulator

TCS, two-component system

Chapter 1 General introduction

1.1 Two-component signal transduction

Bacteria need to adapt toward rapid changes in the environment in order to survive and obtain nutrients for growth. One of the many strategies used by prokaryotes involves the use of a signaling cascade called two component signal transduction (TCS), which involves two types of proteins: a sensor histidine kinase (HK) and response regulator (RR) (Figure 1.1) (1). These proteins have structurally conserved domains. The kinase (phosphodonor) domain can be associated with a variety of sensor domains that allows effective translation of environmental cues into an autophosphorylation and phosphotransfer reaction to a RR (phosphoacceptor), which can be associated with a variety of output domains. Together, these proteins work to regulate different physiological responses like cell-to-cell communication, transcriptional regulation, regulation of virulence factors, chemotaxis and other physiological processes (2-7). The number of TCS proteins varies from one organism to another. For example, in *Escherichia coli* there are ~64 proteins involved in TCS (HKs and RRs), while in *Haemophilus influenzae* there are ~11 proteins involved in TCS (8,9). The sensor domain is the most diverse region in HKs, for example 9% of HKs have a GAF (cGMP phosphodiesterases) domain, 31% of HKs contain a HAMP (signal transducer) domain and 31% have at least one PAS (Per-Arnt-Sim) domain (10,11). Usually binding of a small ligand causes conformational changes on the sensor

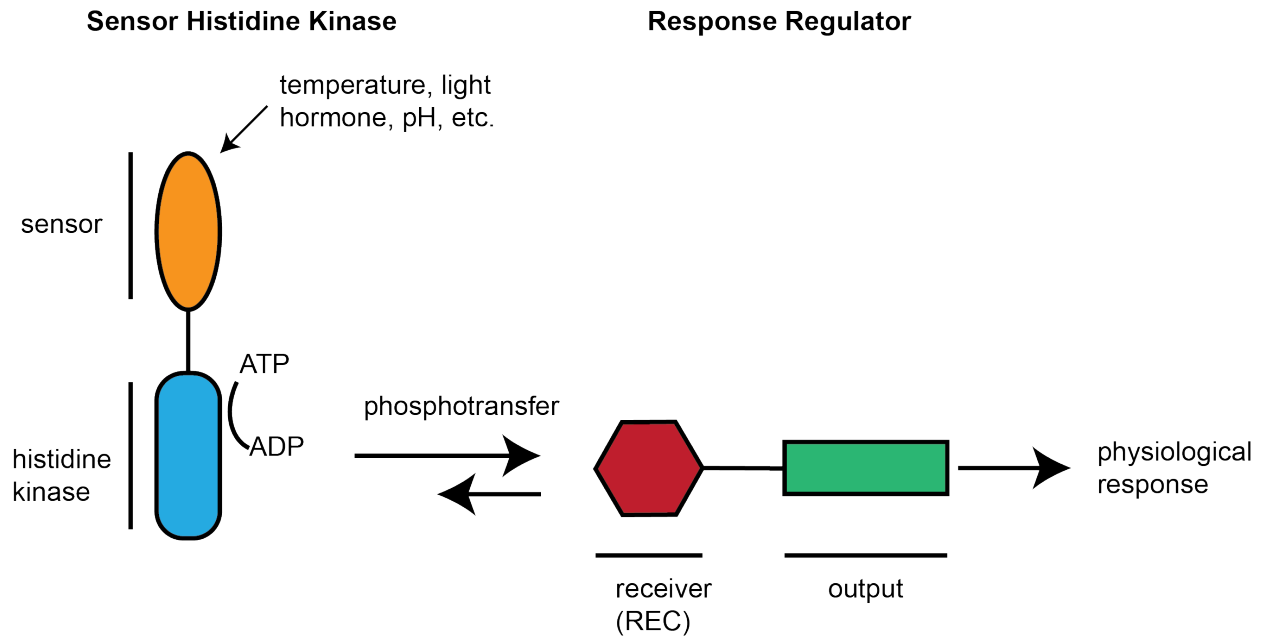


Figure 1.1 Two component signal transduction

The sensor domain of the histidine kinase senses an environmental stimulus, which leads to activation of the autophosphorylation reaction. Subsequently the histidine kinase phosphorylates an aspartate residue in the receiver domain of the response regulator. This allows the response regulator to regulate physiological changes.

domain, which are transferred to the dimerization and histidine phosphotransfer domain (DHp) and the catalytic domain (CA) of the HK (3). These changes induce an autophosphorylation reaction, where the CA domain binds an ATP molecule and transfers the γ -phosphate to a conserved histidine residue in the DHp domain (3). This in turn allows the HK to transfer the phosphate group to the cognate RR. The RR is minimally composed of a receiver domain (REC), which contains the conserved aspartate residue that gets phosphorylated by the HK. Even though many RRs only harbor the REC domain, others contain an effector domain, which dictates the function of the protein upon phosphorylation. Similarly to the sensor domains in HKs, output domains in RRs are diverse (e.g. DNA binding domain, diguanylate phosphodiesterases, RNA binding domain, protein phosphatase and histidine kinase) (12).

Prokaryotes need to cope with limiting nutrient environments as sensing nutrient rich environments can confer survival advantage to a species. For example, the TCS NtrB/NtrC is one of the most well characterized signaling pathways found in many prokaryotes like *E. coli*, *Salmonella typhimurium* and *Klebsiella pneumoniae*. This signaling cascade regulates several genes required for nitrogen assimilation, where NtrB is the HK and NtrC is the RR (a transcription factor) (1). NtrB responds to the intracellular ratio of 2-ketoglutarate and glutamine by activating its autokinase activity, leading to the phosphorylation of NtrC, which results in the increased expression of glutamine synthase (13). Another role that TCS play in prokaryotic cells is that of quorum sensing or cell-cell communication. This allows the bacteria to sense cell density by detecting a series of hormones secreted by bacterial cells known as auto-inducers (AI) (14). For instance, the quorum sensing *E. coli* regulator proteins QseB/QseC,

act together to regulate flagella and motility (15). The CheA/CheY TCS is involved in the regulation of bacterial chemotaxis. The sensor domain of CheA binds small ligands that activate the autophosphorylation of the histidine residue and subsequently phosphotransfers the phosphate to the downstream RR CheY (16,17). This allows CheY to bind the flagellar machinery and induce a clockwise (CW) or counter clockwise (CCW) rotation, allowing the bacteria to swim towards nutrient rich environments. Additionally, TCS can regulate virulence factors in many bacteria. For instance, AgrC/AgrA from *Staphylococcus aureus* regulates the expression of toxic shock syndrome toxin 1 (TSST-1) and α -, β - and δ -hemolysins among others (4,18,19). Other physiological processes where TCS have an important role is sporulation in *Bacillus subtilis* (KinA/Spo0F) (20), phosphate homeostasis (PhoR/PhoB) (21), iron homeostasis and antibiotic resistance (PmrA/PmrB) (22). These are only a few examples of how TCSs plays a central role in bacterial physiology.

1.2 Histidine kinases

The first component of TCS is the sensor HK, which can be located either in the membrane or as a soluble protein in the cytosol. The prototypical HK is a homodimer that contains one or more highly diverse sensor domains and a conserved kinase core that allows for the autophosphorylation reaction on a conserved histidine residue upon detection of a specific signal (Figure 1.2) (23). For the past two decades many groups have focused their studies at understanding the molecular

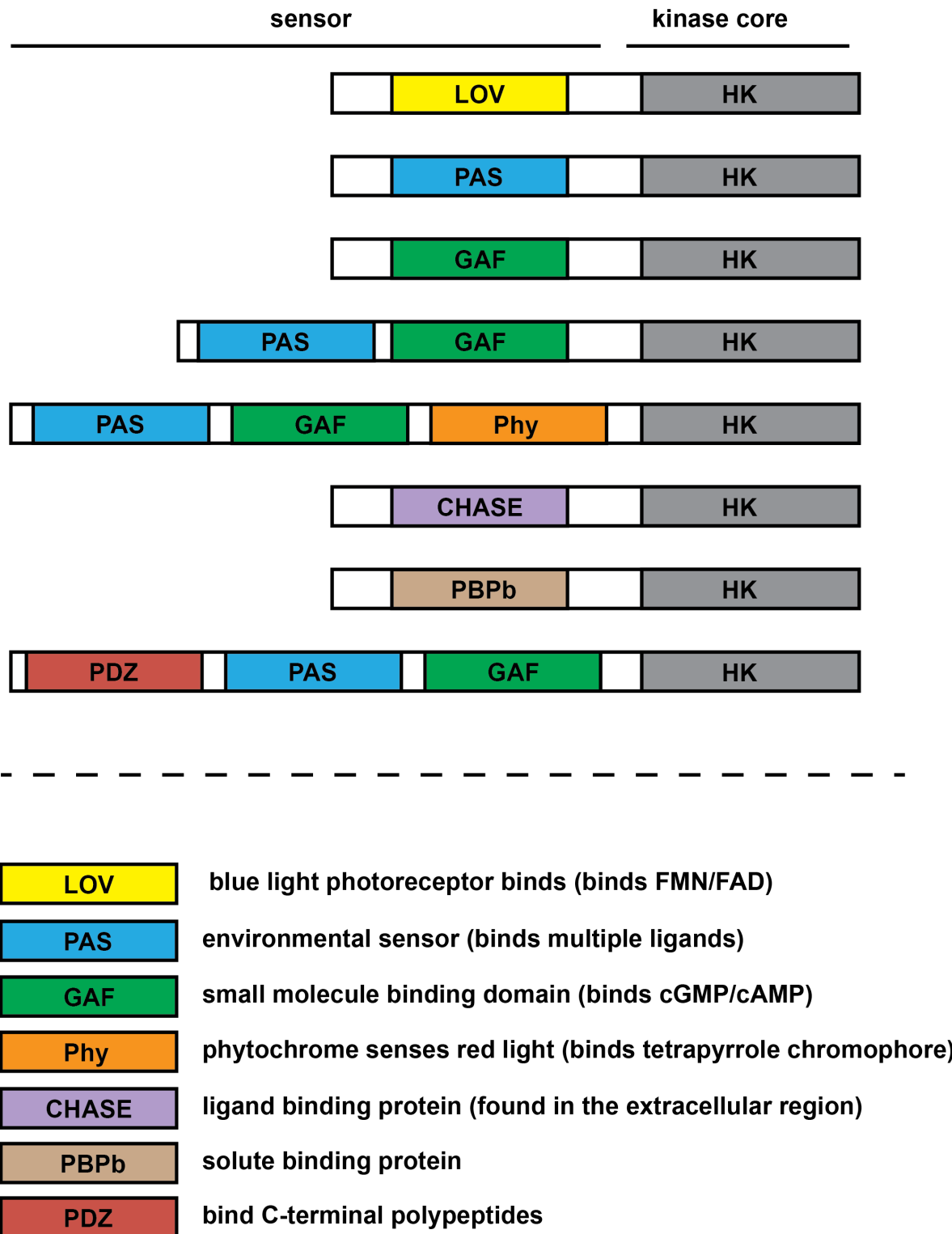


Figure 1.2 Schematic representation of histidine kinases with different sensor domain organization.

Diversity of sensor domains that regulate histidine kinase activity. Source SMART database (11).

mechanisms of how diverse sensor domains can regulate the kinase core and autophosphorylation of HKs.

1.2.1 Sensor domains

The sensor domain is the region of the HK that is responsible for sensing environmental cues and regulating the autophosphorylation activity of the kinase core. Analysis of HK sequences show that the sensor domain is the region that varies the most (3), but these domains can be identified using homology searches. Genetic, biochemical and biophysical characterization of many sensor domains has been hampered by the difficulty of identifying the stimulus or ligand the sensor domain recognizes (3) and that many are membrane bound. However, HKs have been classified in three different groups based on the topology of the sensor domain; extracellular, membrane embedded and cytoplasmic (Figure 1.3a) (24).

The most common type of extracellular sensor domains is the PDC domain (PhoQ-DcuS-CitA) (24). The crystal structures of the sensor domain of PhoQ (Mg^{2+} sensor), DcuS (fumarate sensor) and CitA (regulates citrate metabolism) HKs are known (25-28). These PDC domains are composed of 5 anti-parallel β -strands flanked by a N-terminal α -helix and a short C-terminal helix (Figure 1.4). This fold is highly similar to that of the PAS domain, often used by many proteins as environmental sensors (29). But some differences have been identified, especially in residues that are located between the second and third β -strands and a

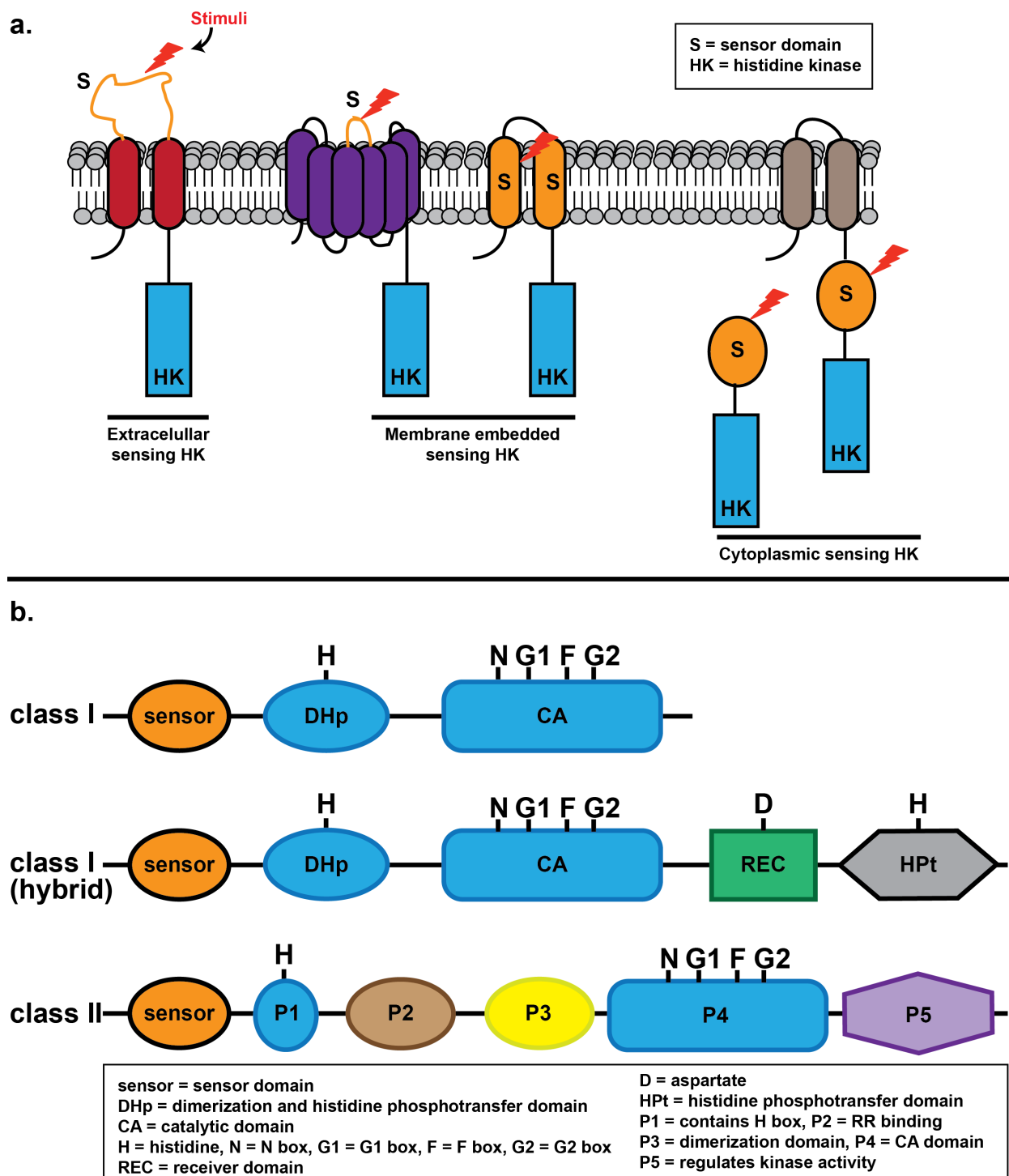


Figure 1.3 Classification of histidine kinases.

a) Classification of histidine kinases based on the localization of the sensor domain (modified from Mascher *et.al.* (30)). b) Classification of histidine kinases based on the homology boxes and localization of H-box (modified from Yamada *et.al.* (31)).

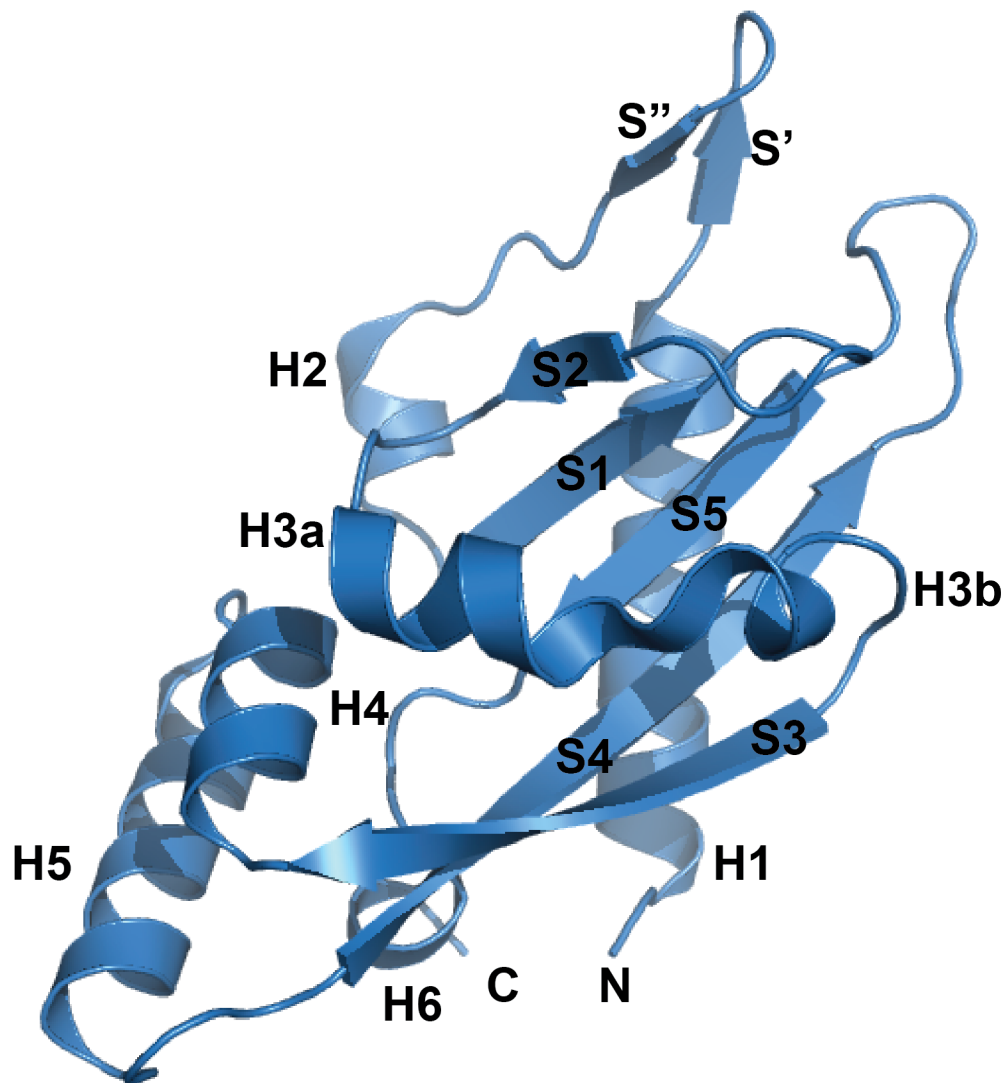


Figure 1.4 Ribbon diagram of PDC domain of PhoQ (43-190) (PDB code: 3BQA). Modified from Cheung *et.al.* (27). Secondary structure elements are labeled in black. The protein contains 5 central β -strands surrounded by 6 α -helices.

N-terminal helix, present only in PDC domains (27). The membrane embedded sensor domains are composed of HKs that have multiple transmembrane regions. For instance, biochemical and structural studies show that the transmembrane region is required for temperature sensing by DesK, but the exact mechanism of temperature sensing is still unknown (32,33). The cytoplasmic sensor domains, unlike the extracellular domains, are composed mainly of PAS domains (24). PAS domains are used as a signaling module by a variety of proteins, often binding small ligands or engaging in protein-protein interaction to initiate a signaling cascade. For instance, the structure of the sensor domain of *Rhizobium meliloti* FixL, a HK that detects oxygen by binding a heme molecule, has been determined (34). Other examples of PAS containing HKs are the *Staphylococcus carnosus* NreB, that senses oxygen using an iron-sulfur cluster (35), and the photosensor LovK that binds a flavin cofactor to sense blue light and redox (36). These examples provide a small glimpse of the diversity of sensor domains, the strategies and environmental cues that can be recognized.

Global analysis of sequenced genomes using the SMART database in April 2014, show that there are ~22,800 HKs (11). The majority of these proteins ~21,500 (94%) belong to bacterial species. Closer examination shows that ~6,800 (31.7%) of these HKs harbor at least one PAS domain. This underlies the importance of structural and biochemical characterization of such widespread sensor in bacteria.

1.2.1.1 PAS domains are modular environmental sensors

PAS domains are a family of environmental sensors that are present from bacteria to

eukaryotes. These domains were initially described in the *Drosophila period* and *single-minded* and the aryl hydrocarbon receptor nuclear transporter (ARNT) (37,38). PAS domains are able to sense a variety of environmental changes like redox, oxygen, light, small ligands and protein-protein interactions (39). The type of environmental cues a PAS domain is able to sense is partly dictated by the cofactors that are associated with the protein. Some PAS domains are known to bind flavin mononucleotide (FMN), flavin adenine dinucleotide (FAD), riboflavin, heme and other natural and artificial small molecules (39). For example, the plant phototropins blue light receptor contains two PAS domains that bind FMN or FAD (40). In the photoactive yellow protein (PYP) the PAS domain binds a 4-hydroxycinnamoyl chromophore to sense blue light (41). The quorum sensing protein LuxP contains two tandem PAS domains that are used to interact with another protein LuxQ (42). This in turn allows the bacteria to sense cell density and regulate many processes like virulence factors and bioluminescence (42).

The sequence identity between PAS domains is below 20%, making conventional identification very difficult (29). But essentially all proteins identified by Pfam as PAS domains and whose structure has been deposited in the protein data bank (PDB) have very similar fold (Figure 1.5) (43,44). This consists of 5 antiparallel β -strands surrounded by several α -helices. In the core of the structure, there is sometimes a cavity that is used by some PAS domains to bind small ligands or cofactors (29). The photosensors, found in plants and in some prokaryotes, are a good example of a PAS domain binding a small ligand. In some cases, the ligand is a flavin cofactor that allows the PAS domain to sense blue light. These types of

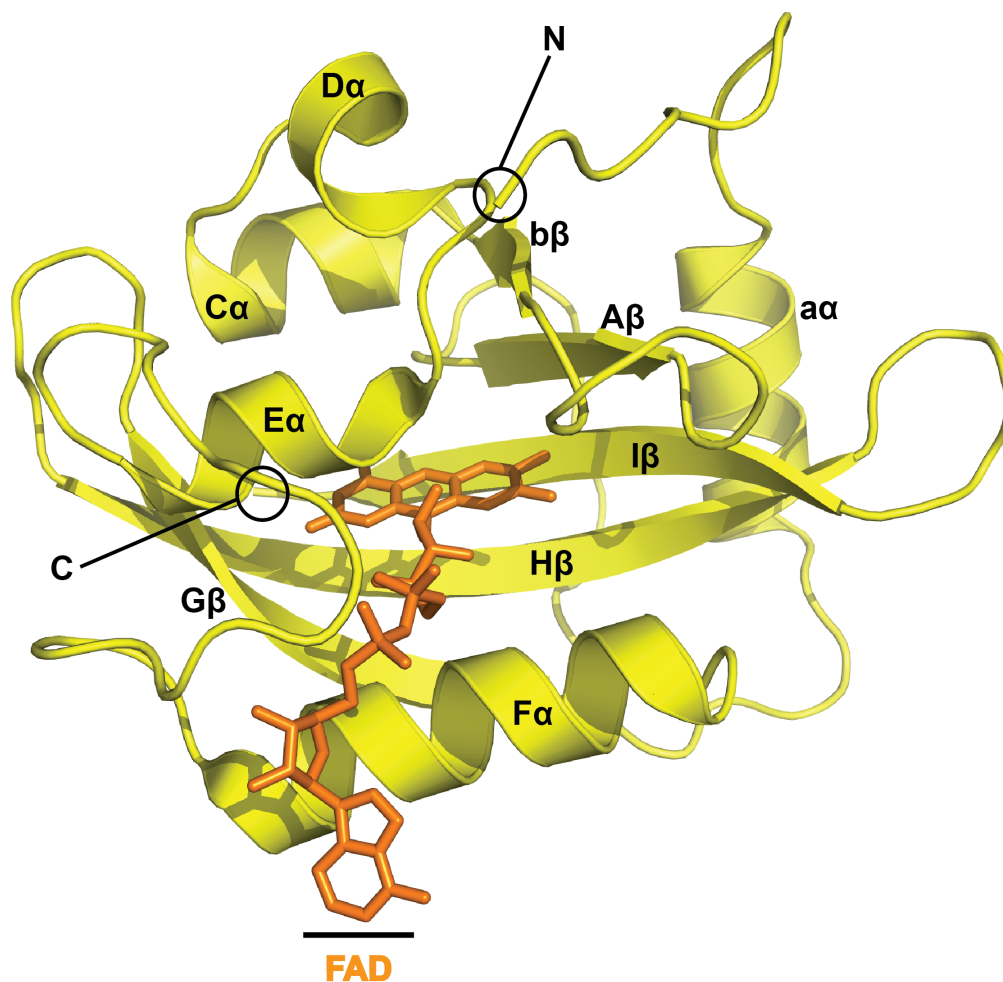


Figure 1.5 2.0 Å crystal structure of *N. crassa* VIVID shown in ribbon diagram.

Modified from Zoltowski *et.al.* (45). Secondary structure elements are labeled in black. VIVID adopts the conserved fold of the PAS domain with 5 central β-strands surrounded by α-helices, with a non-conserved N-terminal helix/strand pair (αα, bβ). Inside VIVID, a flavin adenine dinucleotide (FAD).

photosensors have been categorized in a sub-family within the PAS domain called LOV (Light-Oxygen-Voltage) domain (46).

1.2.1.2 LOV domains, a subfamily of PAS domains, which sense blue light and redox

LOV domains are a subfamily of the PAS environmental sensors (39). The LOV domain was identified in phototropins, as a blue-light photoreceptor with serine/threonine kinase activity, involved in plant phototropism (47). In addition to phototropism, phototropins are known to control stomatal opening, light induced chloroplast movement and phototropic bending (48-51). The ability of LOV domains to respond to blue light comes from its capacity to bind a flavin chromophore (FMN/FAD) and a covalent adduct that forms between the C4(a) of FMN and a conserved cysteine residue found inside the LOV domain (40,52). Through sequence analysis, LOV domains are known to contain a conserved GRNCRFLQ motif that can be used to identify potential members of this family within the PAS domains (46).

Recently, light regulated HKs (LOV-HKs) have been identified in prokaryotes like *Brucella abortus*, *Brucella melitensis*, *Erythrobacter litoralis*, *Pseudomonas syringae* and *Caulobacter crescentus* (36,53). Furthermore, such proteins have been linked to control pathogenesis in some bacterial species and fungi (54). LOV domains are found to be associated not only with kinase domains, but also with DNA binding domains (55-57), STAS (sulfate transporter anti-sigma factor antagonist) domains (58,59) and GGDEF and EAL (diguanylate phosphodiesterases) domains (46). Finally, isolated LOV domains have also been identified to

play a role in circadian rhythm maintenance, like in the case of *Neurospora crassa* VIVID (VVD) (Figure 1.5) (60). These examples showcase the diversity of output domains that LOV domains can regulate (Figure 1.6).

1.2.1.3 LOV domain photocycle

Characterization of flavin containing proteins has been mainly done using UV-visible spectroscopy. Flavin chromophores are non-covalently bound to the LOV domain in the resting state (dark state). Upon blue light exposure (~400-450 nm), chemical changes in the isoalloxazine ring of the flavin chromophore allow the sidechain of a conserved cysteine to form a covalent adduct to the C4(a) of the isoalloxazine ring (Figure 1.7). This chemical changes in the flavin results in a loss of three maxima in the UV-visible spectra between 400-500 nm (light state) (61,62). This process is reversible with the covalent adduct spontaneously breaking and reverting the LOV domain back to the dark state in the order of seconds to hours (52,63).

1.2.2 Kinase domain

The kinase domain of the HK is usually located in the cytosol and is composed of the dimerization and histidine phosphotransfer (DHp) and catalytic (CA) domains, known in the Pfam database as His_kinase_A and HATPase_c respectively (Figure 1.8d) (43,44). Within these domains there are preserved regions that are well conserved among HKs. These regions

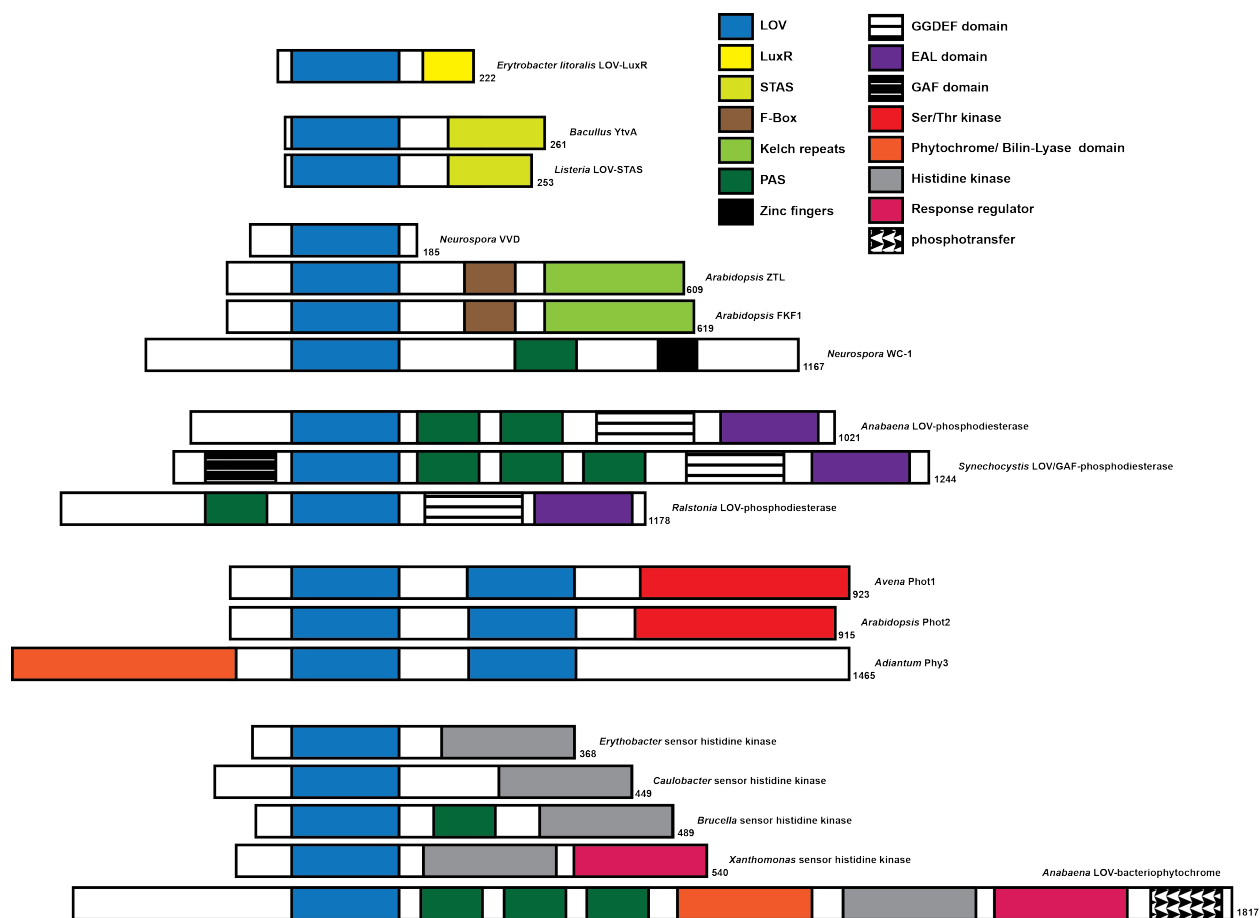


Figure 1.6 Diversity of output domains attached to LOV domain.

Adapted from Crosson *et.al.* (46).

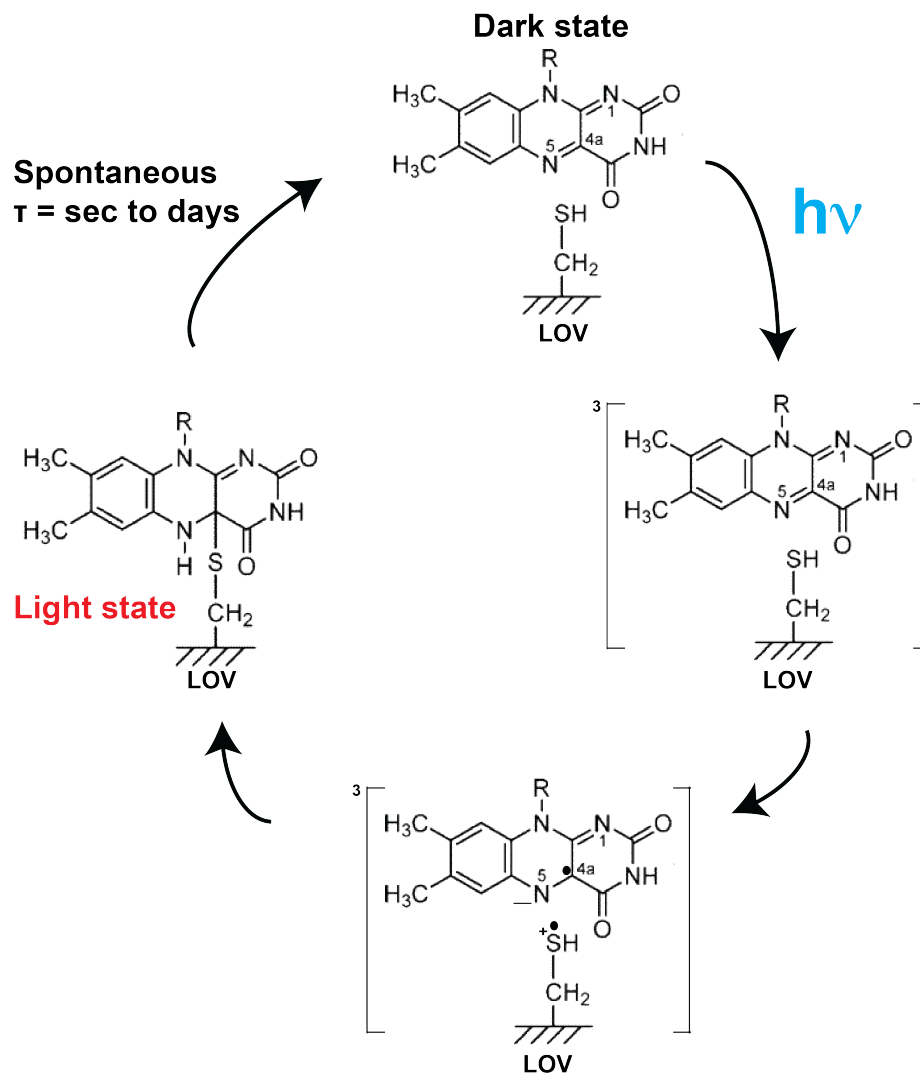


Figure 1.7 The LOV domain photocycle.

Adapted from Schleicher *et.al* (61). Light illumination allows the non-covalently bound flavin to form a covalent adduct to the LOV domain, forming the light state. The light state spontaneously returns to the dark state in the order of seconds to days.

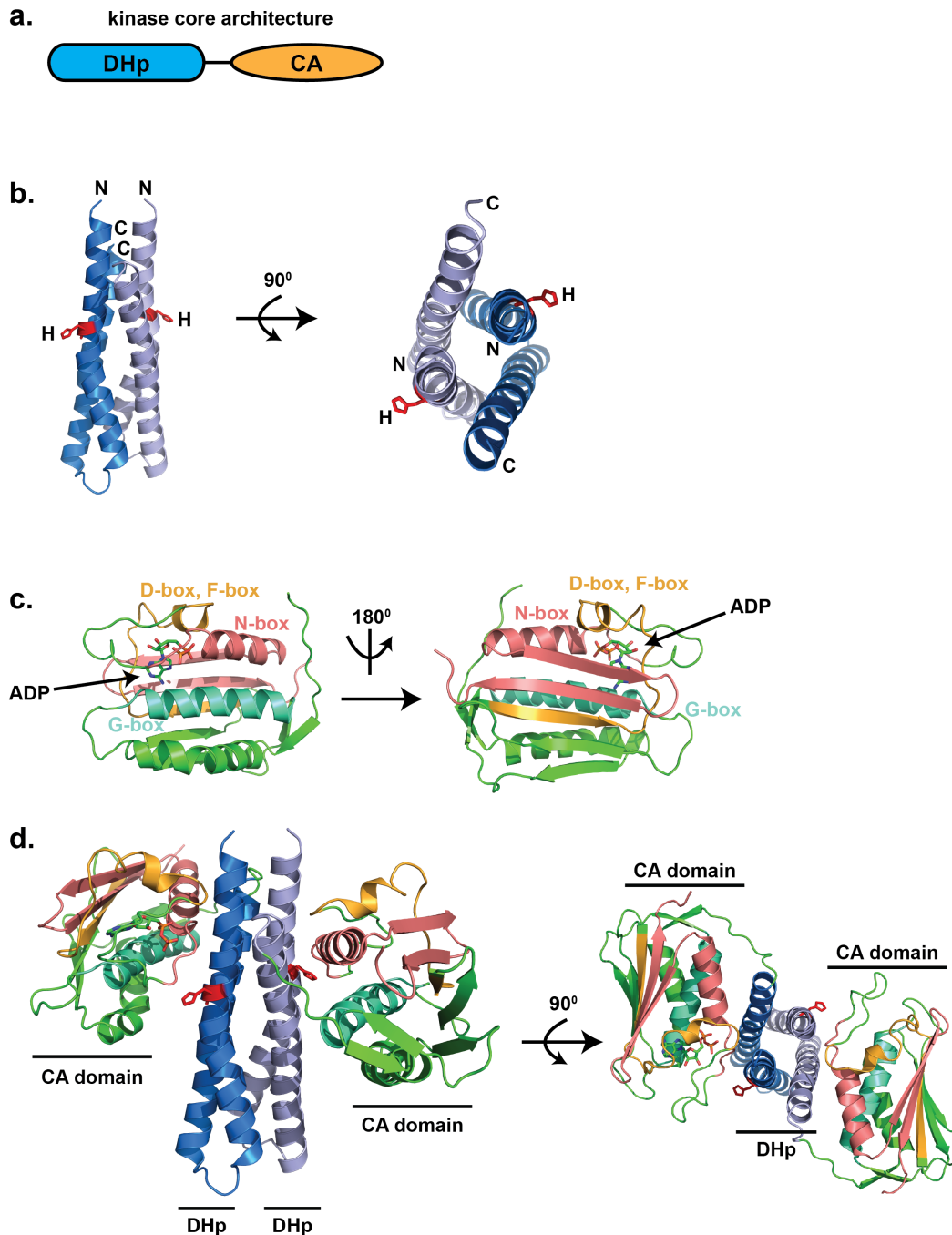


Figure 1.8 2.8 Å crystal structure of the kinase core of *Thermotoga maritima* HK853

a) Schematic representation of the kinase core. The kinase core contains two main domains the DHp and the CA domain. b) DHp domain of HK853, highlighted in red is the phosphoaccepting histidine, which forms part of the H-box. c) CA domain of HK853, highlighted is are homology boxes (D-, F-, N-, G-) important for nucleotide binding. d) Structure of DHp and CA domain of HK853. Showing the relative position of the CA domain to phosphoaccepting histidine.

have been named H-, N-, D-, F- and G- homology boxes after characteristic residues found in these regions (3,64,65). The DHp domain contains the conserved histidine residue (H box) that gets phosphorylated upon activation. The CA domain, which contains the rest of the homology boxes (N, D, F, G), is responsible for ATP binding and phosphate transfer to the histidine residue (3). Together, these domains are required for the autophosphorylation reaction, recognition and phosphotransfer to the aspartate residue in the REC domain of the cognate RR.

The simplest HKs, only containing the sensor, DHp and CA domains, are the most common type (>75%) (66,67) among prokaryotes and are termed class I HKs. However, other types of HKs incorporate additional domains, including hybrid class I and class II HKs (Figure 1.3b) (31,68). About ~4.2% of HKs from the SMART database contains an additional histidine phosphotransfer domain (HPt) and REC domain (10,11). These types of HKs, also known as hybrid HKs, initially transfer the phosphate to a histidine residue in the DHp domain followed by phosphorylation of the aspartate residue in the REC domain and finally phosphotransfer to a second histidine residue in the HPt domain (His-Asp-His) (31). The class II HK are more complex by having additional domains in the kinase core (P1, P2, P3, P4, P5) (Figure 1.3b) (31). The chemotaxis protein CheA is an example of a class II HK that contains all 5 domains (68). Through structural studies of CheA, it is known that the P1 domain contains the conserved histidine residue (H-box), P2 is responsible for RR binding, P3 mediates dimerization of the HK, while P4 binds ATP and P5 regulates kinase activity (68-73).

Analysis of 348 HKs based on sequence similarities shows that over 90% of these proteins fall into one of 11 subfamilies (HPK₁-HPK₁₁) (65). The criteria for classification of the HKs

within the different subfamilies are based on sequence conservation in the H-box and N-box. Recently a new class of HKs with sequence homology to the *Agrobacterium tumefaciens* BphP2, an HK involved in light perception, were identified and classified as HWE_HKs (74). Around 2% of all bacterial genomes, based in the SMART database, contain an HWE_HK, including the marine α -proteobacterium *E. litoralis* that contains two blue-light regulated HWE_HKs (EL362 and EL368) and which will be the subject of discussion in chapter 3.

1.2.2.1 Kinase domain structure and signaling mechanism

Many studies have aimed at understanding how the sensor domain can initiate autophosphorylation in the kinase core. In solution, almost all HKs exist in a preformed homodimer that is mediated by the DHp domain (3). The crystal structure of the *Thermotoga maritima* sensor kinase HK853 revealed the architecture of the DHp domain and CA domain (75), showing that it is composed of a four-helix bundle, where each subunit forms two antiparallel α -helices (Figure 1.8b). The four helices pack against each other forming a hydrophobic core, exposing the conserved histidine residue (one per subunit) to solvent.

The CA domain adopts a α/β sandwich fold (Bergerat fold) (76,77), differentiating it from Ser/Thr/Tyr kinases, but similar to the ATPase domain of the GHL ATPase superfamily, whose members include GyrB (gyrase), Hsp90 (heat shock protein chaperone) and MutL (DNA mismatch repair protein) (77). As a result, the CA domain has been included in the ATPase superfamily, which was renamed to the GHKL superfamily of ATPase/Kinase (77). In the CA

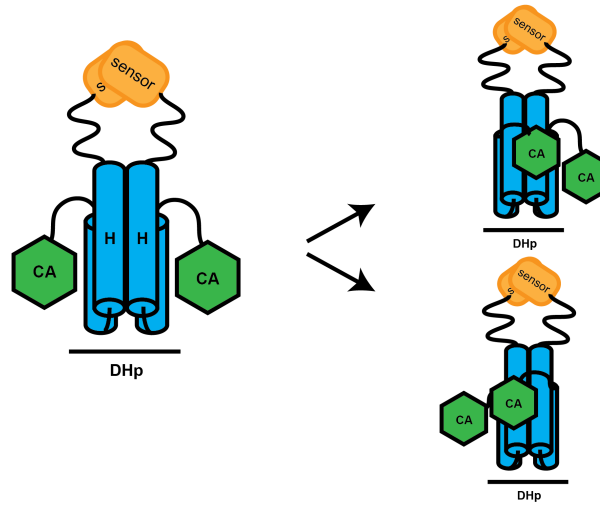
domain of HK853, one layer is formed by five β -strands while the second layer is composed of three α -helices that together enclose a hydrophobic core. Additionally, there is a polypeptide fragment that is composed of a short α -helix (D-box, F-box) (76) (Figure 1.8c). Furthermore, the structure reveals that it is in this region where ATP binds. Additionally, the N-box of HKs contains an asparagine residue which is responsible for coordinating an Mg^{2+} ion (77). Mg^{2+} ion is a very important cofactor assisting in connecting ATP to the protein via solvent-mediated hydrogen bonds (77). This features can be observed in other structures of CA domain, suggesting a common mechanism of ATP binding.

Even though there is much structural and biochemical information collected on individual HK domains (DHp and CA), there is poor understanding on how all three domains (sensor domain-DHp-CA) interact. The structure of the entire DHp/CA kinase core of *Geobacillus stearothermophilus* KinB and *T. maritima* HK853 have revealed some details of histidine phosphorylation by the CA domain (78,79). With the structure of HK853, it has been postulated that the CA domain undergoes conformational changes to position itself in contact with the phosphoaccepting histidine in order for the phosphorylation reaction to occur (Figure 1.9a) (78). The crystal structure of *G. stearothermophilus* KinB was solved in the presence of the HK inhibitor Sda, a 46 amino acid peptide (80). In this Sda/KinB complex, Sda was found to function as a barricade between the CA domain and the DHp domain, preventing autophosphorylation, phosphotransfer and phosphatase activity (Figure 1.10) (79). These structures provided insight on how the CA domain contacts the DHp domain for the autophosphorylation reaction, but does not answer how the sensor domain is able to regulate the

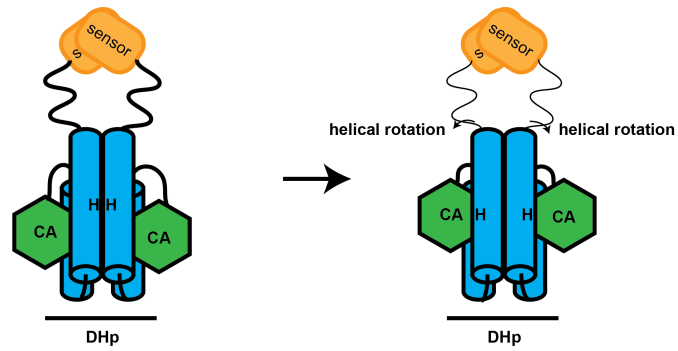
Figure 1.9 HK activation models.

a) Based on the crystal structure of *T. maritima* HK853 (PDB:2C2A) (78). Upon activation the CA domain positions itself in contact with the DHp domain. Subsequently the conserved histidine is phosphorylated. b) Based on the crystal structure of YF1 (PDB:4GCZ) (81). Activation of the HK leads to rotation of the DHp, exposing the conserved histidine residue for phosphorylation by the CA domain. c) Based on the crystal structure of CpxA (PDB:4BIU) (82). Activation of the HK induces bending of the DHp domain, positioning the histidine residue in close proximity to the CA domain.

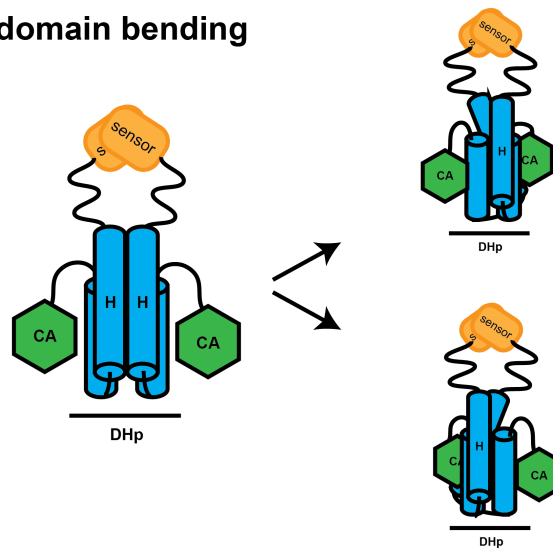
a. CA domain proximal to DHp domain



b. Rotation of DHp domain



c. DHp domain bending



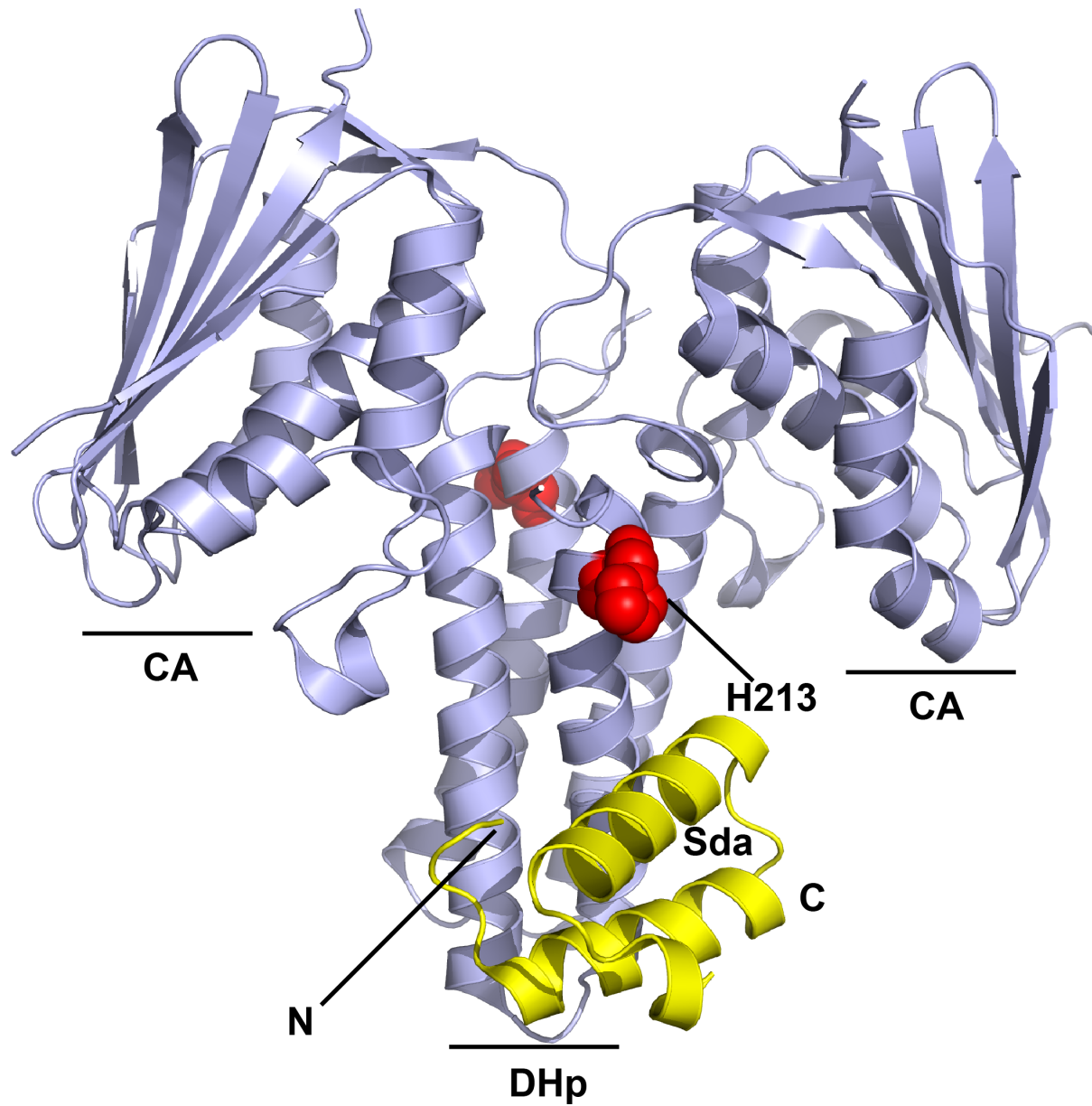


Figure 1.10 Crystal structure of KinB bound to the Sda inhibitor.

Modified from Bick *et.al.* (79). Sda binds in a way that does not allow positioning of the CA domain proximal to the DHp domain for phosphorylation of the histidine residue (H213).

kinase core. Recently, the full-length structures of HK (sensor-DHp-CA) were described (YF1 and VicK) (Figure 1.11) (81,83). In the structure of the artificially-engineered YF1 protein, the PAS-B domain of *Bradyrhizobium japonicum* FixL was replaced by the LOV domain of *B. subtilis* YtvA, resulting in a HK that responds to blue light instead of oxygen (Figure 1.11a) (84). Based on the structure and previous biochemical data, it has been proposed that the signal is propagated from the sensor domain to the kinase core by rotational movement in the coiled-coiled linker (81,84). The VicK structure (Figure 1.11b) suggested that the basis of phosphorylation and dephosphorylation is based on helical bending of the DHp domain (83). This movement allows the CA domain access to the histidine residue for phosphorylation. Finally, the crystal structure of the entire cytoplasmic region of CpxA, a HK involved in *E. coli* response to envelope stress was solved. The structure showed that the CA domain was positioned within distance of the conserved histidine residue as a result of helical motions in the DHp domain (82). Based in these structures, three modes of signal transduction leading to have been proposed that consist of i) movement of the CA domain proximal to the histidine residue in the DHp domain (Figure 1.9a), ii) helical rotation of the coiled-coiled linker and DHp domain (Figure 1.9b) and iii) helical bending of the DHp domain (Figure 1.9c).

1.3 Response regulators

The second component of the TCS signal transduction is the RR. It contains the REC domain, which harbors the phosphoaccepting aspartate (3). REC domains have been described

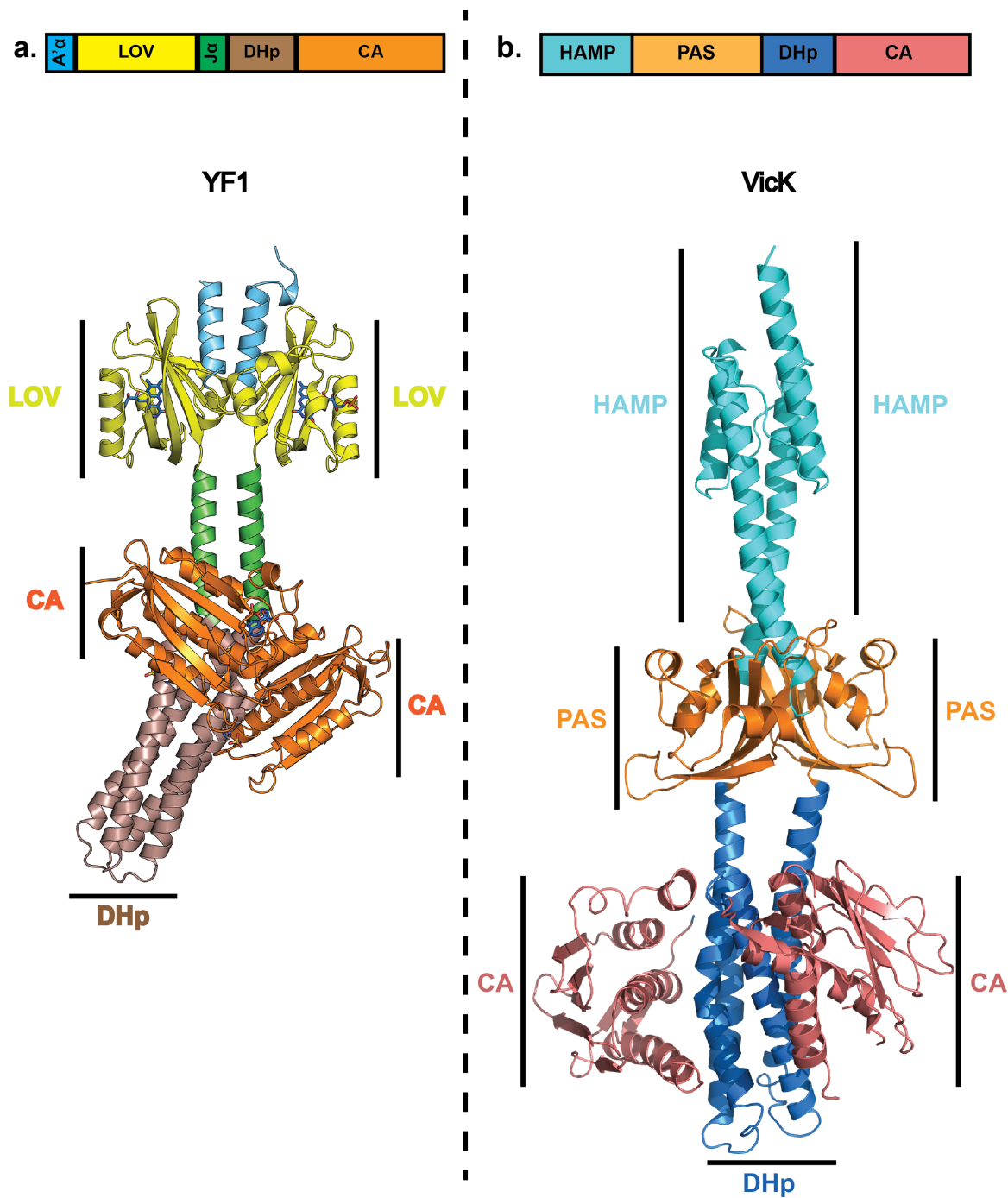


Figure 1.11 Full-length structure of the hybrid histidine kinase YF1 and the cytoplasmic portion of VicK from *Streptococcus mutans*.

a) Crystal structure of YF1 (PDB: 4GCZ) modified from Diensthuber *et.al.* (81). Schematic representation of YF1 histidine kinase: in yellow the LOV domain of *B. subtilis* YtvA and in orange/brown the kinase domain of *B. japonicum* FixL. b) Crystal structure of the sensor kinase VicK (PDB: 4I5S). The HAMP domain is located N-terminus to the sensor domain, and is used to transmit signal from the membrane to the kinase core

as switches, which cycle between the phosphorylated (ON) and the dephosphorylated (OFF) state. Analogous to REC domains, the guanine nucleotide-binding proteins (GNBP) found in eukaryotic signaling have a similar mode of regulation (85). In response to environmental changes, these proteins function as molecular switches cycling between OFF (GDP bound) and ON (GTP bound) states, controlling physiological processes like cell growth (85). The prototypical RR contains an N-terminal REC domain followed by a variable C-terminal effector domain (3). The effector domains often dictate the specific biochemical/functional role the RR may partake inside the cell (i.e. HTH effectors involved in DNA binding). However, a subset of RRs without effector domains have been identified, leading to a subgroup known as single domain response regulators (SDRR) (86). For instance, the chemotaxis protein CheY is a well-studied SDRR that participates in regulation of bacterial motility (16,87). Other SDRRs include Spo0F, involved in *B. subtilis* sporulation (88,89), and DivK, a *C. crescentus* SDRR with an essential role in cell division (90,91).

1.3.1 Receiver domain structure

The CheY superfamily has served as the basis to identify other REC domains (92). REC domains serve as the minimal functional subunit of the RR, as they contain the phosphoaccepting aspartate as well as additional residues to regulate activation like seen in CheY or Spo0F. As of April 2014, ~280 structures of RRs have been deposited in the PDB database (93). Most of the REC domain structures solved so far resemble that of the chemotaxis protein CheY, which was

one of the earliest structures to be solved in this group (94,95). The structure revealed a $(\beta/\alpha)_5$ fold, consisting of 5 parallel central β -strands surrounded by 5 α -helices (Figure 1.12a) (94,95). Furthermore, the phosphoaccepting aspartate (D57 in CheY) is located at the C-terminal region of β_3 (Figure 1.12b). The loop region between β_1 and α_1 in CheY contains two aspartate residues (D12, D13) that together with D57 form a carboxylate cluster. This is the region where a divalent cation, typically Mg(II), binds to aid in the phosphorylation reaction (96,97). Finally at the C-terminus, there is a set of highly conserved residues: threonine/serine (T87 at the end of β_4), phenylalanine/tyrosine (Y106), lysine (K109) and proline (P110) at the end of β_5 that important for activation of the REC domain (Figure 1.12b) (97). Sequence alignment of other RRs reveals a general conservation of residues found in CheY, suggesting a common regulatory strategy among REC domains (92,97).

1.3.2 Response regulator activation

While TCS are found in some fungi and plants (98,99), their absence in higher eukaryotes (mammals) has motivated the interest in understanding the molecular mechanism of activation of these proteins, to develop new therapies for treating the increasing number of multiple antibiotic resistant infections (100). Biochemical studies have shown that REC domains can be phosphorylated by their cognate HK (101) or can catalyze an autophosphorylation reaction from a small ligand phosphodonors, like carbamoyl phosphate or acetyl phosphate (102). This reaction leads to a number of conformational changes along the REC domain that results in the

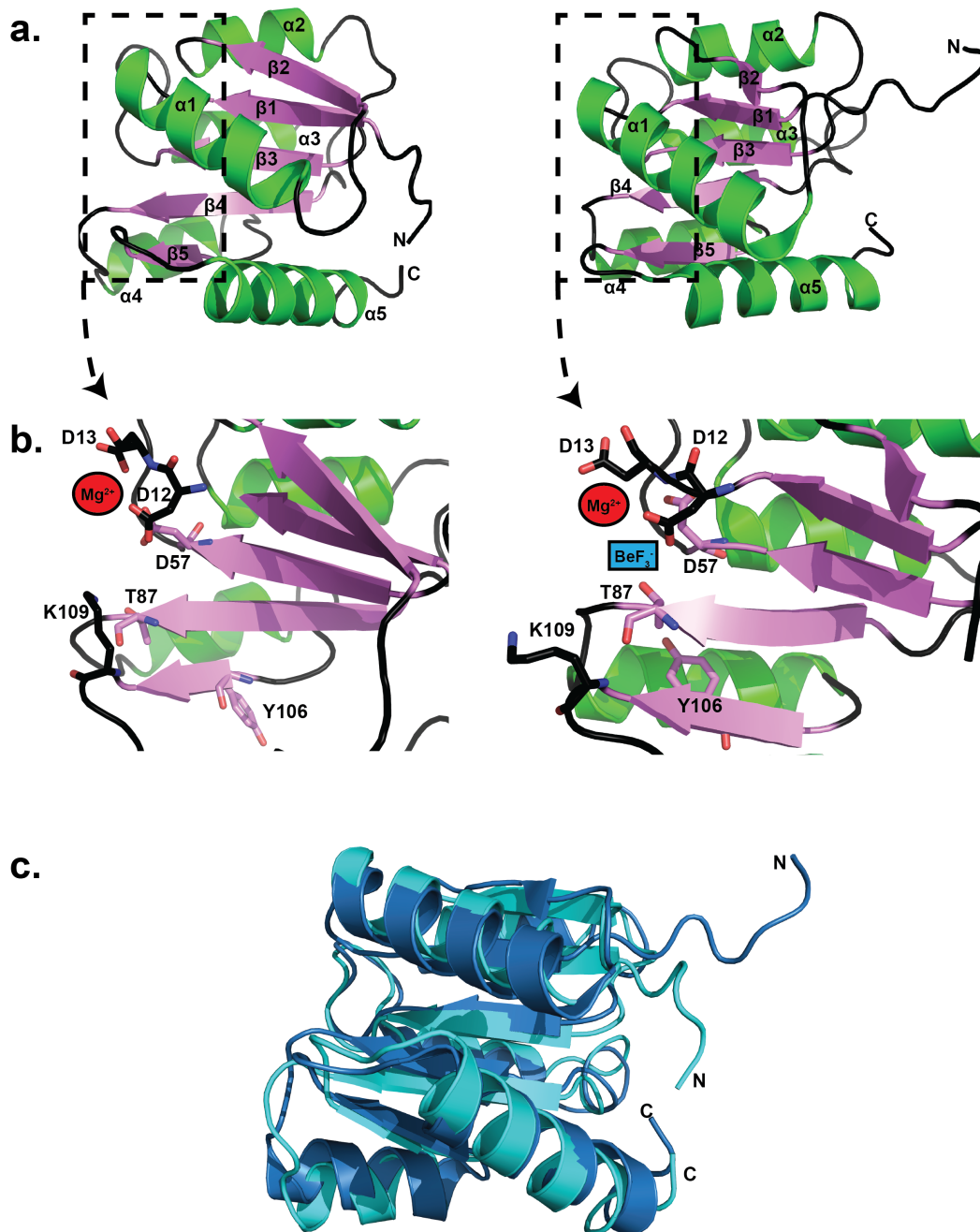


Figure 1.12 Structure of CheY in inactive and active conformations.

a) Crystal structure of CheY in the inactive conformation (left) (PDB:2CHE) (95) and solution structure of CheY in the active conformation (right) (PDB:1DJM) (103). b) Close up of active site of CheY in the inactive (left) and active (right) conformation, with predicted site of Mg^{2+} and BeF_3^- binding. Y106 exhibits a sidechain rotation towards T87 in the active state. c) Superimposition of CheY in the inactive (light blue) and active (dark blue), shows minimal changes between structures.

regulation of the effector domain.

Structural analyses of RRs in the active and inactive conformation have been performed to understand the molecular mechanism of phosphorylation-mediated activation of the REC domain. These studies have provided insight on the general mechanism of RR activation, particularly by identifying the roles of the residues conserved among REC domains (92). For instance, in the loop region between $\beta 1$ and $\alpha 1$, CheY contains two aspartate residues that together with the phosphoaccepting aspartate form a carboxylate cluster that is used for divalent cation binding (96). These residues and the associated cation are used to catalyze the phosphorylation reaction of the aspartate residue (97). In CheY (PDB: 2CHE), the preferred divalent cation is Mg^{2+} , as shown by functional and structural studies (104,105), but other REC domains are known to bind other cations, like Ca^{2+} and Mn^{2+} (106). In the structures of NtrC and Spo0F (PDB: 1NTR, 1FSP) two aspartate residues can be observed at this position and in close proximity of the phosphoaccepting aspartate (Figure 1.13) (95,107,108). The divalent cation help catalyze the phosphotransfer reaction by hydrolyzing the phosphate group from the HK to the conserved aspartate at the end of the central β -strand 3 (96,104). In addition to these residues, the conserved threonine/serine at the end of the β -strand 4 helps stabilize the phosphorylated state (109). Upon phosphorylation of the REC domain, the sidechain of the conserved threonine/serine (Thr 87 in CheY) rotates to position the hydroxyl in close proximity of the phosphate to form a hydrogen bond (97). Similarly the sidechain of the conserved lysine residue at the β -strand 5 rotates in the direction of the phosphoaccepting aspartate to form a salt

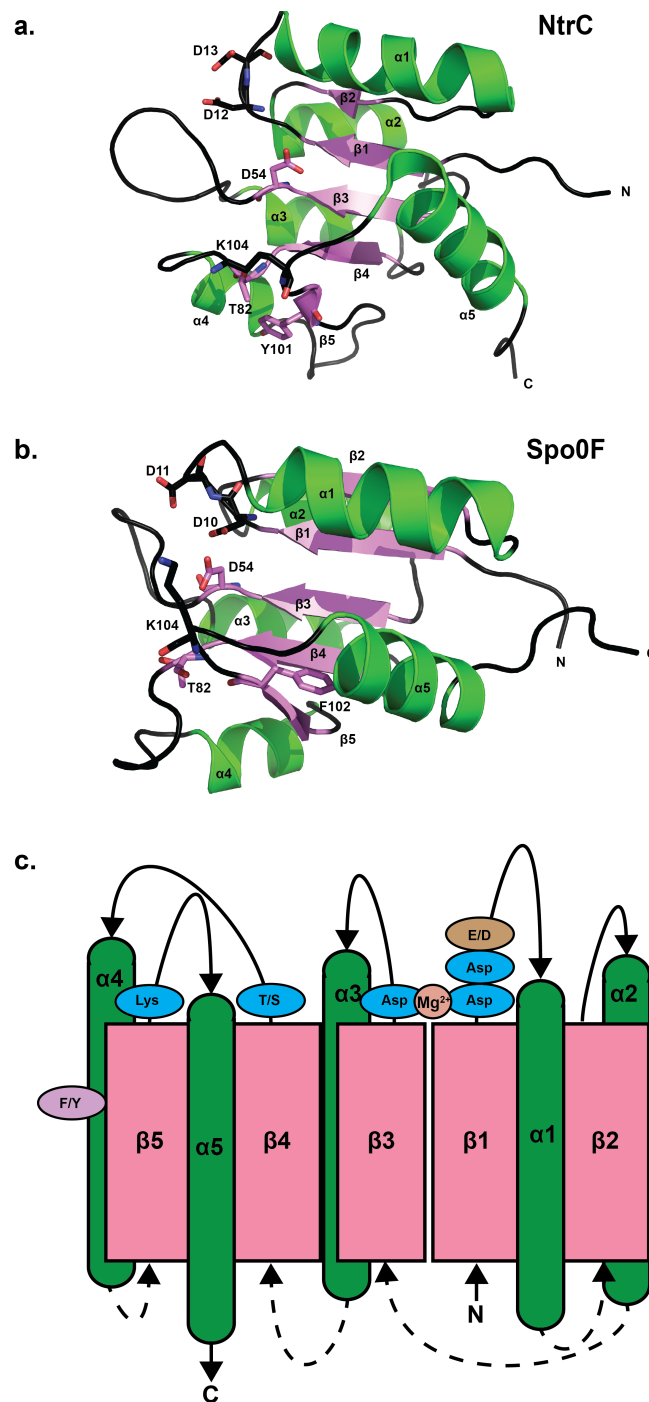


Figure 1.13 Structure of the REC domain of NtrC and Spo0F.

a) Solution structure of NtrC (PDB:1NTR) (107), active site residues and secondary structure elements are labeled in black. b) Solution structure of Spo0F (PDB:1FSP) (108), active site residues and secondary structure elements labeled in black. c) Schematic representation of REC domains (adapted from Bourret, R.B. (97)). Residues that play a key role in REC domain phosphorylation are shown in light blue.

bridge with the phosphate group, stabilizing the active state (97,110). Functional studies revealed that mutation of the lysine residue in CheY does not abolish phosphorylation, but fails at inducing clockwise flagellar rotation (tumbly swimming), suggesting that this residue has a role in the activation of the protein, but not phosphorylation (110). Finally an aromatic residue (phenylalanine/tyrosine) in $\beta 5$ position of the REC domain is highly conserved. In this case, the sidechain rotation previously discussed (ser/thr) stabilizes a rotameric conformation of the phenylalanine/tyrosine residue within a hydrophobic cavity, in what is known as the Y-T coupling (97,103,111). Comparing the structure of activated CheY to other REC domains revealed similar conformational changes upon activation (e.g. Spo0A and FixJ) (112).

Recently NMR methods sensitive to millisecond timescale dynamics, like the Carr-Purcell Meiboom-Gill relaxation dispersion (CPMG RD) approach, have been very useful to study conformational changes of RRs in solution (113,114). This experiment allows direct measurement of the relaxation time of the spin of any nucleus, which is influenced by the chemical environment. For instance, these methods have been used to obtain kinetic, thermodynamic and structural information for processes that occur in the microsecond to millisecond time scale (μs -ms). Processes that occur within this time scale include, sidechain reorientation, loop motion and secondary structure changes (114).

This type of NMR method has been used to analyze the effects of phosphorylation in CheY and NtrC^r. Conformational changes of unphosphorylated CheY in the microsecond to millisecond (μs -ms) timescale revealed that the protein spontaneously switches between inactive and active-like conformations (115). While the inactive ground state is much more populated

without phosphorylation, this post-translational modification shifts the equilibrium towards the active state. These types of studies will expand the existing knowledge of RR activation at the molecular level. In the case of the nitrogen sensing TCS (NtrB/NtrC), the REC domain of NtrC has been extensively studied to understand the effects of phosphorylation in activation of the REC domain (107,116). Using solution NMR relaxation dispersion methods, it was shown that in solution NtrC^r is in equilibrium between two different folded conformations (inactive and active) (117,118). When NtrC^r is in the unphosphorylated state, it is primarily in the inactive conformation with a small population sampling the active state. Activation of the REC domain, using small phosphodonors (102) or a small ligand known to mimic the phosphate group (BeF₃⁻) (119-121), shifts the equilibrium towards the active conformation. Many of the conformational changes that occur upon phosphorylation were concentrated at the C-terminal region, from α -helix 3 to β -strand 5 ('3445' switch region) (116), which was first identified by comparing wild type NtrC^r to different partially active mutants (122). Finally, NtrC^r also contains the conserved aromatic residue (tyrosine) at the β -strand 5, suggested to be involved in the Y-T coupling, which is important for the activation of REC domains (92,97). However, recent evidence shows that the Y-T coupling in NtrC^r might not be critical for the activation of the REC domain, but rather to play a role in protein-protein interaction (123). Mutational and relaxation dispersion NMR experiments showed that removing the tyrosine residue did not affect the phosphorylation mediated activation of NtrC^r, nor the stability of the phosphorylated state. With more REC domains being examined with a combination of solution structural and dynamic methods, more details on the dynamics of activation will be revealed.

1.3.3 Effector domain diversity

The REC domain of the RR is able to be phosphorylated by the HK or small phosphodonors, regulating its downstream activity, determined by the associated effector. Genome wide analyses of signal transduction proteins have given insight on the diversity of effector domains in RRs (12,86,124). As a result of these studies, the authors maintain a list of RRs that has been manually curated to contain a non-redundant collection of prokaryotic genomes (<http://www.ncbi.nlm.nih.gov/Complete-Genomes/RRcensus.html>). Additionally, RRs found in this list have been classified by their domain architectures. For instance, as of 2011 there were ~27,000 RRs found between prokaryotes and archaea. Approximately ~4,600 (17%) are SDRRs, ~16,600 (61%) have a DNA binding domain, ~280 (1%) contain a RNA binding domain and ~3,200 (11.8%) contain an effector domain with an enzymatic activity (Figure 1.14). The last group included in this list was classified as “other”, which constitute about ~2,400 (9%) of RRs and are only found in specific groups of bacteria.

The largest group of RRs (61%), function as transcriptional regulators, with six different subfamilies: OmpR, NarL, NtrC, LytR, ActR and AraC (12,124). The second largest group of RRs comprising 14% is the SDRR, which only contain the modular REC domain. This class of RRs is versatile and is found to be involved in a variety of physiological responses. For example, the well-characterized chemotaxis protein CheY is a SDRR that regulates flagellar rotation upon phosphorylation (16,125). In the soil bacterium *R. meliloti*, two CheY proteins

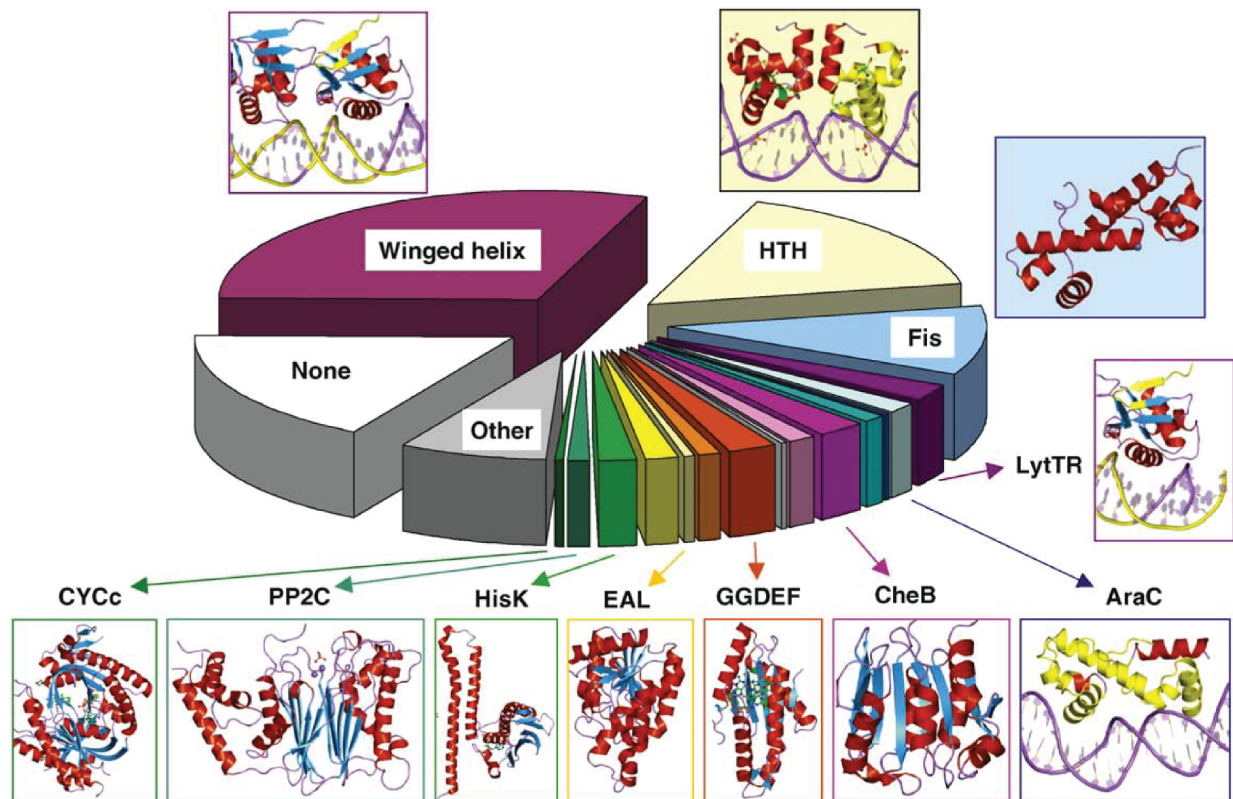


Figure 1.14 Classification of RRs by their output domain.

Figure adapted from Galperin, M.Y. (12).

are required to effectively regulate chemotaxis. In this case, CheY2 is the main regulator of flagellar rotation, while CheY1 acts as a phosphate sink for the system (126), exemplifying the ability of members of the same class of protein to have two distinct roles in the cell. SDRRs have also been shown to function as allosteric regulators. For example, the SDRR DivK plays an important role in the cell cycle of *C. crescentus*. Phosphorylated (DivK~P) localizes to one of the poles and induces stalked cell morphology in one premature daughter cell where as the other premature daughter cell differentiates into a swarmer cell (127). Followed by the SDRR, the next most abundant class of RRs are those with an enzymatic activity (11.8%). For example PleD is a RR in *C. crescentus* that contains a GGDEF domain, used to synthesize c-di-GMP (127). Other known effector domains with enzymatic activity are EAL domains (diguanylate phosphodiesterases), HisK (histidine kinase) and PP2C (protein phosphatase) (12). Finally the least abundant of effector domains (1%) are the RNA binding domain (i.e. AmiR, ANTAR) (128).

1.3.4 Atypical response regulators

Recently a new class of RR has been described, named atypical or pseudo RRs (97). This class of protein contains a REC domain with many of the conserved residues and structure of REC domains, but lacking the phosphoaccepting aspartate or other essential features. One example of this emerging class of RRs is the *Myxococcus xanthus* FrsZ, which regulates social motility. This protein lacks the phosphoaccepting aspartate, the threonine/serine residue and

does not bind Mg^{2+} and BeF_3^- (129). But interestingly, the conserved aromatic residue (tyrosine) at the β -strand 5 seems to be important for the function of this protein (129). In *Synechoccus*, NblR is involved in transcriptional regulation after nutrient or high light stress. This orphan atypical RR does not need to be phosphorylated to become active (130). Substitution of putative phosphoaccepting aspartate to an alanine, did not affect the activity of this transcriptional regulator. It was proposed that the activation of this pseudo-RR involves sensing of redox state inside the cell and the formation of a disulfide bond (130). However, mutational analysis showed that the mechanism of activation is not dependent of disulfide bond formation and must involve some sort of heterodimer formation that has yet to be discovered (131). These are some examples of REC domains that lack conserved residues and appears to not use phosphorylation to regulate physiological roles.

1.4 Blue light regulated two-component systems

Light is an important source of energy for many organisms. The widespread presence of photoreceptors in prokaryotes (e.g. LOV domains) suggests that light plays an important role in the lifestyle of many bacteria, even those not traditionally thought to be phototropic or photosynthetic. LOV domains are found linked to HKs and are known to regulate kinase activity by light (53,63). For instance, the soil bacterium *C. crescentus* contains a light regulated TCS LovK/LovR, which is known to regulate cell attachment and osmotic stress response (36,132). In this particular case, light activates the soluble HK (LovK), while the

SDRR (LovR) regulates cell attachment, as seen in microfluidics experiments (36).

Furthermore, LovK/LovR has been also implicated to regulate the general stress response pathway of *C. crescentus* (132). During osmotic stress, a second TCS PhyK (HK) and PhyR (RR) are responsible for mediating stress dependent survival. Phosphorylated PhyR activates an EcfG-family sigma factor by interacting with the anti-sigma^{EcfG} factor NepR (133).

Transcriptional reporter assays and survival assays under osmotic stress demonstrated that LovK/LovR regulates and is regulated by PhyK/PhyR by a complicated network of crosstalk between HKs and RRs (132).

A homologous TCS with high similarity to the one described in *C. crescentus* has been also identified in the marine α -proteobacterium *E. litoralis* (53,63). This microorganism was identified in an effort to understand the metabolism of aerobic anoxygenic phototropic (AAP) bacteria (134-136). *E. litoralis* contains three soluble LOV-HKs (EL346, EL368 and EL362), named after their number of amino acids, that can phosphorylate two RRs, LovR (EL_LovR) and PhyR (EL_PhyR) (63,101). *E. litoralis* is not a genetically tractable microorganism, complicating the functional characterization of the light-regulated TCS. However, it provides an excellent system to study how a known stimulus (blue light) affects the activation of a LOV-HK and phosphorylation of the cognate RR. The biochemical and biophysical characterization of two of the LOV-HKs (EL368 and EL362) and the target RRs (EL_PhyR and EL_LovR) are the subject of discussion in the coming chapters.

Light not only serves as a stimulus for TCSs involved in stress response, but also it can be used to regulate infectivity. *Brucella melitensis* and *Brucella abortus* are example of

microorganism that uses light to regulate virulence. Studies have revealed that the LOV-HK in *B. abortus* is required for replication inside the macrophage (53). Furthermore, mutation of the cysteine, responsible for covalent adduct formation between the LOV domain and the chromophore, did not restore wild type replication rates. This suggests that the LOV-HK plays an active role in the infectivity of *B. abortus*, and that it requires light for activation.

1.5 Relevance of two-component systems

Antibiotic resistance has become an increasing public health issue in the recent years. Methicillin resistant *S. aureus* (MRSA), multi-drug resistant *Mycobacterium tuberculosis* and multi-drug resistant *Neisseria gonorrhoea* infections have become increasingly difficult to treat due to resistance to available drugs (137-139). TCSs play a central role in many of bacterial responses to external stimuli. This signaling cascade, which is composed by a HK and a RR, contains conserved features that allows for efficient signal transduction between proteins (kinase core and REC domain) and a diversified input and output domains that give the ability to universally use the same biochemical reaction for different circumstances. Because the proteins involved in TCSs share many properties, it has been considered as a potential target for antimicrobial agents (140). For instance, a combination of computational and experimental methods identified 8 compounds that can inhibit DNA binding of the PhoP RR from *Salmonella enterica* (141). The biochemical and biophysical data suggests that the compound may bind to the α 4- β 5- α 5 region of the REC domain or inhibition of the DNA binding domain.

Understanding the molecular details of TCS signal transduction is key to develop new and more efficient therapies in a post-antibiotic era.

Chapter 2 Experimental procedures

2.1 General growth conditions and strain construction

E. coli were cultured in LB liquid medium or in LB agar (15g/L) at 37 °C supplemented with appropriate antibiotic concentrations: chloramphenicol, 20 mg/mL; gentamicin, 15 mg/mL; kanamycin, 30 mg/mL; or spectinomycin-streptomycin, 50 mg/mL-30 mg/mL. EL368, EL_LovR and EL_PhyR were cloned in plasmids containing the vanillate (Pvan) or xylose (Pxyl) inducible promoters (pMT528, pMT585, pMT644, pMT674) using NdeI, EcoRI and XhoI restriction sites. Plasmids were transformed to *E. coli* DH5 α cells and subsequently purified using Promega Wizard Plus miniprep DNA purification systems.

C. crescentus strains bearing the transcriptional reporter plasmid pRKlac290 were grown in peptone-yeast extract (PYE) agar plates (15 g/L) at 30 °C. Liquid cultures of *C. crescentus* were grown in M2 defined medium supplemented with 0.15% xylose (M2X) as the carbon source. Competent *C. crescentus* strains were generated by growing overnight cultures to OD₆₆₀ ~0.6. Cells were centrifuged for 3 min at ~11,900 xg, resuspended with sterile H₂O and repeated three times. Approximately 70 mL of cells are mixed with desired plasmid (pMT528, pMT585, pMT644, pMT674) and electroporated using a Bio-Rad Gene Pulser Xgene. Post-electroporation fresh PYE media was added and let the cells recover for 2 hr at 30 °C. Subsequently, strains were plated on PYE plates with appropriate antibiotics: chloramphenicol,

1 mg/mL; gentamycin, 5 mg/mL; kanamycin, 25 mg/mL; oxytetracycline, 2 mg/mL; spectinomycin-treptomycin, 100 mg/mL-5 mg/mL. Cells were grown in liquid PYE media and stocks were frozen in 25% glycerol.

2.2 Cloning, expression and purification of LOV-HK and response regulator proteins

DNA-encoding sequences of the LOV-HK proteins EL368, EL346 and EL362 (NCBI Gene locus tags ELI_02980, ELI_04860, and ELI_07650, respectively) and anti- σ factor (locus tag ELI_10225) were amplified from *Erythrobacter litoralis* HTCC2594 genomic DNA (135), and cloned into the pHis-G β 1-parallel expression vector (142). Response regulators (locus tags in Table 3.1) were amplified from *Erythrobacter litoralis* HTCC2594 genomic DNA and cloned into the pHis-parallel expression vector (143). Mutants EL368 (C93A), EL362 (R150G) and EL_LovR (E12A, D13A, E14A, D56A, P95A, N54K) were generated with QuickChange II XL site-directed mutagenesis kit (Stratagene). *Escherichia coli* BL21(DE3) cells transformed with those vectors were grown at 37 °C in LB media containing 100 μ g/mL of ampicillin to an A_{600} of 0.8, then induced overnight at 18 °C by the addition of 0.4 mM isopropyl β -D-thiogalactoside (IPTG). Cells were harvested, resuspended into 50 mM Tris pH 8.0, 100 mM NaCl buffer, lysed by extrusion and centrifuged at 48,000 g for 45 min. The supernatant fraction was initially loaded onto a Ni²⁺ affinity column (Chelating SepharoseTM Fast Flow, GE Healthcare) pre-equilibrated with the above buffer plus 25 mM imidazole. Proteins were eluted using a 25 to 500 mM imidazole gradient, and then digested with His₆-TEV protease (144). Cleaved target

proteins were separated from their tags and TEV protease using a Ni²⁺ affinity column; flowthroughs were collected and concentrated (Amicon Ultra, Millipore). A final gel filtration step used HiLoad 16/60 Superdex 75 or HiLoad 26/60 Superdex 200 columns (GE Healthcare), with both columns pre-equilibrated in 50 mM Tris pH 8.0, 100 mM NaCl buffer. All protein-containing fractions were analyzed by SDS-PAGE and stored at -20 °C with 50% glycerol (v/v). For the three LOV-HK proteins, all purification steps were performed under dim red light. Protein concentrations were measured at A₄₄₆ for EL368 and Pierce Bradford assay (145) for EL_LovR. Protein production in complex media and purification were performed as described (63), with protein concentrations measured using Bradford assays (Pierce) (145). U-¹⁵N labeled and ¹⁵N,¹³C labeled proteins were obtained by transforming protein expression plasmids into *Escherichia coli* BL21(DE3) cells grown in M9 minimal media containing 1 g/L of ¹⁵NH₄Cl for U-¹⁵N samples, supplemented with 3 g/L [¹³C₆] glucose for U-¹⁵N/¹³C labeled samples. Cultures were shaken at 37 °C to an A₆₀₀ of 0.6-0.8, before gene expression was induced with 0.5 mM isopropyl β-D-thiogalactopyranoside at 18 °C. Protein purifications were conducted as previously reported (63).

2.3 Visible absorption spectroscopy

UV-vis absorbance spectra of EL368, EL362 and EL362 (R150G) were collected on a Varian Cary 50 spectrophotometer using a quartz cuvette with 1 cm path length. Dark state samples were kept in the dark until data collection; light state samples were generated via flash

illumination. Dark state recovery time constants were obtained by monitoring the increase in absorbance at 446 nm in 20 min intervals for 10 hr at room temperature. Data points were fitted to a two-phase exponential decay function using the software Prism (GraphPad Software Inc.). All proteins were in 50 mM Tris pH 8.0, 100 mM NaCl, 5 mM DTT solutions.

2.4 Autophosphorylation Assays

EL368 autophosphorylation reactions were performed at room temperature in 50 mM Tris pH 8.0, 100 mM NaCl, 5 mM MgCl₂ and 5 mM DTT. Reactions were initiated by adding mixtures of radiolabeled [γ -³²P]ATP (10 – 50 μ Ci, 6000 Ci/mmol, Perkin Elmer) and cold ATP (0.05 – 2 mM) in buffer with EL368 (5 μ M final concentration) in dark (dim red light) or light (protein sample previously illuminated with photographic flash) conditions. At the appropriate time points, aliquots were removed and quenched into 4x SDS-PAGE sample buffer (50 mM Tris pH 6.8, 200 mM NaCl, 40 mM EDTA, 0.2% bromophenol blue, 10% (v/v) β -mercaptoethanol, 4% (w/w) SDS and 20% (v/v) glycerol. Samples were immediately immersed in liquid N₂ and stored at -80 °C, before SDS-PAGE analysis. After electrophoresis, the dye front and unincorporated ATP were removed with a razor blade. Subsequently, gels were dried under vacuum at 80 °C for 45 min and exposed for 30 to 60 min to a phosphoimager screen that was subsequently scanned with a Fujifilm FLA-5100 phosphoimager. Band intensity measurements were performed with MultiGauge software (Fujifilm). Initial rates of ³²P incorporation were calculated by fitting the first time points to a linear equation; the [ATP]

dependence of these rates were fit to a Michaelis-Menten equation to extract K_m and k_{cat} parameters using Prism. EL362, EL362 (R150G) dark/lit states (5 μ M) were autophosphorylated as mentioned above, but with 500 μ M unlabeled ATP and 50 μ Ci of [γ - 32 P]ATP (6000 Ci/mmol, Perkin Elmer).

2.5 Phosphotransfer profiling

Initially, EL368 or EL346 LOV-HK proteins (10 μ M) were autophosphorylated in 50 mM Tris pH 8.0, 100 mM NaCl, 5 mM MgCl₂, 5 mM DTT, 4.5 μ Ci [γ - 32 P]ATP (6000 Ci/mmol) and 1 mM ATP for 10 min at room temperature under white light conditions. Response regulators were diluted to 10 μ M in the same buffer without nucleotides. Equimolar mixtures of phosphorylated EL368 or EL346 and response regulators (5 μ M each) were made and incubated at room temperature for 30 s and 10 min intervals. Samples were treated and imaged for 32 P incorporation as described above.

2.6 Phosphotransfer kinetic measurements

To obtain the phosphotransfer rate of EL368 to the cognate response regulator EL_PhyR (gene locus ELI_10215), 5 μ M EL368 in nucleotide-free buffer was mixed with 100 μ M EL_PhyR containing 25 μ Ci [γ - 32 P]ATP (6000 Ci/mmol) and 1.5 mM ATP. Aliquots were removed at appropriate time points, and treated as described above with the exception that the band corresponding to the phosphorylated response regulator was measured. Initial rates for the

dark state were obtained with reactions performed under dim red light; lit state EL368 samples were generated by flash illumination prior to the beginning of the reaction and kept under regular white light room illumination. Phosphotransfer of EL362 (5 μ M) was done as previously stated for EL368, but with 500 μ M of ATP, and 5 μ M of the cognate response regulator EL_LovR (gene locus ELI_07655).

2.7 Phosphatase assay

EL_PhyR phosphatase assays were performed at room temperature in 50 mM Tris, 100 mM NaCl, 5 mM DTT, 5 mM MgCl₂ at pH 8.0. 10 μ M of EL368 was pre-incubated for 10 min with an equimolar concentration of EL_PhyR and 30 μ Ci of [γ -³²P]ATP. After pre-incubation 5 mM AMPPNP was added to the reaction to stop further phosphorylation from ATP. For reactions with the EL_LovR (wild type or D56A) proteins, 10 μ M of these proteins were added simultaneously with 5 mM AMPPNP. Aliquots were removed at 0.25, 0.5, 1, 2, 5, 10 and 15 min. Samples were treated as described above. EL_LovR and EL_PhyR (20 μ M) were incubated with EL368 (10 μ M) in 50 mM Tris (pH 7.5), 100 mM NaCl, 5 mM DTT at room temperature. Proteins were incubated for 10 min with 0.5 mM ATP and 25 μ Ci [γ -³²P] ATP (6000 Ci/mmol, PerkinElmer), with 10 μ L aliquots taken at 0.5, 1, 5 and 10 min intervals. Samples were treated as previously described (63). Phosphatase assays were done by incubating 5 μ M EL368 and 20 μ M EL_LovR in 10 mM Tris (pH 7.5), 50 mM NaCl, 10 mM MgCl₂, 1 mM DTT. Proteins were incubated with 500 μ M ATP and 70 μ Ci [γ -³²P] ATP (6000

Ci/mmol, PerkinElmer) for 10 min. After this 10 min incubation, 5 mM AMP-PNP was added to prevent additional phosphorylation and 10 μ L aliquots were collected at 0.25, 0.5, 0.75, 1, 1.5, 2, 3, 6, 10, 15, 20 and 25 min timepoints. Samples were then treated as described in (63).

2.8 Size exclusion chromatography and multiple angle laser light scattering

The oligomerization states of EL368, EL362 and EL_LovR were determined with integrated size exclusion chromatography and light scattering (SEC-MALS). 500 μ L of 20 μ M EL368, EL368(56-368), EL362 and EL362(R150G) dark/lit samples were injected at 0.5 mL/min flow onto Superdex 75 10/300 or Superdex 200 10/300 analytical columns (GE Biosciences), pre-equilibrated with 50 mM Tris pH 8.0, 100 mM NaCl, 5 mM MgCl₂ and 5 mM DTT buffer. Using a 0.5 mL/min flow rate, these samples were detected post-elution using inline miniDAWN TREOS light scattering and Optilab rEX refractive index detectors (Wyatt Technology). All the procedures were performed at 5 °C. Data analyses and molecular weight calculations were carried out using the ASTRA V software (Wyatt Technology). The same approach was also used to study the complex of the EL_PhyR response regulator and its anti- σ factor. 500 μ L samples containing EL_PhyR (30 μ M), anti- σ factor (40 μ M) individually or mixed were applied onto Superdex 75 10/300 in line with MALS pre-equilibrated with the above-mentioned buffer. To study the interaction with the phosphorylated state of response regulator, EL_PhyR by itself or mixed with anti- σ factor was incubated with 0.5 μ M EL368 and 2 mM ATP for 30 min prior to injection.

The oligomerization state of EL_LovR was determined by size exclusion chromatography coupled to inline multiangle light scattering (SEC-MALS). 500 μ L of 20 μ M EL_LovR was injected onto a Superdex 200 10/300 analytical gel filtration column (GE Biosciences) pre-equilibrated with 50 mM Tris (pH 8.0), 100 mM NaCl, 5 mM DTT buffer. In conditions that required magnesium, 10 mM MgCl₂ was added to sample and column buffers. 10 mM carbamoyl phosphate and 10 mM MgCl₂ was incubated with EL_LovR for 10 min to generate the phosphorylated state. Elution volumes were calibrated to apparent molecular weights using the following standards: thyroglobulin (670 kDa), gamma-globulin (158 kDa), ovalbumin (44 kDa), myoglobin (17 kDa) and vitamin B12 (1.4 kDa). Post-chromatography, eluting protein was detected using inline miniDAWN TREOS light scattering and Optilab rEX refractive index detectors (Wyatt Technology). All sample collection was done at 4 °C. Data analyses and molecular weight calculations were carried out using the ASTRA V software (Wyatt Technology).

2.9 NMR solution structure determination and relaxation experiments

Samples used for protein assignment of active EL_LovR contained 500 μ M of ¹⁵N-¹³C labeled protein in 20 mM HEPES (pH 7.5), 3 mM NaN₃, 5 mM BeCl₂, 15 mM NaF, 10 mM MgCl₂ and 10% D₂O. NMR data were collected at 25 °C on Varian Inova 600 and 800 MHz spectrometers and processed using NMRPipe (146) and NMRViewJ (One Moon Scientific) (147). Chemical shift assignments for backbone and sidechains were obtained from 3D HNCACB,

CBCA(CO)NH, HNCO, H(CCO)NH, C(CO)NH and HCCH-TOCSY experiments (148).

Interproton distance restraints were obtained from 3D ^{15}N , ^{13}C simultaneous edited NOESY spectra (149). Hydrogen bond restraints were defined from backbone amide ^2H exchange protection factors (150) obtained from $^{15}\text{N}/^1\text{H}$ HSQC data collected on lyophilized U- ^{15}N EL_LovR protein resuspended in 99.9% D_2O (25 °C, pH 7.5) to identify H-bond donors, while H-bond acceptors were identified from manual NOESY analysis. ϕ and ψ angle restraints were obtained from chemical shift analyses using TALOS-N (151). Mg^{2+} and BeF_3^- ions were not explicitly included in the structure calculations, although both were present in the samples used for structural restraint measurements. Structures were calculated with automated NOESY spectra assignment using ARIA 2.2 (152).

2.10 Limited proteolysis and Mass Spectrometry analysis

Limited proteolysis was carried out by mixing EL_LovR (390 μM = 5 mg/mL) with trypsin (w/w 1 trypsin: 90 EL_LovR) in 50 mM Tris (pH 7.5), 100 mM NaCl, 5 mM DTT. For experiments requiring Mg^{2+} and BeF_3^- , 10 mM of MgCl_2 and 5 mM/15 mM of BeCl_2/NaF were added, respectively. After mixing EL_LovR and trypsin, 10 μL aliquots were taken at 1, 3, 6, 10 and 15 min timepoints and stopped with 4 \times SDS-PAGE sample buffer (50 mM Tris (pH 6.8), 200 mM NaCl, 40 mM EDTA, 0.2% bromophenol blue, 10% (v/v) β -mercaptoethanol, 4% (w/w) SDS, and 20% (v/v) glycerol) for gel electrophoresis analysis. For mass spectrometry analysis, EL_LovR was digested for 3 min and the reaction was stopped with 4 mM phenylmethylsulfonyl

fluoride (PMSF). Molecular masses of resulting fragments were obtained by LC-MS with Agilent 6540 Q-TOF instrument (UT Southwestern Proteomics Core Facility).

2.11 Titration with $MgCl_2$ and BeF_3^-

A 2 M stock solution of $MgCl_2$ was prepared and titrated into 500 μ M U- ^{15}N labeled EL_LovR in 10 mM Tris (pH 7.5), 50 mM NaCl, 1 mM DTT, 10% D_2O , at 25 °C. $^{15}N/^1H$ HSQC spectra were collected with 0-10 mM $MgCl_2$ present, processed as described above, and analyzed for peak intensity changes using NMRViewJ software (147) titration analysis. For BeF_3^- titration stock solutions of $BeCl_2$ and NaF were prepared at 1 M and 0.5 M respectively. $BeCl_2$ (ranging from 0-20 mM) was titrated to 500 μ M protein in buffer containing 10 mM Tris pH 7.5, 50 mM NaCl, 1 mM DTT, 10% D_2O and 50 mM NaF. NaF (ranging from 0-50 mM) was titrated to 500 μ M protein in buffer containing 10 mM Tris pH 7.5, 50 mM NaCl, 1 mM DTT, 10% D_2O and 1 mM $BeCl_2$. Data collection, processing and analysis were as described above.

2.12 β -galactosidase assays

To test for the ability of EL368, EL_PhyR and EL_LovR to regulate SigT activity, *C. crescentus* strains bearing the transcriptional reporter plasmid pRKlac290 were inoculated on fresh peptone-yeast extract plates (PYE) containing selection marker as described in Foreman *et. al.* (132). Freshly grown cultures (~5 mL) were inoculated on ~7 mL of M2X medium

containing 1 $\mu\text{g}/\text{mL}$ oxy-tetracycline, 0.5 % of xylose and 0.5 mM of vanillate. To assay for SigT activity, overnight cultures were diluted to an OD_{660} of 0.025 with ~ 7 mL of fresh M2X medium and allow to outgrow for 16 h at 30 $^{\circ}\text{C}$ to ensure uniformity. Subsequently cultures were diluted to OD_{660} of 0.1 with ~ 12 mL fresh M2X medium split into 2 mL cultures and allowed to outgrow for 1 h at 30 $^{\circ}\text{C}$. Half of the culture was subjected to osmotic stress by adding 150 mM final concentration of sucrose and an equal volume of water (unstressed) to the control tube. Cultures were grown for 4 h at 30 $^{\circ}\text{C}$ and shaking before measuring the β -galactosidase activity. 600 μL of Z-buffer (60 mM Na_2HPO_4 , 40 mM NaH_2PO_4 , 10 mM KCl, 1 mM MgSO_4) and 200 μL of *o*-nitrophenyl- β -D-galactopyranoside were added to 200 μL of chloroform-permeabilized cells. Upon development of medium yellow color, the reaction was stopped by addition of 1 mL of 1 M sodium carbonate (NaCO_3) and absorbance was measured at 420 nm on a Varian Cary 50 spectrophotometer. Miller units were calculated using the following equation:

$$\text{Miller units} = \frac{(A_{420} \times 1,000)}{A_{660} \times t \times v}$$

where t is reaction time in minutes and v is volume of cells used in mL.

Table 2.1 *C. crescentus* and *E. coli* strains used in this study

	Genotype	Reference
<i>C. crescentus</i>		
FC642	CB15/pRKlac290-P _{sigU}	(132)
FC1628	CB15 <i>vanR</i> ::pMT528 <i>xyiX</i> ::pMT585/pRKlac290-P _{sigU}	(132)
FC1708	CB15 Δ <i>lovKR vanR</i> ::pMT528 <i>xyiX</i> ::pMT585/pRKlac290-P _{sigU}	(132)
FC1711	CB15 Δ <i>lovKR vanR</i> ::pMT528- <i>lovK xyiX</i> ::pMT585- <i>lovR</i> /pRKlac290-P _{sigU}	(132)
VO06	CB15 Δ <i>lovKR vanR</i> ::pMT528- <i>el368 xyiX</i> ::pMT585- <i>el_lovR</i> /pRKlac290-P _{sigU}	This study
FC1190	CB15 Δ <i>lovKR</i> /pRKlac290-P _{sigU}	(132)
FC814	CB15 Δ <i>phyR</i> /pRKlac290-P _{sigU}	(132)
VO20	CB15 Δ <i>phyR \Delta</i> <i>lovKR xyiX</i> ::pMT585-6x-His- <i>el_phyR</i> /pRKlac290-P _{sigU}	This study
VO21	CB15 Δ <i>phyR \Delta</i> <i>lovKR xyiX</i> ::pMT585- <i>el_phyR</i> /pRKlac290-P _{sigU}	This study
VO22	CB15 Δ <i>phyR xyiX</i> ::pMT585-6x-His- <i>el_phyR</i> /pRKlac290-P _{sigU}	This study
VO23	CB15 Δ <i>phyR xyiX</i> ::pMT585- <i>el_phyR</i> /pRKlac290-P _{sigU}	This study
VO26	CB15 Δ <i>phyR \Delta</i> <i>lovKR vanR</i> ::pMT528-6x-His- <i>el368 vanR</i> ::pMT674-6x-His- <i>el_phyR xyiX</i> ::pMT585-6x-His- <i>el_lovR</i> /pRKlac290-P _{sigU}	This study
FC1631	CB15 <i>vanR</i> ::pMT528- <i>lovK xyiX</i> ::pMT585- <i>lovR</i> /pRKlac290-P _{sigU}	(132)
FC1681	CB15 Δ <i>phyR \Delta</i> <i>lovKR</i> /pRKlac290-P _{sigU}	(132)
VO27	CB15 Δ <i>phyR \Delta</i> <i>lovKR vanR</i> ::pMT674-6x-His- <i>el_phyR</i> /pRKlac290-P _{sigU}	This study
VO29	CB15 Δ <i>phyR \Delta</i> <i>lovKR vanR</i> ::pMT528-6x-His- <i>el368 vanR</i> ::pMT674-6x-His- <i>el_phyR</i>	

vanR::pMT644-6x-His-el_lovR/pRKlac290-P_{sigU}

This study

E. coli

FC338	TOP10/pMT528 (pVCHYC-1)	(153)
FC339	TOP10/pMT585 (pXGFPC-2)	(153)
MTLS4340	TOP10/pMT644 (pVGFPC-4)	(153)
MTLS4396	TOP10/pMT674 (pVGFPC-6)	(153)

Chapter 3 Enzymatic analysis of LOV-HK in *Erythrobacter litoralis* HTCC2594

(Published as: Blue Light Regulated Two-Component Systems: Enzymatic and Functional Analyses of Light-Oxygen-Voltage (LOV)-Histidine Kinases and Downstream Response Regulators)

Fernando Corrêa[†], Wen-Huang Ko[†], Victor Ocasio[†], Roberto A. Bogomolni and Kevin H. Gardner

Biochemistry, **2013**, 52: 4656-4666

([†]: F.C, W.-H.K., V.O. contributed equally to this manuscript)

Abstract

Light is an essential environmental cue for diverse organisms. Many prokaryotic blue light photoreceptors use Light, Oxygen, Voltage (LOV) sensory domains to control the activities of diverse output domains, including histidine kinases (HK). Upon activation, these proteins autophosphorylate a histidine residue before subsequently transferring the phosphate to an aspartate residue in the receiver domain of a cognate response regulator (RR). Such phosphorylation, activates the output domain of the RR, leading to changes in gene expression, protein-protein interactions or enzymatic activities. Here we focus on one such light sensing LOV-HK from the marine bacterium *Erythrobacter litoralis* HTCC2594 (EL368), seeking to

understand how kinase activity and subsequent downstream effects are regulated by light. We found that photoactivation of EL368 led to a significant enhancement in the incorporation of phosphate within the HK domain. Further enzymatic studies showed that the LOV domain affected both the LOV-HK turnover rate (k_{cat}) and K_m in a light-dependent manner. Using *in vitro* phosphotransfer profiling, we identified two target RRs for EL368 and two additional LOV-HKs (EL346 and EL362) encoded within the host genome. The two RRs include a PhyR-type transcriptional regulator (EL_PhyR) and a receiver-only protein (EL_LovR), reminiscent of stress-triggered systems in other bacteria. Taken together, our data provide a biochemical foundation for this light-regulated signaling module of sensors, effectors and regulators that control bacterial responses to environmental conditions.

3.1 Introduction

Organisms have developed stimulus-response coupled mechanisms to sense and to adapt to the myriad of physical and chemical changes in their surroundings. A common example of such signaling in prokaryotes is provided by phosphorelay systems based on two types of proteins: a sensory histidine kinase (HK) and a downstream response regulator (RR); activation of the former leads to RR phosphorylation that induces cellular responses via changes in downstream gene expression or interactions within a signaling pathway (23,154). Light is one of the prevalent stimuli sensed by bacteria, because of its dual and opposing roles as vital source of energy and as a potentially damaging factor to intracellular components. As such, a diverse

set of photosensory proteins has evolved to allow these organisms to detect and cope with light throughout the UV and visible spectrum.

A prevalent type of blue light photosensor is provided by the Light-Oxygen-Voltage (LOV) domains (155,156), a subset of the broader family of Per-ARNT-Sim (PAS) group of environmental sensors (157). These proteins non-covalently bind FMN or FAD in the dark; upon blue light exposure, a covalent adduct is formed between the flavin isoalloxazine C4a position and a nearby cysteine residue. This bond is stable under illumination, but spontaneously breaks in the dark with a timescale of seconds to hours (52,158). Notably, formation of this bond triggers conformational changes at the central β -sheet of the protein that are propagated to a wide array of downstream domains (60,159,160), including HKs, HTH DNA-binding domains, phosphodiesterases, sigma factor regulators (STAS) domains (46,155). In LOV-containing HKs (LOV-HKs), light exposure typically leads to an enhancement in the overall kinase activity of the protein (36,53,161), implicating an important role of these proteins in sensing and responding to light stimulus. While this has been validated for several LOV-HKs (36,46,53,132,155,162-165), the mechanisms that allow LOV domains to control HK activity remain an active topic of investigation. Such information would benefit both basic knowledge of signal transduction in an essential class of sensory proteins while also facilitating the development of optogenetic tools to control complex signaling pathways.

To this end, we used a series of biochemical tools to characterize the enzymatic mechanisms and signaling pathways of the three predicted LOV-HK proteins from the marine bacterium *Erythrobacter litoralis* HTCC2594 (53): EL368, EL346 and EL362. Both EL368 and EL346

undergo light-dependent activation of autophosphorylation kinase activity; in contrast, EL362 contains a point mutation within the critical LOV domain, rendering it insensitive to light. Mechanistically, steady state enzymatic analysis of EL368 showed that the observed photoactivation stems from changes in both k_{cat} and K_{m} parameters upon illumination. *In vitro* phosphotransfer profiling of EL368 and the two other *E. litoralis* LOV-HKs (EL346 and EL362) reveal two downstream targets: a PhyR-type anti-, anti-sigma RR and a single domain RR. Examination of their biochemical properties and comparison with the genetically-identified *Caulobacter crescentus* LovK/LovR stress signaling system (132) suggests that these substrates are homologs of the *C. crescentus* PhyR and LovR proteins, leading us to designate them as EL_PhyR and EL_LovR, respectively. Intriguingly, all three LOV-HKs phosphorylate EL_LovR while EL_PhyR is targeted more specifically by only EL368 and EL346. This type of signaling network is reminiscent of general stress responses in several α -proteobacteria (166,167), particularly via parallels with the *Caulobacter crescentus* pathway where PhyR regulates an operon containing an EL368-homolog and its cognate RR (132). Altogether, our findings suggest that LOV-HKs may participate in conserved branched transduction pathways in bacteria essential to biological responses to stress.

3.2 Results

3.2.1 Characterization of light-dependent enzymatic activity

In addition to a conventional HWE-type HK domain (74), EL368 contains an N-terminal

LOV domain, conferring kinase activation upon blue light exposure (53). Measurements of the autophosphorylation activity of EL368 using $[\gamma\text{-}^{32}\text{P}]\text{ATP}$ as substrate in the dark and light show that the protein is approximately four times more active in the lit state ($v: 0.007\pm 0.001\text{ s}^{-1}$) than in the dark ($v: 0.002\pm 0.001\text{ s}^{-1}$) (Figure 3.1 a,b). Changes in kinase activity upon light illumination have also been reported for other natural LOV-HKs (36,53,161) along with an engineered variant of FixL (84), clearly indicating that light-induced conformational changes in the LOV domain can allosterically affect the overall activity of the HK domain. However, the underlying mechanisms of such regulation remain unclear. In a very simplistic enzymatic model, the sensor domain could influence overall enzyme activity through changes in the affinity for various substrates (K_m), V_{\max} or a combination of both. To address which of these enzymatic parameters are affected by illumination, we determined the net kinase activity of EL368 at varying concentrations of ATP. Figure 3.1b shows that the autophosphorylation reaction catalyzed by the enzyme supports a classical Michaelis-Menten kinetics mechanism in both conformational states. Upon activation the enzyme presents a four times overall increase in its catalytic rate ($V_{\max}(\text{dark}): 0.002\pm 0.0001\text{ s}^{-1}$, $V_{\max}(\text{lit}): 0.009\pm 0.0005\text{ s}^{-1}$). On the other hand, there is a slight, but measurable decrease of affinity for ATP in the lit state ($385\pm 52\text{ }\mu\text{M}$) in comparison to the dark state ($131\pm 31\text{ }\mu\text{M}$). Similar ATP affinities have been reported for other HKs (168-171).

One practical issue for measurements of dark state kinase activity is the very slow photorecovery to the dark state observed for this enzyme ($\sim 2\text{ hr}$, Figure 3.2), which would lead to the accumulation of lit state conformers upon incidental exposure to light. While we took

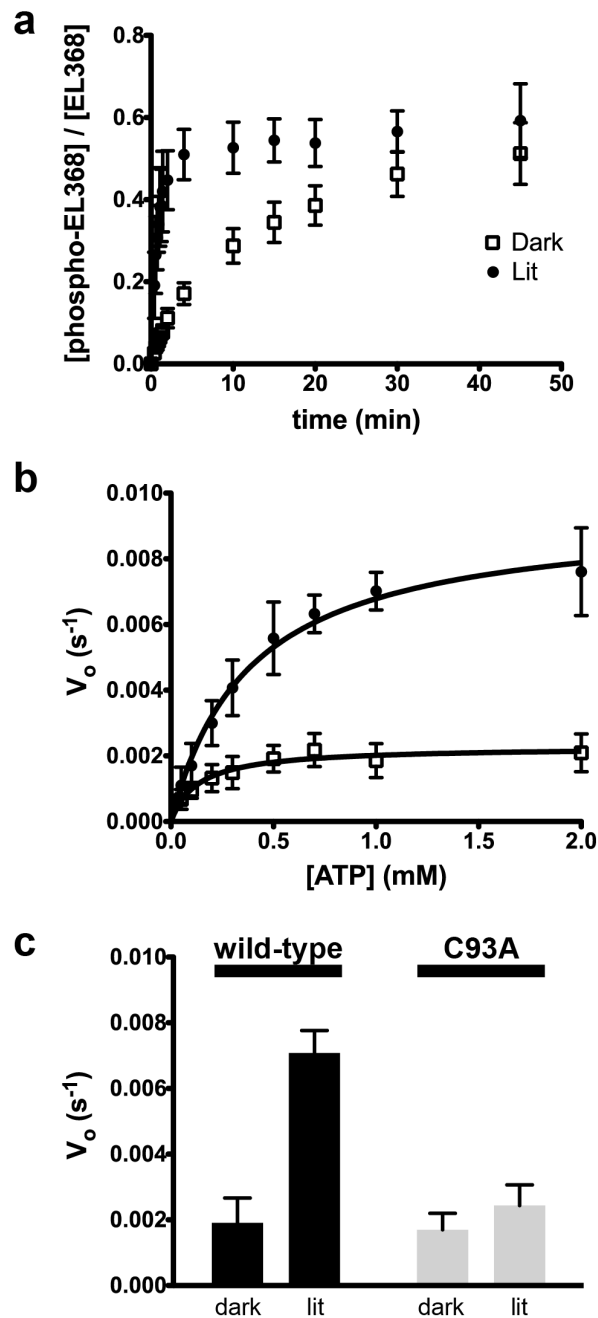


Figure 3.1 Light enhances the phosphorylation activity of EL368.

(a) Time course of phosphate incorporation into EL368 either in dark or white light conditions. Upon light exposure, the enzyme has a higher kinase activity and achieves steady state equilibrium more quickly than the dark state. (b) Initial velocities obtained at different ATP concentrations were fit to a Michaelis–Menten equation (black line). (c) EL368 (C93A) demonstrates that kinase activity observed in the dark state does not arise from residual cysteinyl-flavin adduct formation.

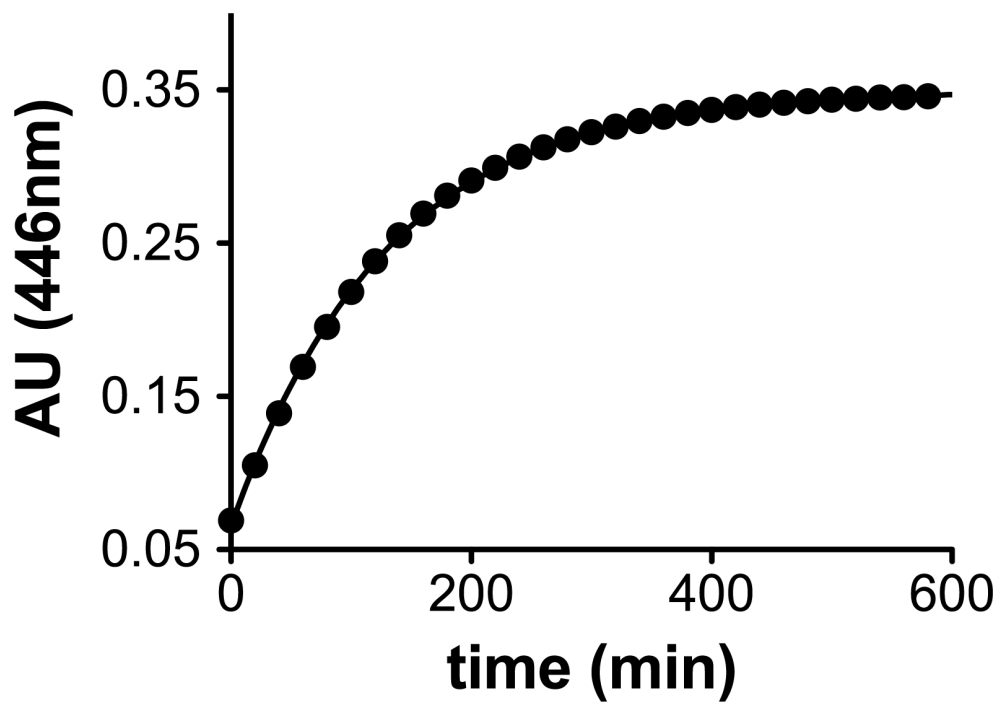


Figure 3.2 EL368 undergoes a reversible photocycle.

The increase in absorbance at 446 nm was monitored every 1200 s for a total of 36000 s; data were subsequently fit to a one phase exponential curve (line).

reasonable steps to avoid such exposure, such artifacts could lead to aberrantly high background levels of activity in such phosphorylation assays. To rule this out, we engineered a mutant version (C93A) that binds to flavin but cannot form the cysteinyl adduct. As expected, the mutant displayed a dark state activity (v : $0.002 \pm 0.0005 \text{ s}^{-1}$) comparable to wild type (v : $0.002 \pm 0.001 \text{ s}^{-1}$), and only minimally affected by light (v : $0.002 \pm 0.001 \text{ s}^{-1}$) at 1 mM ATP (Figure 1c). Low levels of dark state phosphorylation have also been reported in other LOV-HK systems (36,53,161).

3.2.2 LOV domain stabilizes dimeric conformation

Most HKs studied to date function as dimers, with *cis* or *trans*-autophosphorylation between subunits of the oligomer (75,168,172,173). To examine whether EL368 also operates as a dimer, we took advantage of the long-lived lit state (~2 hr) used SEC-MALS to examine the solution oligomerization state of the protein in the dark and light. Results demonstrated that EL368 is primarily a very stable and light-independent dimer in solution (Figure 3.3). In addition, the minor changes in the elution profile between light and dark conditions suggests that there are no drastic changes in the shape of the enzyme upon activation, in agreement with data reported for the *C. crescentus* homolog LovK (174).

Secondary structure predictions of EL368 by Jpred (175) indicates that the N-terminal LOV domain is preceded by an additional 56 residue-long region (Figure 3.4). Previous studies of other LOV domains have demonstrated that such additional regions can affect photocycle

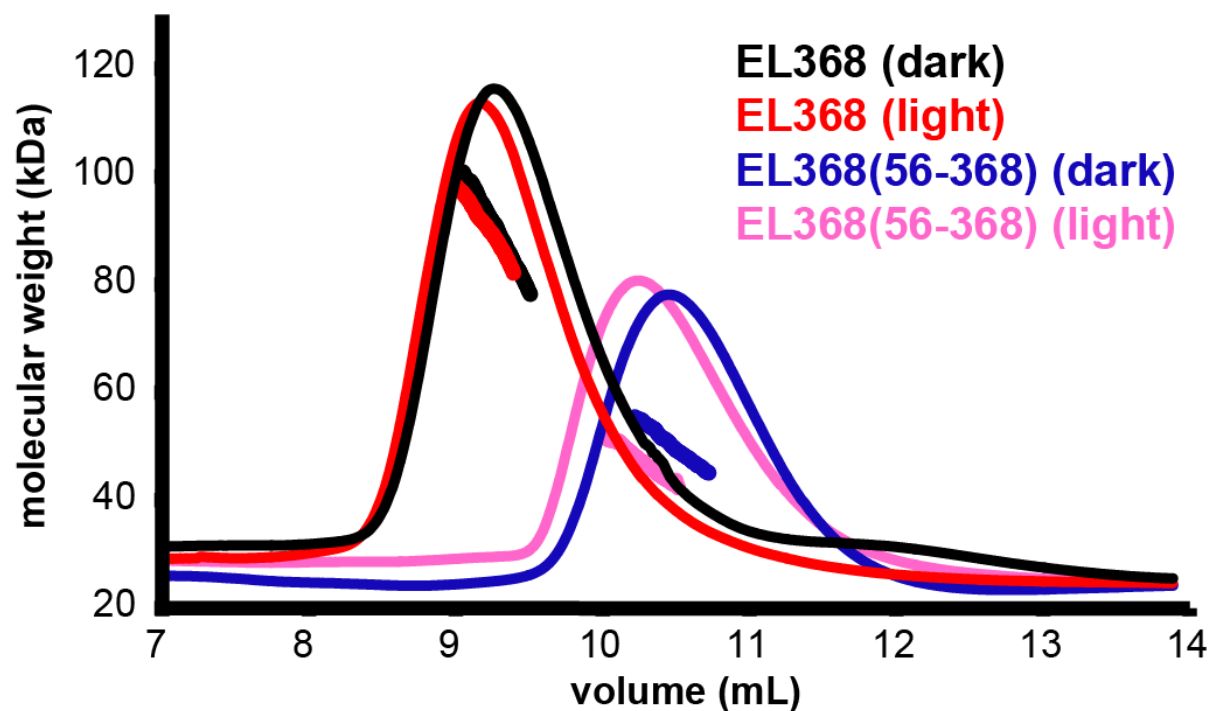


Figure 3.3 Dimeric solution structure of EL368 is stabilized by elements located N-terminal of the LOV domain.

SEC-MALS traces correspond to full-length EL368 (black, dark state; red, light) and EL368(56-368) (blue, dark; magenta, light); dRI traces from the Optilab rEX are shown as solid lines, plotted on the same relative scale, while MALS-derived mass distributions are plotted as individual points. Full-length EL368 is dimeric regardless of illumination, as SEC elution profiles and mass distributions are unaffected by light (apparent MW~90 kDa at the center of the peak, compared to the monomer MW of 41.1 kDa). Removal of 55 residues prior to the predicted LOV domain generates EL368(56-368) and destabilizes the dimer (apparent MW ~50kDa at the center of the peak, compared to the monomer MW of 35.2 kDa).

lifetime and oligomerization state (174,177), leading us to examine their influence in EL368. To do so, we constructed a truncated form of the protein, EL368 (56-368). While removal of that segment did not affect the binding to flavin or solubility of the molecule, SEC-MALS showed that this deletion affected the protein oligomerization state by biasing it towards lower molecular weight (Figure 3.3). The molecular weight distributions obtained for dark and lit samples suggest that protein eluted as a mixture of monomers and dimers, with minimal light-dependent effects.

3.2.3 Light regulated two-component signaling: Identification of target response regulators and influence of light stimulus on phosphotransfer

Two component systems are often composed of HKs and RRs found in operons, where they usually form an exclusive phosphotransfer pair. Nevertheless, HKs can be found as “orphans” without candidate RRs nearby in the genome, complicating identification of cognate pairs from sequence alone (101,178). Analysis of the *E. litoralis* genome (135) shows that EL368 is encoded as an orphan HK, with the nearest predicted RR over 80 kb away. To further characterize the influence of light stimulation at the phosphotransfer step and suggest a functional role for EL368, we proceeded to identify RR substrates using phosphotransfer profiling. This technique, based on comparisons of the ability of HKs to phosphorylate candidate RRs, takes advantage of the *in vitro* kinetic preference HKs exhibit for their *in vivo* cognate RR (179).

The *E. litoralis* genome is predicted to encode 23 RRs (124) (Table 3.1), 21 of which we successfully expressed in *E. coli*. 12 of these proteins expressed as full-length constructs; the other 9 were expressed as isolated receiver domains. This approach, which considerably increased the total yield of soluble protein compared to the full-length forms, takes in consideration the fact that receiver domain defines the complex specificity and phosphotransfer catalysis (179). We were unable to obtain sufficient quantities of two proteins for further analysis, as they either went into inclusion bodies (ELI_11255) or failed to express (ELI_11920). With these reagents in hand, *in vitro* profiling of EL368 in a very short timescale (30 s) shows that the enzyme efficiently phosphorylated EL_LovR and EL_PhyR (Figure 3.5a). Extension of the reaction to 10 min allowed the protein to phosphorylate 4 additional response regulators at lower levels, although these may reflect non-specific crosstalk given the prolonged incubation time (179) (Figure 3.5b).

In addition to EL368, *E. litoralis* also contains two other LOV-HKs: EL346 (53) and EL362 (*vide infra*). The former one is also predicted to be an orphan HK, therefore we performed the same biochemical-mapping scheme. Interestingly, EL346 demonstrated a kinetic preference for the same two RRs initially recognized by EL368 (Figure 3.6a; summarized in Figure 3.5c). Nevertheless, in a longer reaction time point, it phosphorylated only one additional substrate (ELI_09195) (Figure 3.6b). EL362 exhibited a different specificity and several other unique properties, discussed below.

To address whether a light stimulus would affect phosphotransfer as well as autophosphorylation, we conducted kinase assays in the dark and light with mixtures of EL368

Locus Tag	Domain Disposition	Tested as
ELI_07655	1—Receiver—121	Full-length
ELI_04825	1—Receiver—170	Full-length
ELI_14085	1—Receiver—122	Full-length
ELI_07690	1—Receiver—130	Full-length
ELI_09195	1—Receiver—119	Full-length
ELI_11255*	1—Receiver—121	-----
ELI_10215	1—Anti-anti- σ (PhyR)—Receiver—266	Full-length
ELI_02135	1—Receiver—DNA binding (OmpR)—251	Full-length
ELI_02515	1—Receiver—DNA binding (OmpR)—231	Full-length
ELI_03645	1—Receiver—DNA binding (OmpR)—225	Full-length
ELI_05400	1—Receiver—DNA binding (OmpR)—229	Full-length
ELI_11920**	1—Receiver—DNA binding (OmpR)—248	-----
ELI_14230	1—Receiver—DNA binding (OmpR)—231	Fragment (1-123)
ELI_09055	1—Receiver—DNA binding (LuxR)—219	Fragment (1-157)
ELI_09265	1—Receiver—DNA binding (LuxR)—198	Fragment (1-115)
ELI_02325	1—Receiver— σ^{54} interaction domain—HTH—472	Fragment (1-142)
ELI_05325	1—Receiver— σ^{54} interaction domain—HTH—454	Fragment (1-141)
ELI_06265	1—Receiver— σ^{54} interaction domain—HTH—458	Fragment (1-139)
ELI_06275	1—Receiver— σ^{54} interaction domain—HTH—470	Fragment (1-127)
ELI_12660	1—Receiver—DNA binding (LytR)—265	Fragment (1-141)
ELI_12895	1—Receiver—DNA binding (LytR)—246	Full-length
ELI_11250	1—Receiver—Methylesterase (CheB)—342	Fragment (1-132)
ELI_01510	1—Receiver— <i>No predicted function</i> —419	Full-length

Table 3.1 Predicted response regulators in *Erythrobacter litoralis* HTCC2594 as described (124) (http://www.ncbi.nlm.nih.gov/Complete_Genomes/RRcensus.html). Locus tags are provided from NCBI Gene.

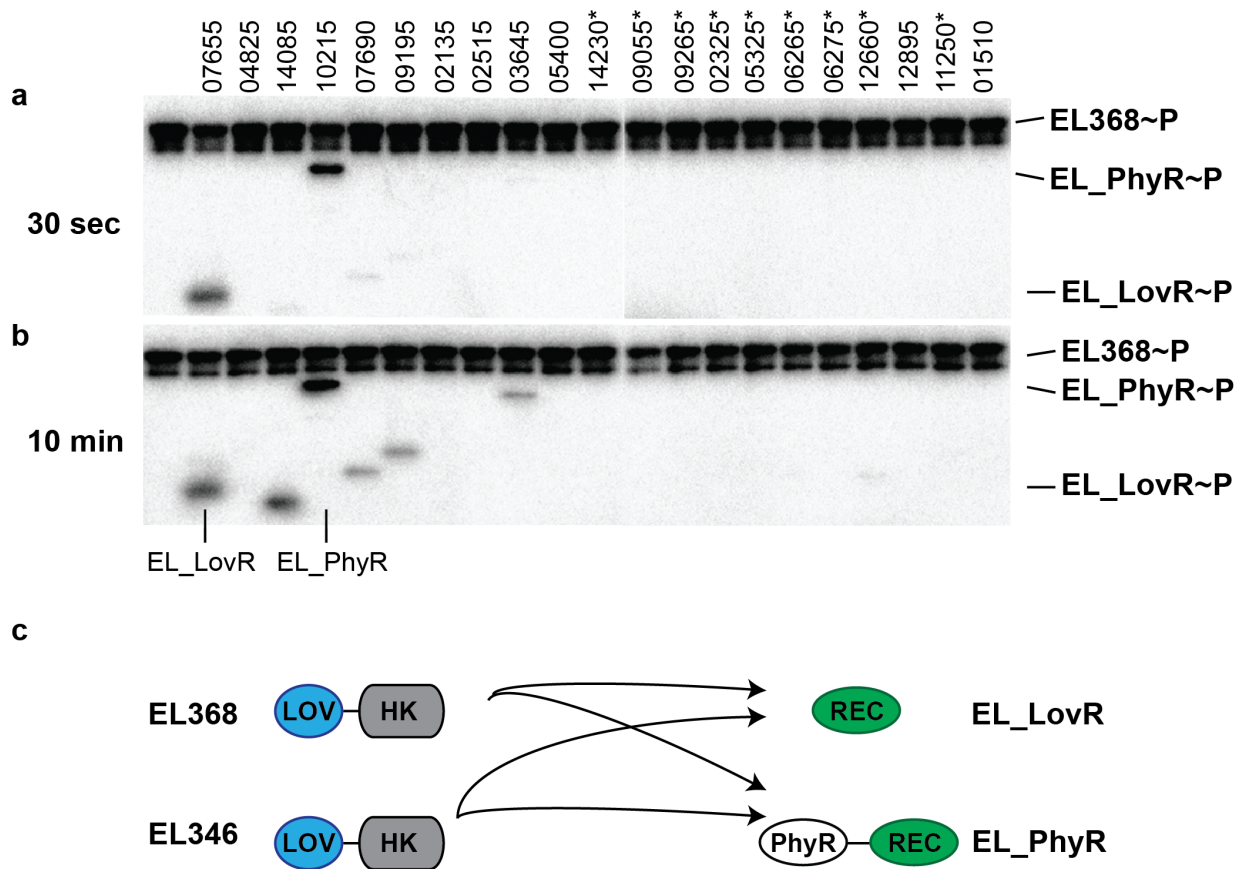


Figure 3.5 Phosphotransfer profiling of EL368.

HK was profiled against 21 RR of *E. litoralis* with phosphotransfer reaction times of 30 s (a) and 10 min (b). In the longer time reaction, several RRs are phosphorylated by the enzyme; however, in a much shorter time point only two kinetically preferred protein substrates (EL_PhyR and EL_LovR) are phosphorylated. Asterisks (*) indicate RR fragments containing only the receiver domain as described in Table 3.1. For optimum resolution, this SDS-PAGE gel was run longer than the comparable gels shown in Figures 4 and 6; EL368 appears as a doublet here as a result. (c) Schematic summary of phosphorylation patterns among the EL368 and EL346 LOV-HK proteins and their RR substrates.

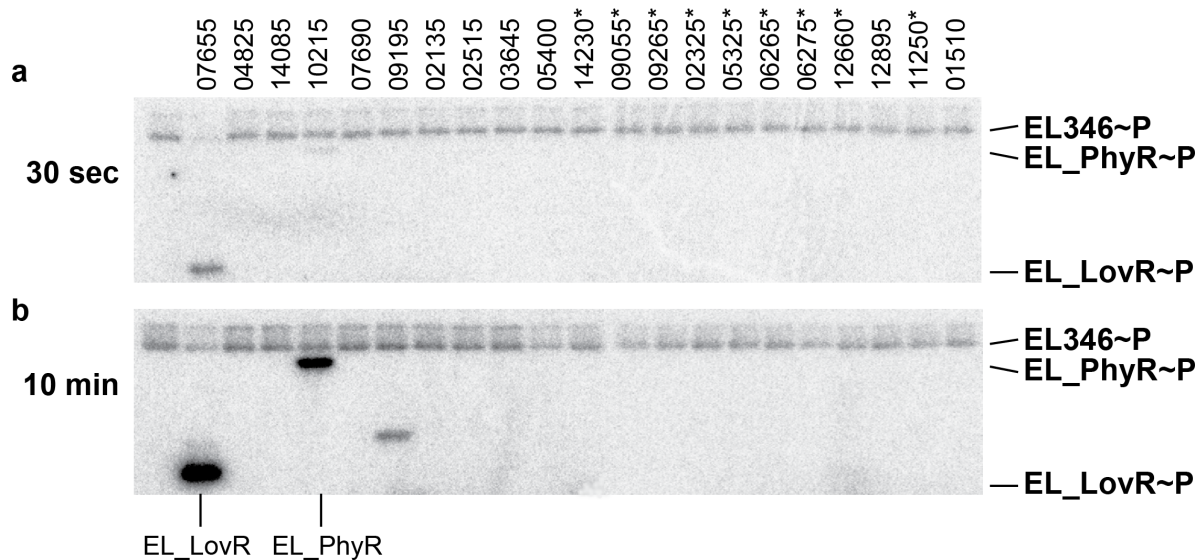


Figure 3.6 Phosphotransfer profiling of the EL346 HK.

HK was profiled against twenty-one *E. litoralis* RR proteins with phosphotransfer reaction times of 30 s (a) and 10 min (b). In the short incubation, EL346 preferentially phosphorylates only two protein substrates: ELI_07655 (EL_LovR) and ELI_10215 (EL_PhyR); at longer times, an additional substrate (ELI_09195) becomes phosphorylated, although this may reflect non-specific crosstalk given the extended duration of the incubation (101). Reaction conditions were the same as used for EL368 (5 μ M EL346, 5 μ M RRs in 50 mM Tris pH 8.0, 100 mM NaCl, 5 mM MgCl₂, 5 mM DTT, 1 mM ATP, 4.5 μ Ci [γ -³²P] ATP at room temperature. *: substrates used were REC-only truncations as described in Table 3.1.

and its substrates (1:20 ratio). These experiments utilized EL_PhyR as a substrate, as EL_LovR exhibited substantial phosphatase activity (*vide infra*). Following the same trends observed for the autophosphorylation, the amount of phosphorylated RR in the light was higher than in the dark state (v (dark): $0.001 \pm 7 \times 10^{-5}$ mol RR (mol kinase) $^{-1}$ s $^{-1}$, v (lit): $0.0080 \pm 3 \times 10^{-4}$ mol RR (mol kinase) $^{-1}$ s $^{-1}$), suggesting that the control exerted by photoactivation primarily affects the levels of phosphorylated HKs that in turn lead to an increase in the population of phosphorylated RRs (Figure 3.7).

3.2.4 EL368 controls a transduction cascade involving an sigma/anti-sigma interaction system

To initially suggest potential functions of the two LOV-HK substrates, we used a bioinformatics approach with Hidden Markov Model domain identification implemented by Pfam (180). This revealed that EL_PhyR combines a C-terminal REC domain with a N-terminal sigma (σ) factor like domain, analogous to the PhyR response regulator. PhyR itself is found in an operon with genes for σ and anti- σ factors and a very conserved upstream promoter consensus sequence with -35 (GGAACC) and -10 (CGTT) elements (166,167,181-183). Under stress conditions, PhyR is activated and binds to the anti- σ factor, increasing the number of free σ subunits that may bind to DNA leading to the transcription of target genes (166). Notably, the chromosomal region of EL_PhyR shows that it has a similar arrangement as the PhyR regulon (Figure 3.8a), reinforcing the analogy between these proteins.

To test the hypothesis that EL_PhyR may serve as a PhyR homolog, we examined a critical

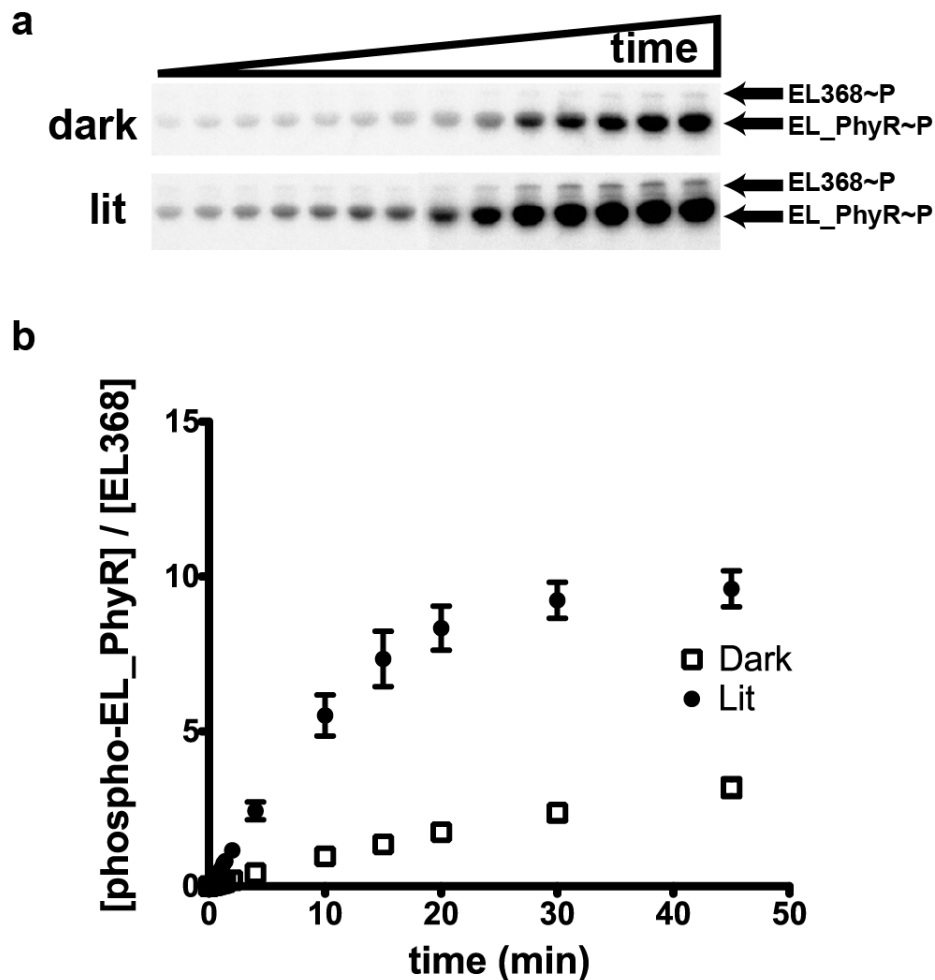


Figure 3.7 Influence of light on the EL368 phosphorylation of the EL_PhyR substrate.

(a) Time course of EL_PhyR by EL368 under dark and light conditions. (b) Quantitation of phosphorylation levels observed in panel a. As observed in the autophosphorylation reaction, light stimulates the phosphorylation activity of the enzyme. The linear phase of the curves (up to 55 s) was used to calculate the initial rates of phosphotransfer.

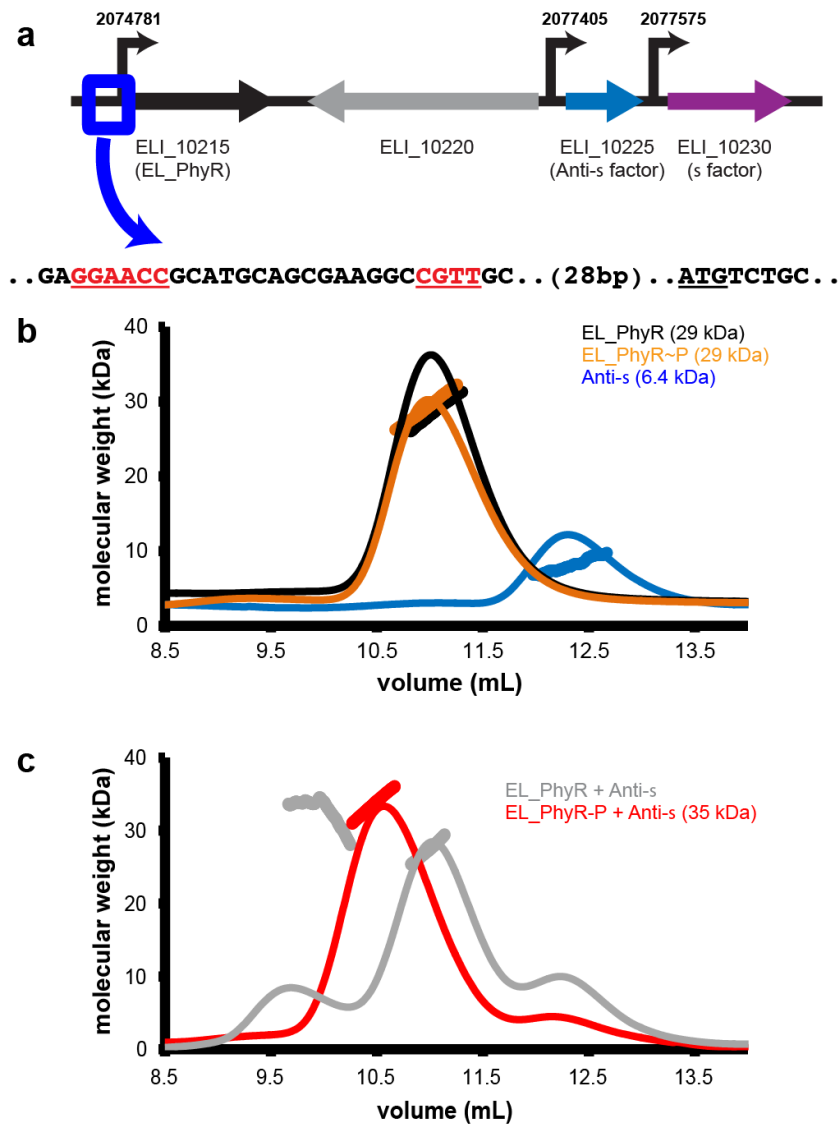


Figure 3.8 EL_PhyR binds to an anti- σ factor upon activation.

(a) Top: Representation of the chromosomal region of EL_PhyR gene. Arrows indicate open reading frames for response regulator EL_PhyR (phyR-like) and anti- σ and σ factors. The coordinates to the initiation codon of each gene are indicated by curved arrows. Bottom: DNA sequence of the 5' region of the EL_PhyR gene, the putative promoter sequence (red), and the initial residues of the protein. (b) SEC-MALS results of the isolated versions of the inactive and active forms of EL_PhyR and the anti- σ factor. (c) SEC-MALS data of combinations of inactive EL_PhyR and anti- σ compared with a mix of the activated EL_PhyR/anti- σ . Changes in the elution volumes and MW distributions of mixtures of EL_PhyR and anti- σ factor show the binding of the two proteins when the response regulator is phosphorylated. Phosphorylated state of the response regulator was generated by adding it to EL368 and ATP and incubating by 30 min at room temperature before injecting in a Superdex 75 10/300GL column. dRI and MW data are shown as described in Figure 3.2.

function: binding of phospho-EL_PhyR to the predicted anti- σ (NepR) by using SEC-MALS experiments with mixtures of both proteins. To generate active RR, we added very small amounts of EL368 (0.5 μ M) and ATP (1 mM) prior injection onto the system. Phosphorylation did not trigger any drastic change in oligomerization state or shape of NepR, which remains monomeric (Figure 3.8b); the anti- σ was also monomeric in solution. When both proteins were incubated together, we observed an interaction between the two only when the RR was activated, as demonstrated by a shift in elution volume to 10.6 mL and increase in molecular weight corresponding to formation of a 1:1 heterodimer of EL_PhyR (MW \sim 28 kDa) and NepR (MW \sim 6.4 kDa). We note that a minor population of the inactive RR is also capable of forming some complex with the anti- σ (grey line, 9.8 mL), but differences in both the efficiency of forming this complex and its SEC elution volume suggest that this minor complex substantially differs from the dimer formed by activated protein.

The second substrate, EL_LovR, is annotated by Pfam analysis (180) as a single domain response regulator containing only a REC domain (SDRR). These molecules serve several roles in signaling pathways, from forming protein complexes with downstream elements to serving as phosphate sinks that modulate pathway activity (86,124). The combination of EL_LovR and the PhyR homolog EL_PhyR is reminiscent of an analogous stress response system identified in *C. crescentus* (132). In this system, the SDRR is proposed to act as a phosphate dump based solely on genetic approaches; to provide a biochemical validation for this model and demonstrate its function, we assayed the effects of EL_LovR on the stability of the EL_PhyR~P complex. To do so, we preincubated EL368, [γ - 32 P]ATP and the EL_PhyR

substrate under illumination, efficiently generating the EL_PhyR~P complex, before stopping further kinase activity by adding an excess of non-hydrolyzable AMPPNP. Aliquots taken from this reaction afterwards shows that the EL_PhyR~P complex is normally stable over the 15 min duration of the assay (Figure 3.9a). However, when the SDRR is added simultaneously with AMPPNP, we instead see a rapid decrease in EL_PhyR~P accompanied by a transient accumulation of EL_LovR~P (Figure 3.9b), followed by its rapid dephosphorylation. These data are consistent with EL_LovR serving as a phosphate sink that can rapidly deactivate the EL_PhyR by promoting phosphate turnover. This activity requires the phosphoaccepting D56 residue within the SDRR; mutation to alanine greatly slows these effects while dramatically lowers phosphorylation levels (with low residual phosphorylation likely occurring on nearby residues (184)) (Figure 3.9c). Taken together our data suggests that the HK-PhyR-SDRR signaling module reported by genetics in *C. crescentus* can be reconstituted *in vitro* with these *E. litoralis* proteins.

3.2.5 EL_LovR forms a two-component system with a “blind” LOV histidine kinase:

Non-flavin binding protein has impaired kinase activity

Analysis of chromosomal region near EL_LovR revealed another LOV-HK, (ELI_07650, named here as EL362) located 18 bp upstream of the RR, suggesting that they might both be located in a shared operon. Phosphotransfer assays confirmed that the enzyme could indeed use

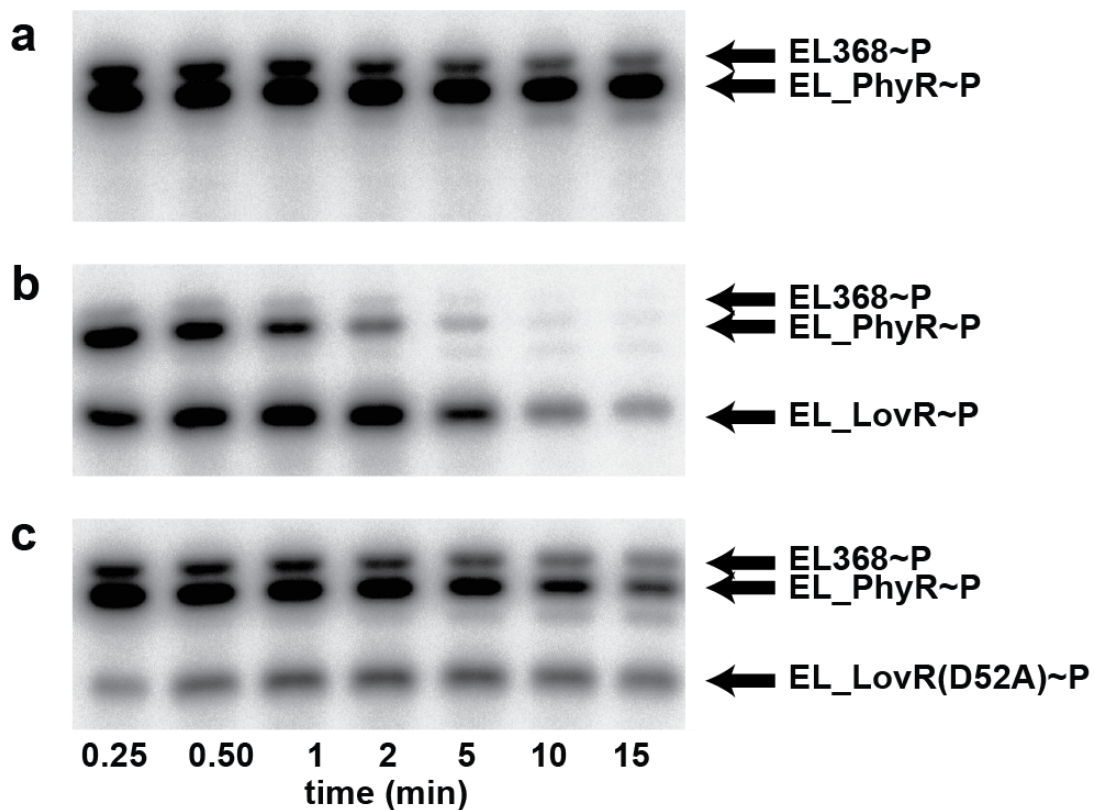


Figure 3.9 Presence of EL_LovR induces phosphate loss of EL_PhyR.

(a) Phosphatase assay of EL_PhyR after phosphotransfer by EL368, demonstrating that phosphorylated EL_PhyR is stable up to 15 min. (b) EL_PhyR rapidly loses phosphate when incubated with unphosphorylated EL_LovR. (c) The phosphoaccepting Asp52 residue is involved in the phosphate turnover of EL_PhyR, as shown by the reduced efficiency of EL_LovR D56A in this process.

EL_LovR as a substrate (Figure 3.10); comparable assays with EL_PhyR and an unrelated response regulator showed no phosphorylation (Figure 3.10). Interestingly, EL362 also appears to contain a LOV domain based on the presence of the highly conserved GRNCRFLQ motif characteristic of the LOV family (46) (Figure 3.11). Nonetheless, we were unable to demonstrate flavin binding to purified recombinant EL362 protein. This was explained by the presence of an unusual Arg residue at the position of a normally conserved glycine within the I β strand of the putative LOV domain (Figure 3.12). We have confirmed that the mutation which generates the Arg 150 residue was found within DNA isolated from strains regrown in our laboratory, as well as being present in the original genomic sequencing data. A homology model of this domain clearly shows that the large Arg sidechain would protrude directly into the flavin-binding site, blocking chromophore binding (Figure 3.13a). To confirm this hypothesis, we generated a EL362 (R150G) mutant which reverts this position to the most abundant residue among LOV domains. This change restores both flavin binding and LOV photochemistry to EL362 (Figure 3.13b), as exhibited by illumination triggering the expected loss of absorbance near 450 nm and subsequent dark state recovery over approximately 3 hr. Re-establishment of the flavin binding restored photosensitivity to the kinase activity: dark and lit state samples of EL362 (R150G) showed autophosphorylation rates of $0.008 \pm 7 \times 10^{-4} \text{ s}^{-1}$ vs. $0.010 \pm 7 \times 10^{-4} \text{ s}^{-1}$ (Figure 3.13c). Notably, both these levels are higher than the wild type enzyme ($0.001 \pm 1 \times 10^{-3} \text{ s}^{-1}$, unaffected by illumination).

We anticipate that these changes in the LOV domain substantially change the domain

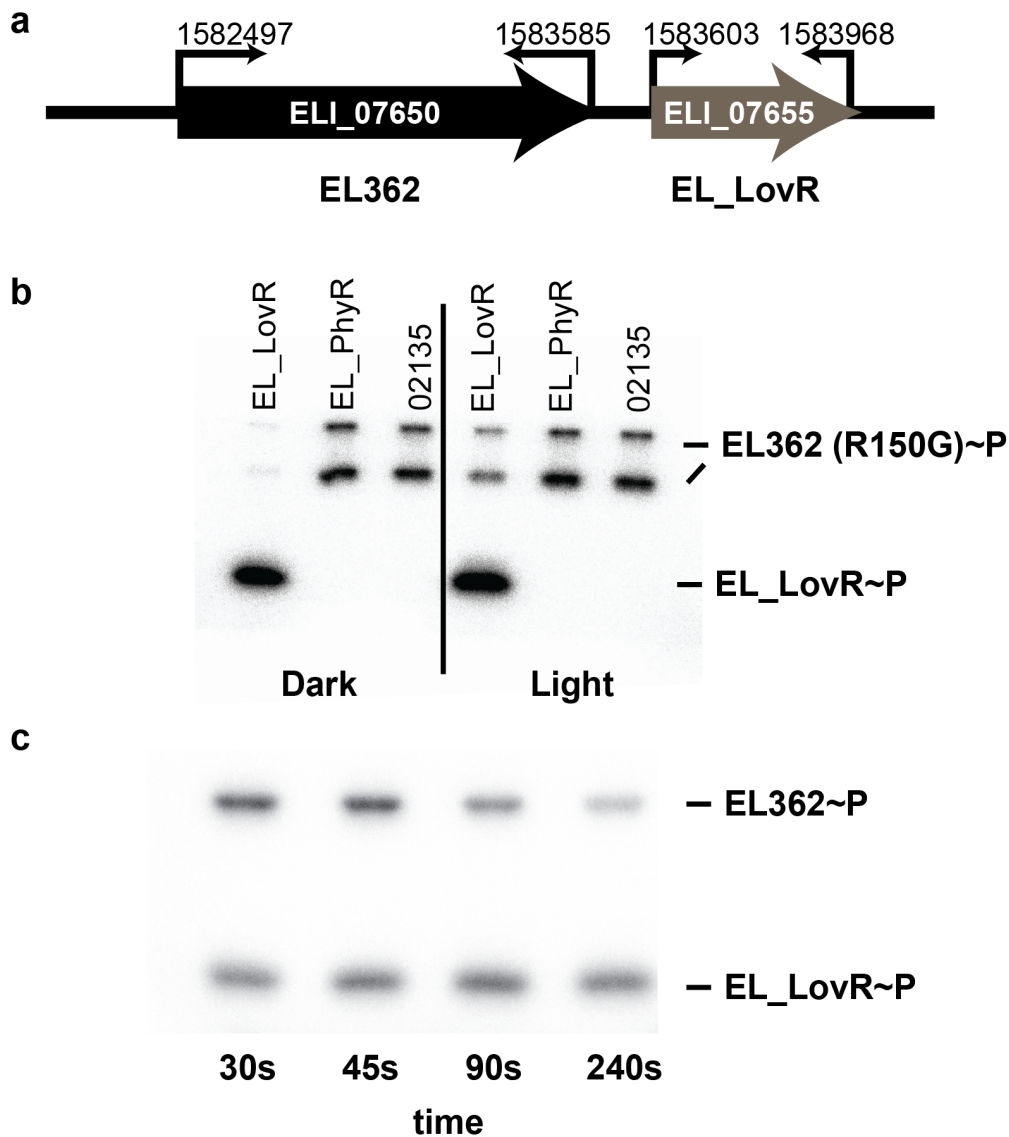


Figure 3.10 EL362 forms a two-component system with its downstream cognate response regulator, EL_LovR.

a). Schematic representation of the chromosomal region near EL362 (ELI_07650) and the EL_LovR response regulator (ELI_07655). Arrows indicate the boundaries of the open reading frames for each gene, with start and stop codon locations as indicated by the arrows. b). Phosphotransfer reaction between EL362(R150G) and EL_LovR, EL_PhyR and a unrelated RR from *E. litoralis* genome (02135). Results show that EL362(R150G) specifically phosphorylates EL_LovR when incubated for 60 s, and the extent of phosphorylation is light-dependent. As noted in the text, wildtype EL362 exhibits minimal and constitutive kinase activity; the R150G point mutant restores light dependence by allowing chromophore binding. c). Extended phosphotransfer reaction between EL362 and EL_LovR (30, 45, 90 and 240 s). Assay conditions: 10 μ M EL362 or EL362 (R150G), 10 μ M EL_LovR in 50 mM Tris pH 8, 100 mM NaCl, 5 mM MgCl₂, 300 μ M ATP, 50 μ Ci [γ -³²P] ATP at room temperature.

```

EL368      MTDGDGRDLPLKGEISAQAGREFDTSRLDLRAIIDPRDLRVDPTLRFLET'TQQTRLAICI
EL362      MDDQPTTRANRVGHP--ESSRQAYSS--ESGATHGSLAFPGASGLLFEQAMAQTRMAVCL
          * *           *           *           *           *           *           *           *
EL368      SDPHQPDPCPVVYVNVQAFDLDTGYAREEIVGRNCRFLQGADTDPEQVRKLREGIAAERYTV
EL362      TDPHQPDHPVFCNAAFERLTGYEEKDII GRNCRFLQGARTDESQVARIRDALAKEEVAV
          ***** *           * *           * *           * *           * *           * *           *
EL368      VDLLNYRKDGIPFVNAVHVGPVIYGEDGTLQYFYGSQWDITDIVAERRKAETQORRIAAELR
EL362      VELLNYRKDGSTFWNALHLGPIYDESGKLYFFRSQWDVTDIHEARAEQRHAKAMAREVS
          * ***** * * * * * * * * * * * * * * * * * * * * * *
EL368      HRTGNIFAVLNAIIGLTSRRERDVSEFADKLSERVSALASAHMTIMDEPDQEAVAIDDL
EL362      HRLKNVFSVIAGIVNITG-RSMDARPVASRINERVQALGRAYEPT-LDEAFMGTIIEVQQA
          * * * * * * * * * * * * * * * * * * * * * * * *
EL368      VTGVMKPYRNRFAERVTTSGPKIELGPRSVTALGLALHELATNAVYKALSVDAGRVEIS
EL362      IRAILAPY-DPEGDRVSLENGVVRTEPNAISSIGLTLHELASNAIKYGALSNETGTIDVS
          * *           * *           *           *           * *           * *           * *           *
EL368      WSREDGD-----VTLVWQEQGGPTVSQEQSEPVKNGTMLIDGMIASLTGSIERDFAAAG
EL362      WHHERDDHRRRLVIDWKESGGPTIEGPPE--TGGTGFDISETLLSYNGTLEKRWDRDG
          * * *           * * * * * *           * *           * *           * *           *
EL368      LQAKITLPVHQPE
EL362      LQAKITLPVHQPE
          * *           *

```

Figure 3.11 EL368 and EL362 have a high degree of sequence identity.

A BLAST (185) alignment of EL368 and EL362 show that they are very similar throughout, including the highly-conserved “GRNCRFLQ” sequence found in many LOV domains (red).



Figure 3.12 The EL362 LOV domain contains an unconserved arginine residue in the Iβ strand.

Sequence alignment with other LOV domains identified by BLAST (185) searching with the EL362 LOV domain sequence demonstrates the substitution of a conserved Gly/Ala residue for an Arg, placing this new large sidechain within the chromophore binding site (Fig. 3.13).

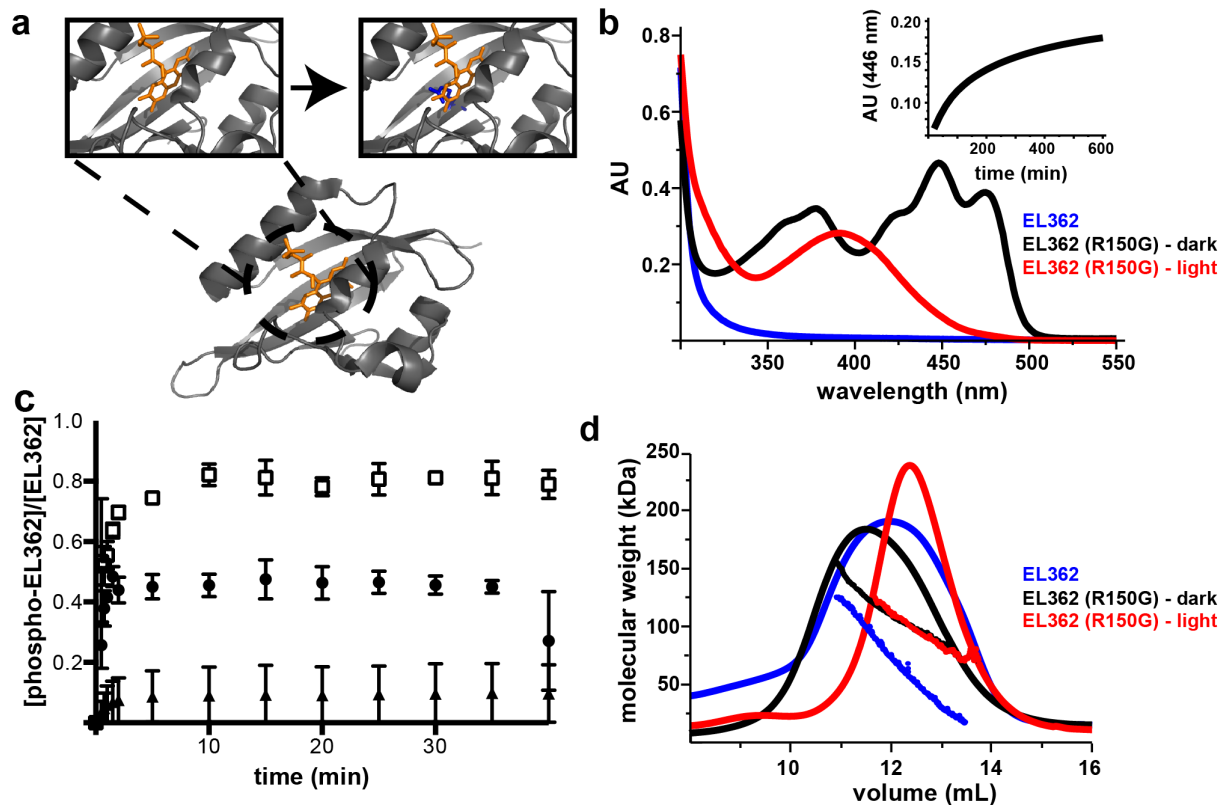


Figure 3.13 Biochemical characterization of EL362: a blind LOV-HK protein.

(a) Predicted effects of R150 residues within the EL362 LOV domain. Bottom center: Structure of a typical LOV domain (*Arabidopsis thaliana* phototropin 2 LOV2 = Atphot2 LOV2, PDB ID 4EEP (186)) showing the location of the internally bound flavin chromophore. Top left: Expansion of the Atphot2 FMN binding site. Top right: Homology model for the predicted site of FMN binding from EL362, superimposing the predicted location of Arg 150 with the FMN bound as seen in other LOV domains. (b) UV-visible absorption spectra of EL362 and EL362 (R150G). The EL362 (R150G) spectrum displays the characteristic vibronic structure of a bound flavin. Upon white light illumination, the flavin undergoes covalent adduct formation. EL362 does not present any spectrum signature indicating the presence of an attached flavin cofactor. EL362 (R150G) photorecovery monitored at 446 nm shows that it undergoes a photocycle after illumination with dark state recovery that takes approximately 3 h. (c) Autophosphorylation kinetics. EL362 (R150G) (filled circles, dark state; open squares, lit state) has overall higher activity than EL362 (filled triangles). (d) SEC-MALS shows that wild type EL362 (monomer MW: 40.7 kDa) is predominantly monomeric in solution (MALS trace ~50 kDa at the center of the peak). Upon restoration of cofactor binding by the R150G point mutation, we observed oligomerization (MALS MW~120 kDa in the dark, ~100 kDa in the light) with some light-dependent effects on the elution peak shape and molecular weight distribution (wild type vs mutant). dRI and MW data are shown as described in Figure 3.3.

structure; given their corresponding perturbations of kinase activity, we asked if they affected the EL362 oligomerization state as seen for EL368 (Figure 3.3). SEC-MALS experiments showed that wild type EL362 eluted as mixture of monomers and higher order oligomers, while the mutant eluted primarily in larger complexes. However, different from EL368, photoexcitation of EL362 (R150G) shifted the elution profile in comparison to its dark state (Figure 3.13d), suggesting a relatively large conformational change. Taken together EL368(56-368) and EL362 show different ways that LOV structure is essential to the activity of the HK domain.

3.3 Discussion

LOV domains are a widespread group of photoswitches that regulate diverse effectors using light-driven allosteric changes (46,155,162). These processes have been studied in several systems, particularly the phototropin class of light-regulated serine/threonine kinases in plants. In these proteins, illumination triggers LOV domain conformational changes that disrupt and unfold a C-terminal “J α helix”, subsequently stimulating kinase activity (159,160). Some LOV-containing proteins appear to work through comparable light-induced release of helical elements, often leading to dimerization (187,188); others alter the conformations of preformed dimers (189). Given the diversity of possible mechanisms and targets, it is important to understand how LOV domains control a variety of effectors, particularly given open questions about the natural regulation of several of these groups (*e.g.* histidine kinases).

Here we provide some biochemical insight into the mechanism of this regulation, showing that illumination activates EL368 via a dual effect, both enhancing the turnover rate for the kinase activity while slightly decreasing the affinity of the protein to ATP (Fig 3.1b). The best-developed mechanistic model for how such regulation might be achieved is based on data from YF1, an engineered LOV-HK protein containing a LOV domain fused onto a HK that is normally controlled by a gas-responsive PAS domain (190-192). This model suggests that light-induced conformational changes at the sensory domain are transmitted to the HK domain through movements in the intervening coiled-coil linker between them, similarly to HAMP domains that often couple sensory and catalytic domains in HKs. Recent crystal structures of both YF1 (192) and a natural PAS-HK protein (83) bolster support for this regulatory model.

We believe that EL368 supports the above-mentioned model for two reasons: i) the presence of coiled coils predicted by the COILS server (193) to be located between V163-R223 to form a DHp domain (Figure 3.4). ii) the presence of a stable LOV dimer interface, which may provide the anchor point needed to trigger the rotational change. Experimental support for this is provided by EL368(56-368) (Figure 3.3) and EL362 (Figure 3.13), which have LOV domains affected by truncation or lack of chromophore binding and correspondingly lower amounts of dimer in solution.

Turning from HK regulation to the subsequent downstream targets, we note that the exciting discovery of prokaryotic LOV photosensory proteins with bioinformatic and biochemical methods (46,132,155,162,194) has significantly preceded their functional characterization. To date, only few of these have had assessed biological roles: several histidine kinases (LovK (36),

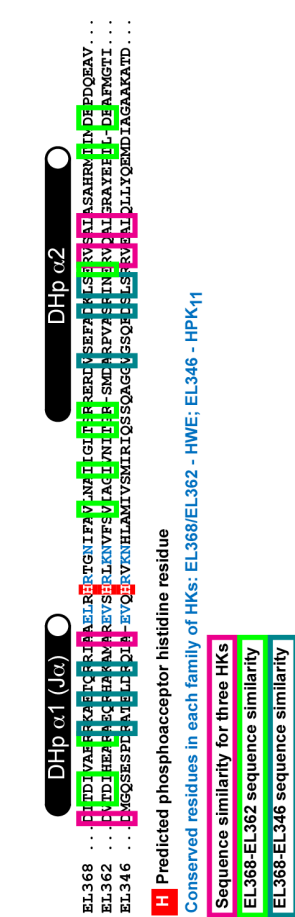
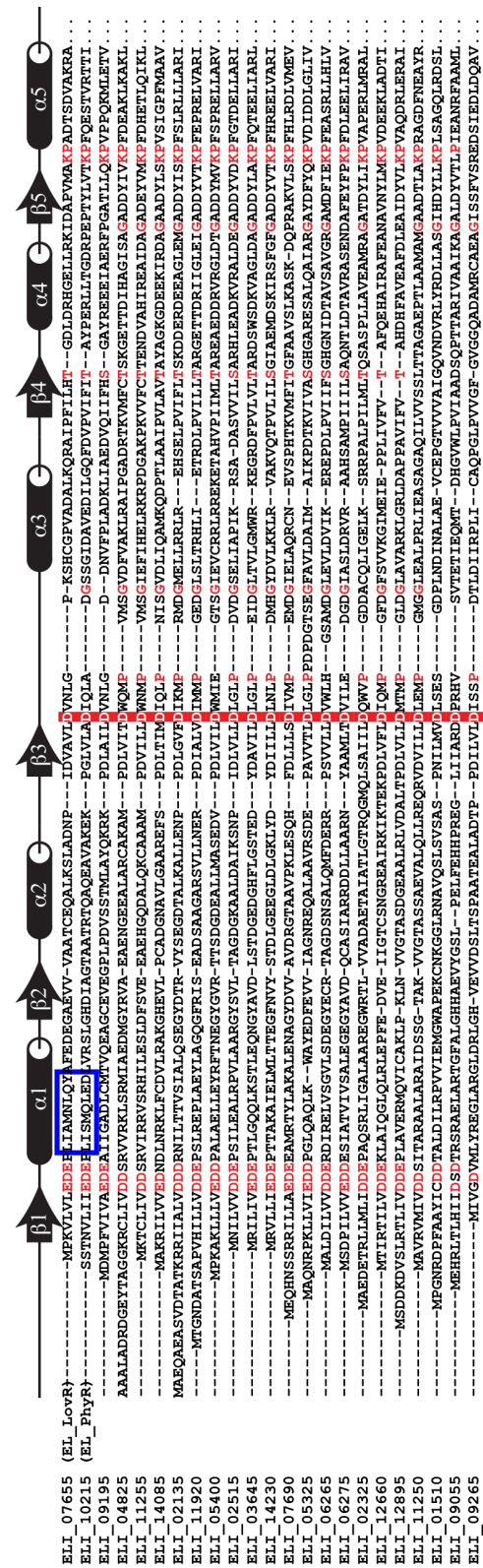
BM-LOV-HK (53), R-LOV-HK (165), Xac-LOV-HK (163)) along with the EL222 DNA binding protein (55) and the anti-sigma antagonist YtvA (195). Here, our investigations of EL368 and two other LOV-HK proteins add to this list, through the use of unbiased phosphotransfer profiling to identify the kinetically-preferred downstream targets of these enzymes. Our data reveal that the three enzymes present a remarkable kinetic preference for the same RR (EL_LovR), which is a potential cognate pair with EL362 based on sequence proximity (Figures 3.5, 3.6, 3.10). EL368 and EL346 also had a kinetic preference for one additional substrate, EL_PhyR (Figures 3.5, 3.6).

Such a “branched” signaling pathway, achieved by multiple enzyme/substrate pairings at the same step, facilitates more complex network behavior than otherwise possible from exclusive links. The biochemical (196) and structural (75,197,198) bases of HK/RR specificity in a two-component pair is defined by residues located near the phosphorylated histidine within the HK DHp domain and mostly by residues in the RR α 1 helix. Inspection of EL_LovR and EL_PhyR sequences show that they share similar α 1 helices compared to the other *E. litoralis* RRs, perhaps specifying their selection by the LOV-HKs (Figure 3.14). On the complementary HK surface, we observe sequence similarities among the DHp regions (Figure 3.14b) as well as differences that may contribute to the differential phosphorylation levels of RR substrates.

Our findings suggest the existence of a complex light-regulated branched pathway in *E. litoralis* involving “many-to-one” (EL346, EL362, EL368 with EL_LovR) and “one-to-many” (EL368, EL346 with EL_LovR and EL_PhyR) HK and RR relationships. “Many to one” relationships allow the cell to integrate multiple inputs into the phosphorylation levels of a

Figure 3.14 Decoding light two-component specificity.

a) Multiple sequence alignment of 23 *E. litoralis* RR receiver domains based on Multalin (199). Highly-conserved residues in the RR family are indicated in red text, while the predicted aspartate phosphoacceptor residues are highlighted by with a red box. The approximate locations of predicted secondary structure elements (175) are indicated above the sequences, as indicated by arrows (β -strand) and cylinders (α -helix). Predicted interfacial residues of EL_LovR and EL_PhyR at the HK-RR complex are indicated by a blue box. b) Sequence alignment of three LOV-HK proteins is depicted. Red boxes indicate the predicted phosphoaccepting histidine residue. Highly conserved residues characteristic for each family of HK are indicated in blue: HWE family (74) – EL368, EL362; HPK11 family (65) – EL346. Colored boxes indicate residues shared by the enzymes: magenta - three enzymes, green - EL368 and EL362 and dark red - EL368 and EL346.



specific RR and consequently undergo appropriate physiological answers for each level (101). EL368 and EL346 both feed into the same EL_LovR and EL_PhyR pathway; this apparent redundancy may be explained by either functional importance (*e.g.* different sensors have differential sensitivity to light) or simply due to a lack of selective pressure against keeping multiple LOV-HK proteins in the genome. We also note that this redundancy provides some robustness in the event of inactivation of one sensor, as perhaps seen by EL368 and EL346 compensating for the impaired function of the non-inducible EL362 kinase (Figure 3.13). We speculate that perhaps EL362 may actually represent a genetic relic of sorts by having served as the ancestral light sensor in this organism (in a conventional operon arrangement with its cognate RR) prior to having suffered an inactivating mutation in its LOV domain. While rigorous testing of the potential *in vivo* roles of multiple LOV-HK proteins will require future experimental validation, we note this redundancy is not restricted solely to *E. litoralis*: multiple eubacteria (including several *Methylobacterium* species) contain two or more LOV-HK genes.

An additional degree of complexity (“one to many” relationship) is added to the transduction pathway by the ability of EL368/EL346 to phosphorylate EL_PhyR in addition to EL_LovR. Our biochemical analyses of EL_PhyR allow us to classify it as a PhyR-like response regulator; an analogous protein in *Methylobacterium extorquens* AM1 (which contains multiple LOV-HK proteins, see above) participates in regulation of σ anti- σ interaction system, which is involved in resistance to multiple environmental stresses through activation of several target genes (166,167). Interestingly, Foreman *et al.* demonstrated that transcription of the LovK-LovR operon in *C. crescentus* is upregulated by the same general stress σ factor (132). In *E. litoralis*

there is no direct evidence that EL368 and EL346 could be regulated by the σ factor. However, analysis of the intergenic region prior to the potential EL362-EL_LovR operon indicates the presence of a putative operator (**GGA**ACT CCG AGC CGC TCA GTC **GGTT**) for the σ binding located 83 nucleotides prior to the start codon of EL362 gene (designated by the EL_ sigT promoter in Figure 3.15), suggesting that *E. litoralis* may adopt a similar system of regulation as observed in the related α -proteobacterium *C. crescentus*. Nevertheless, we do observe some differences between *C. crescentus* and *E. litoralis*, particularly in the latter use of “orphan” HKs to phosphorylate RR proteins distant in the genome (*i.e.* EL368, EL346 with EL_PhyR, EL_LovR). Notably, this allows *E. litoralis* to have a similar light regulated network architecture as observed in *C. crescentus* (132) despite the inability of native EL362 to be controlled by illumination.

3.4 Conclusion

In conclusion, our findings indicate the discovery of a light regulated branched transduction pathway involving a set of several LOV-HKs and stress-related RRs. Additional biochemical and structural studies of these proteins would not only help to understand the molecular mechanisms of activation of HKs, but also enhance our knowledge about the complexity and diversity of two-component signaling systems.

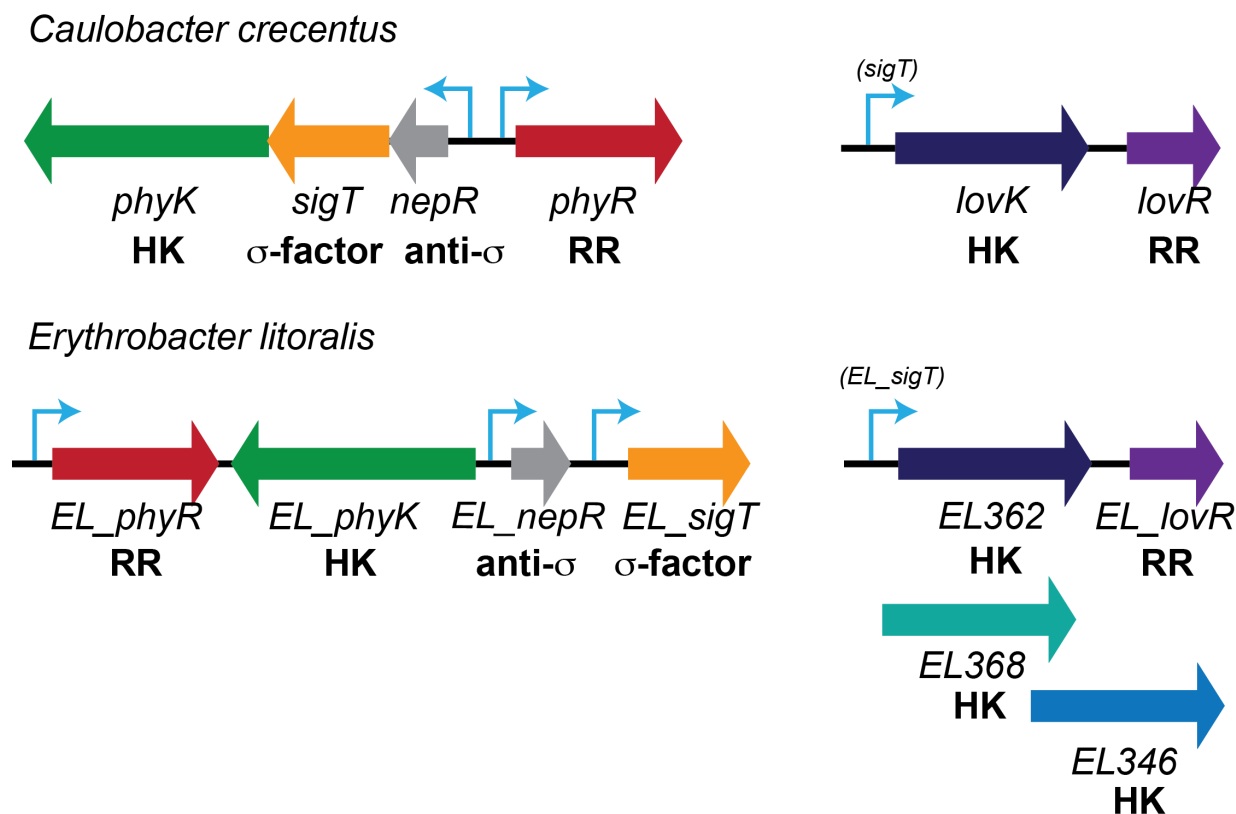


Figure 3.15 Comparison of *Caulobacter crescentus* and *Erythrobacter litoralis* stress-responsive two component systems with LOV-HK proteins.

Top show gene organization for the *phyK-phyR*, *lovK-lovR* two component and *nepR*, *sigT* genes of *C. crescentus* (132). Bottom shows gene organization of homologs found in *E. litoralis*. In addition to the similarities of genomic architecture, we note similar regulatory sigma factors being used to control expression of the *lovK/lovR* and *EL362/EL_lovR* operons.

Chapter 4 Ligand induced folding in a TCS receiver domain

Abstract

To survive and adapt to changes in the environment, bacteria use two component systems. Minimally, these pathways use histidine kinases (HKs) to detect environmental signals, harnessing these to control phosphorylation levels of receiver (REC) domains of downstream response regulators that convert this signal into physiological responses. Studies of several prototypical REC domains suggest that phosphorylation shifts these proteins between inactive and active structures that are globally similar and well-folded. However, it is unclear how globally these findings hold within REC domains in general, particularly within full-length proteins. Here we present EL_LovR, a full-length REC-only protein that is phosphorylated in response to blue light in the marine α -proteobacterium *Erythrobacter litoralis* HTCC2594. Notably, EL_LovR is similar to comparable REC-only proteins used in other bacterial general stress responses, where genetic evidence suggests that their potent phosphatase activity is important to shut off such systems. Size exclusion chromatography, light scattering and solution NMR experiments show that EL_LovR is monomeric and unfolded in solution on its own under conditions routinely used for other REC structure determinations. Addition of Mg^{2+} and phosphorylation induce progressively greater degrees of folding, with the solution structure of the fully-activated EL_LovR adopting the canonical receiver domain fold. Parallel

functional assays show that EL_LovR has a fast dephosphorylation rate, consistent with its proposed function as a phosphate sink. Taken together, our findings demonstrate that EL_LovR undergoes drastic ligand-dependent conformational changes that have not been seen in other RRs with probable effects on the autophosphatase activity of this protein. In conclusion, our work expands the kinds of conformational changes and regulation used by REC domains, critical components of bacterial signaling systems.

4.1 Introduction

Two-component signal transduction (TCS) systems are the most prevalent strategy used by bacteria to sense and adapt to changes in their environment (23,154). Minimally, TCS are comprised of a sensor histidine kinase (HK) and a response regulator (RR) (200). HKs typically contain three types of domains: an environmental sensor, a dimerization and histidine phosphotransfer domain (DHp) and a catalytic domain (CA). Their combined operation allows an HK protein to sense environmental cues via the sensor domain and translate this signal into changes in phosphorylation level on a critical His residue in the DHp domain. With the help of a Mg^{2+} ion, the phosphoryl group is transferred from the phospho-His residue to an aspartate in the receiver domain (REC) of the downstream RR, controlling their function.

While all REC domains share a conserved $(\beta\alpha)_5$ fold (Figure 4.1) and phosphoacceptor region that includes the phospho-accepting aspartate and several nearby acidic residues required

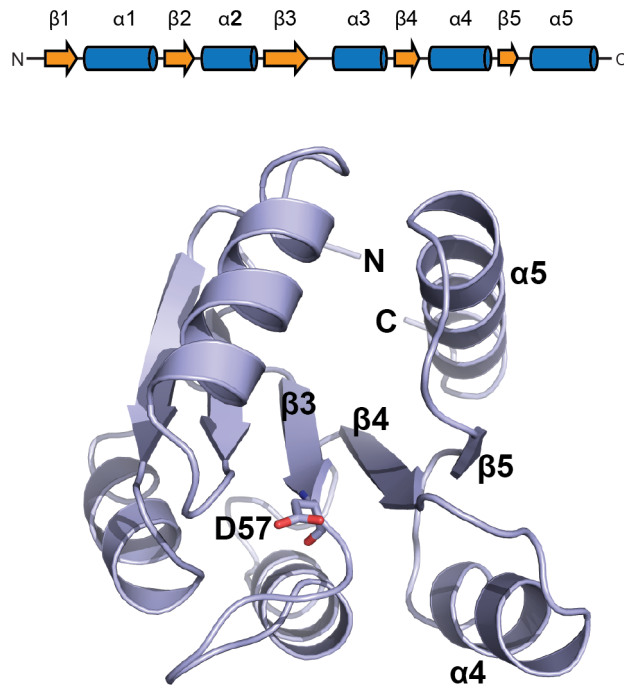


Figure 4.1 Crystal structure of CheY bound to magnesium.

a). Standard secondary structure elements and nomenclature in a typical REC domain. b). Crystal structure of the chemotaxis SDRR protein CheY (95), showing the canonical $(\beta\alpha)_5$ fold of REC domains.

for binding Mg^{2+} ion (104), these domains are found in a wide variety of protein architectures. Some REC-containing proteins contain different types of effectors, such as DNA binding domains, which are directly controlled by phosphorylation, while others contain solely of isolated REC domains. This latter group, collectively referred to as single domain response regulators (SDRR), are fairly prevalent, composing the second largest class of RR proteins (~14%) (2,86). While these proteins lack an effector domain of their own, they can use the $\alpha 4$ - $\beta 5$ - $\alpha 5$ surface at their C-termini to regulate functions of many other diverse proteins. This can often occur by activation-controlled protein/protein interactions; for example, when the CheY SDRR chemotaxis protein is phosphorylated, it interacts with a member of the switch of flagellar motor FliM (201), changing the direction of flagellar rotation. Additionally, it has been reported that CheY can also function as a phosphate sink (86). Another SDRR, DivK plays an essential role in *Caulobacter crescentus* cell division (90) by temporally regulating proteolysis of CtrA, a RR that regulates the expression of many genes involved in cell cycle (91). The sole common theme among these functionally distinct proteins is the REC domain fold.

The widespread use of REC domains in bacterial signaling has led to intense interest in understanding how phosphorylation activates these switches and thereby controls their function. To address these questions, a number of REC domain structures have been solved in their active (103,112,116,202,203) and inactive states (105,107,108,204) and used to generate models of REC signaling. One such model entails the use of phosphorylation to shift a preexisting structural equilibrium, as perhaps best validated by data collected on the REC domain of NtrC (117). When unphosphorylated, this REC domain rapidly interconverts between

well-structured inactive and active-like conformations, with the equilibrium significantly favoring the lower energy, inactive conformation. Upon phosphorylation, the equilibrium shifts to fully populate the active state (117). While elegant, the generality of this signaling model remains somewhat unclear, with some members undergoing non-two state segmental sampling of active-like conformations (CheY (115)) or exhibiting partial unfolding of different secondary structure elements (Sma0114 (203,204)). These examples underscore the need to more completely characterize different REC domain signaling mechanisms in light of the apparent diversity that has been revealed to date.

To this end, we integrated biochemical and biophysical approaches to characterize activation-induced changes in EL_LovR, an SDRR involved in a light regulated TCS (63) found in the marine α -proteobacterium *Erythrobacter litoralis*. EL_LovR, one of the 23 predicted RR encoded in the *E. litoralis* genome (63), is one of two RRs phosphorylated by three light-sensitive HKs in *E. litoralis*, EL346/EL362/EL368 (63). Coupling these data with bioinformatics and genetics analyses showing the importance of a closely related homolog (LovR) in stress responses in *Caulobacter crescentus* (36,132), we hypothesized that EL_LovR has a similar role and sought to investigate how it might be affected by phosphorylation.

Our biophysical analyses revealed that EL_LovR fundamentally requires binding of two ligands – Mg^{2+} ion and phosphorylation – to properly fold into the correct REC domain structure. Contrary to structure predictions indicating that EL_LovR would adopt a canonical REC structure, size exclusion chromatography, limited proteolysis and solution NMR spectroscopy all showed that inactive EL_LovR is disordered with poorly-defined secondary structure elements.

Binding Mg^{2+} ion led to partial folding; further folding was observed either by phosphorylation with enzymatic or small molecule donor or binding to the phosphomimetic beryllium fluoride (BeF_3^-). Using solution NMR spectroscopy, we further confirmed that activated EL_LovR bound to both Mg^{2+} and BeF_3^- adopts the conserved REC domain fold as originally anticipated. Additionally, phosphatase assays indicate that the active state of EL_LovR is short lived with a half-life of approximately 2 min, consistent with expectation of a role as a phosphate sink like its *C. crescentus* homolog LovR (132). These data establish that EL_LovR undergoes an unprecedented ligand-dependent folding reaction, perhaps ensuring that its potent phosphatase activity is restricted to specific circumstances.

4.2 Results

4.2.1 EL_LovR undergoes significant changes in global shape upon Mg^{2+} binding and phosphorylation

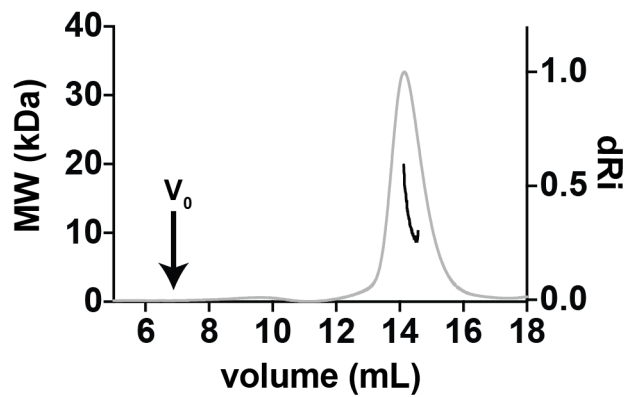
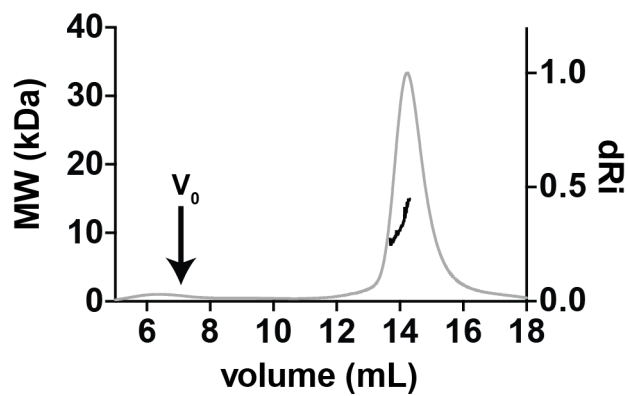
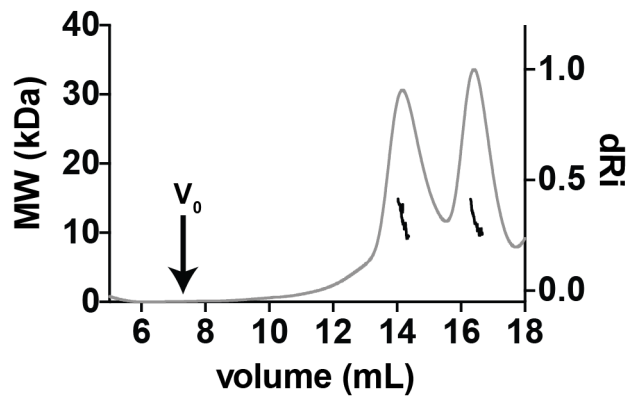
We started our studies by probing the effects of Mg^{2+} binding and phosphorylation on the oligomerization state of EL_LovR. Many RRs change among monomer, dimer and higher order states upon activation (112,205,206). Using an allosteric pathway between the site of phosphorylation and the $\alpha 4$ - $\beta 5$ - $\alpha 5$ interface to generate conformational changes (207) that can affect protein/protein interactions. To determine the oligomeric state of EL_LovR, we used SEC-MALS analysis to obtain two independent types of data regarding protein mass and hydrodynamic behavior. We tested EL_LovR in three different conditions: apo (buffer only),

metal-bound (buffer + 10 mM MgCl₂) and phosphorylated (buffer + 10 mM MgCl₂ + 10 mM carbamoyl phosphate). Under all conditions, light scattering established that EL_LovR is monomeric (~13 kDa); however, we observed substantial changes in hydrodynamic behavior depending on the protein activation state (Figure 4.2). For the apo and Mg²⁺-bound states, the ~14 mL elution volume is much smaller than expected from the EL_LovR sequence, consistent with a ~52.5 kDa particle approximately four times the EL_LovR theoretical molecular weight. We attribute this to an expanded, monomeric EL_LovR given the monomeric molecular weight by MALS. In contrast, comparable studies of phosphorylated EL_LovR (achieved by pre-incubation with carbamoyl phosphate), eluted in two distinct peaks. One elution peak corresponds to the elution volume of the apo and metal-bound state, which we assign to apo-protein. However, the second at a later volume (~17 mL), corresponding much better to the EL_LovR theoretical molecular weight (~13.8 kDa), suggesting that EL_LovR has undergone a significant change in its hydrodynamic radius upon phosphorylation. We attribute this to phosphorylated EL_LovR, with some fraction of the protein either not having been phosphorylated initially or having been spontaneously dephosphorylated due to inherent phosphatase activity in this protein (*vide infra*).

To gain more information on what changes EL_LovR undergoes upon phosphorylation, we used limited proteolysis as a low-resolution structural probe. Using a well-established phosphomimic, beryllium fluoride (BeF₃⁻) (119), to stably activate EL_LovR without issue of potential phosphatase activity, we incubated EL_LovR in varying conditions with trypsin. SDS-PAGE analysis of the resulting samples show that apo- and metal-bound EL_LovR

Figure 4.2 EL_LovR undergoes global conformational changes upon phosphorylation.

a). Superdex S200 10/300 SEC-MALS data indicate that apo EL_LovR eluted at with 14 mL retention volume (differential refractive index, dRi; gray). The molecular weight obtained from multiangle laser light scattering (black) indicates that apo-EL_LovR is a monomer at ~13 kDa while the apparent molecular weight based on elution volume is ~52.5 kDa. b). Comparable to the apo-protein, Mg²⁺-bound EL_LovR eluted at 14 mL and with a monomeric molecular weight, suggesting that Mg²⁺ did not globally change the apo- state structure. c) Phosphorylated, Mg²⁺-bound EL_LovR eluted with in two distinct peaks, one of which resembles the apo- state while the other eluted with a later, 17 mL volume. We interpret the appearance of two peaks as indicating the sample containing both unphosphorylated and phosphorylated forms of EL_LovR due to the rapid phosphatase activity of EL_LovR~P. These data suggest that the overall shape of the molecule changed from an elongated state to a compact state while remaining monomeric ~13 kDa. The void volume (V₀) of this column is approximately 7 mL as indicated on all chromatograms.

a. apo-EL_LovR**b. EL_LovR +Mg²⁺****c. EL_LovR + Mg²⁺ + carbamoyl~P**

undergoes rapid cleavage, completely converting from full length into a stable ~6 kDa fragment within 15 min (Figure 4.3a,b). ESI-MS analysis revealed the protease-resistant fragment to be a 5,851.1 Da segment of EL_LovR, corresponding to residues 8-62. In contrast, activated EL_LovR bound to Mg^{2+} and BeF_3^- remained markedly resistant to trypsin, with only minor proteolysis over time (Figure 4.3c). These results suggest that EL_LovR undergoes significant conformational changes upon activation, consistent with an expanded, protease-accessible protein in the apo- and Mg^{2+} -bound forms folding into a compact, resistant structure upon phosphorylation.

4.2.2 EL_LovR becomes increasingly folded in activating conditions

To obtain residue-level analysis of the EL_LovR folding events implicated by SEC-MALS and limited proteolysis, we collected $^{15}\text{N}/^1\text{H}$ HSQC spectra of apo, Mg^{2+} -bound, Mg^{2+} and BeF_3^- bound samples (Figure 4.4). These data reveal significant improvements in ^1H chemical shift dispersion and homogeneity of peak intensity consistent with protein folding. In the apo form, most of the peaks remain clustered with poor amide proton dispersion in the center of the spectra, with some intense peaks present. These are spectral signatures of disordered protein, likely with limited secondary and tertiary structure. We observed some improvement in peak dispersion and homogeneity upon addition of 10 mM MgCl_2 , including shifting of some peaks outside of the central region. These results indicate conformational changes taking place that were otherwise undetectable with gel filtration or limited proteolysis. To induce the fully active

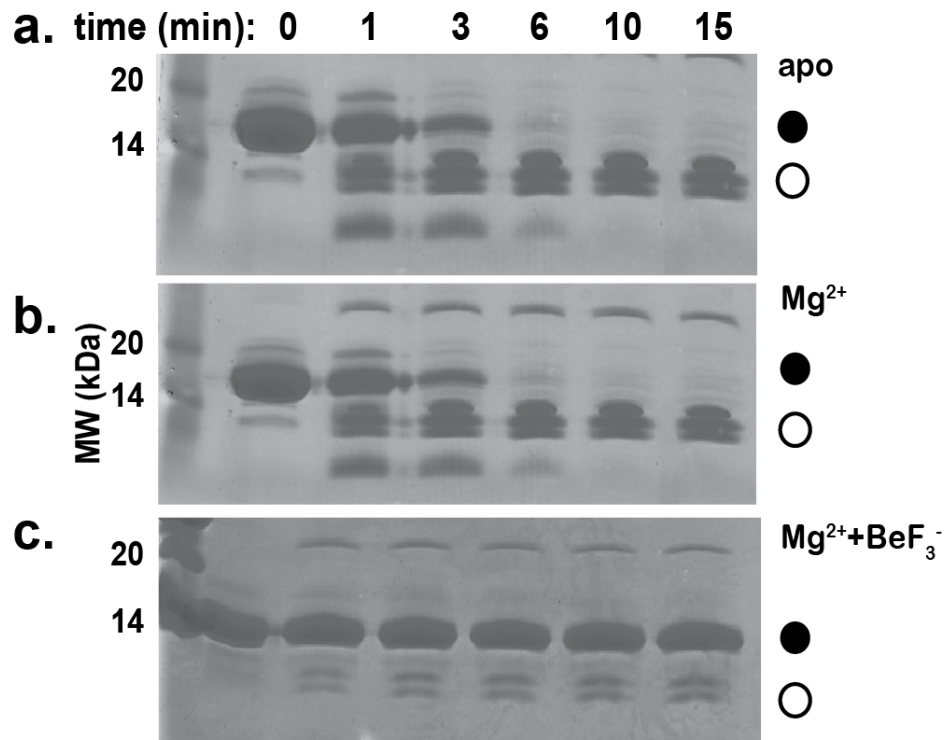


Figure 4.3 EL_LovR~P undergoes phosphorylation-dependent conformational changes to become more resistant to trypsin digestion.

Limited proteolysis of EL_LovR with trypsin in a 1:90 w:w ratio (EL_LovR:trypsin) shows different patterns of cleavage of EL_LovR when phosphorylated. a). Apo-EL_LovR is rapidly cleaved by trypsin from its ~13 kDa full length form (closed circles) into a protease-resistant 5.8 kDa fragment (open circles), identified by ESI-MS to correspond to residues 8-62. b). Mg^{2+} -bound EL_LovR shows a very similar time dependence of trypsin digestion as apo- protein, c). Fully-activated EL_LovR bound to both Mg^{2+} and BeF_3^- was not degraded by trypsin over the same 15 min timecourse as apo- and Mg^{2+} -bound protein, consistent with substantial conformational changes upon activation.

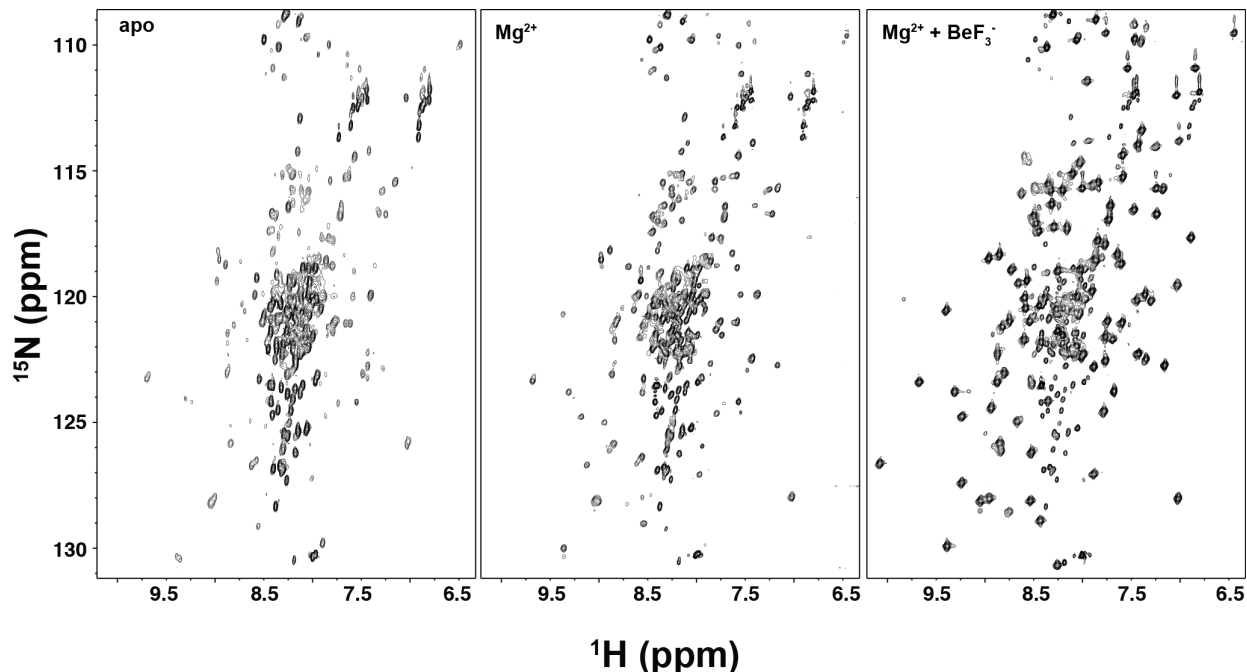


Figure 4.4 EL_LovR progressively becomes more folded with binding to Mg^{2+} and BeF_3^- . $^{15}\text{N}/^1\text{H}$ HSQC spectra were acquired of EL_LovR with varying ligands provided as indicated: Mg^{2+} = 10 mM MgCl_2 ; BeF_3^- =, 5 mM BeCl_2 and 15 mM NaF to generate saturating BeF_3^- . Apo EL_LovR spectra are consistent with mostly disordered proteins, with relatively poor amide proton chemical shift dispersion and heterogeneous peak intensities. Addition of Mg^{2+} improves dispersion and reduces heterogeneity, as well as inducing some peak shifts; all of these signs suggest some degree of ligand-induced stabilization. By adding both Mg^{2+} and BeF_3^- to generate a fully activated state, we observed further improvement in peak dispersion and intensity, consistent with a fully-folded protein.

conformation, we incubated EL_LovR with 5 mM BeF_3^- with the striking generation of outstanding peak dispersion consistent of a well-folded protein (Figure 4.4). Taken together, these data indicate that EL_LovR undergoes a folding event upon activation with BeF_3^- . Consistent with this, ^{15}N -edited NOESY data collected on EL_LovR in inactive and active conditions exhibit drastic differences (Figure 4.5) with very few NOEs observed in the inactive (apo) state in contrast with many short and long range NOEs detected upon addition of Mg^{2+} and BeF_3^- .

We extended this analysis by completing backbone chemical shift assignments on the apo, Mg^{2+} and $\text{Mg}^{2+}/\text{BeF}_3^-$ states of EL_LovR to obtain secondary structure analyses and chemical-shift derived order parameter information (S^2_{CS}) (208) (Figure 4.6). Using standard triple resonance approaches, we obtained backbone chemical shift assignments for 64%, 68% and 100% of residues in these three states. For the apo and Mg^{2+} -bound EL_LovR species, intermediate chemical shift exchange reduced peak intensities to the point of hampering chemical shift assignments in several regions (Figure 4.6a), including the trypsin-susceptible region identified in our limited proteolysis experiments. Those regions that were readily assigned showed significant disorder with fewer (and shorter) secondary structure elements than expected within REC domains (Figure 4.6a). In contrast, EL_LovR incubated with Mg^{2+} and BeF_3^- adopted a more structured conformation, with all REC domain secondary structure elements present (Figure 4.6a).

Further data supporting this ligand-dependent folding process was provided by comparisons of backbone amide order parameters extracted from chemical shifts (S^2_{CS}) (208).

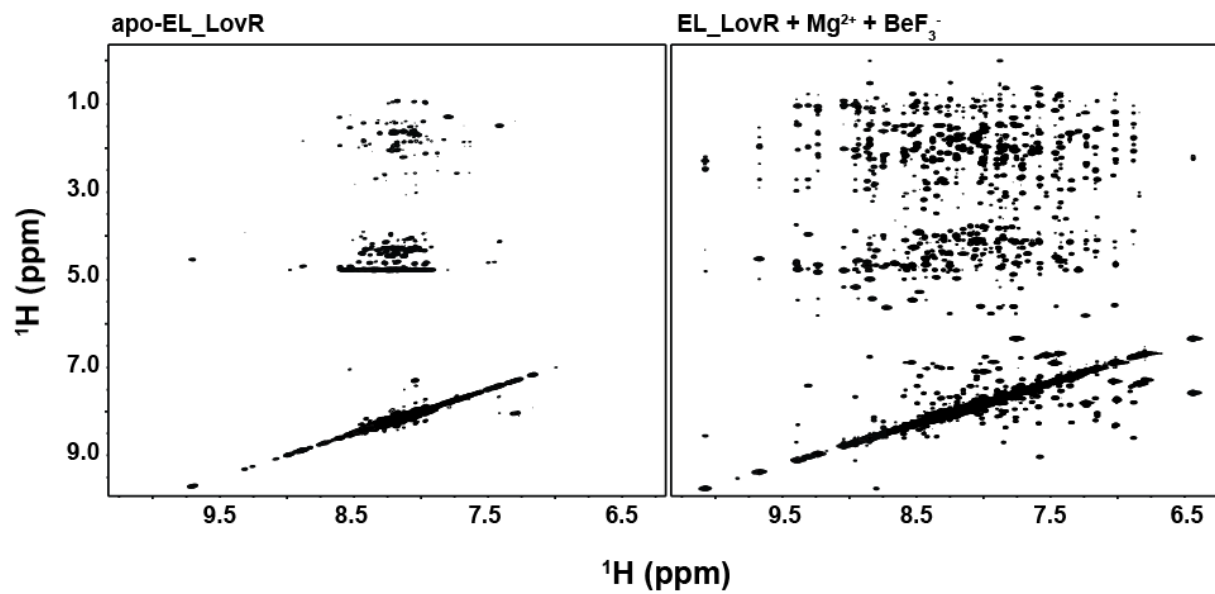


Figure 4.5 NOESY experiment show the lack of long distance NOEs of Apo-EL_LovR compared to EL_LovR + Mg²⁺ + BeF₃⁻

The lack of long distance NOE in Apo-EL_LovR suggests atoms are farther than 5 Å indicating a poorly folded protein. NOESY spectra of EL_LovR with Mg²⁺ and BeF₃⁻ show many interactions within 5 Å, this data was used for structure calculation of EL_LovR in the active state.

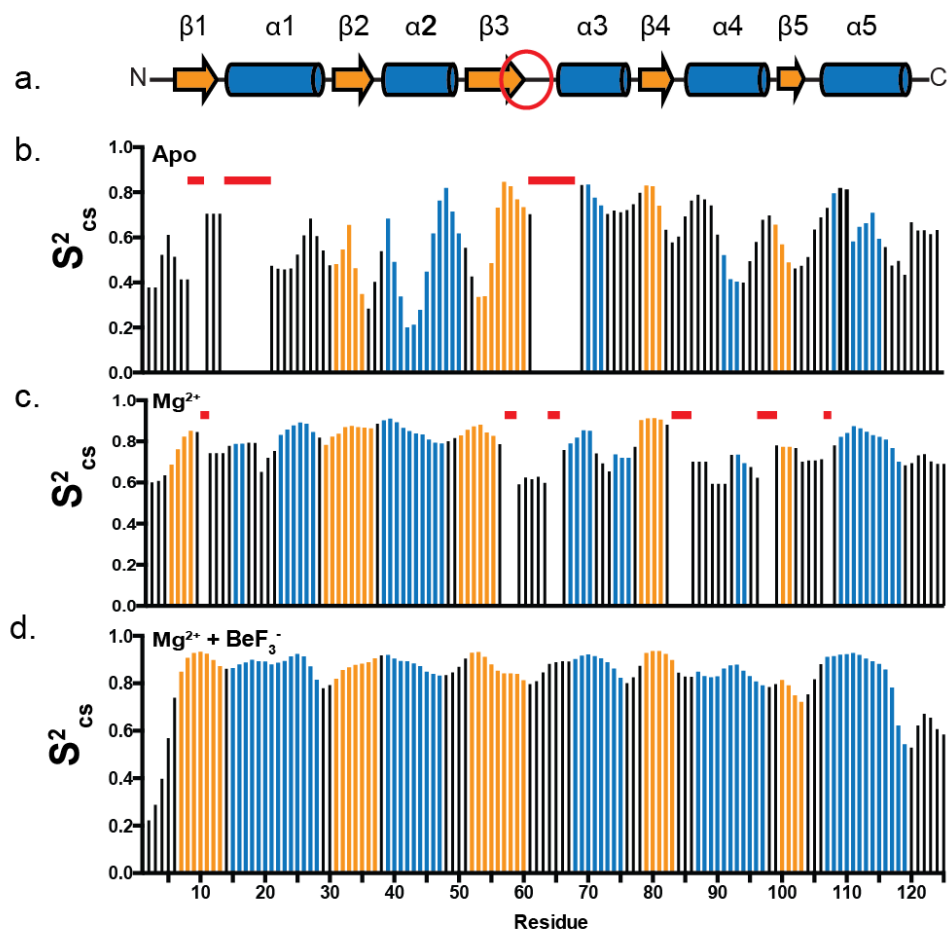


Figure 4.6 Ligand binding to EL_LovR induces the formation of stable secondary structure.

a) Predicted secondary structure elements of EL_LovR based on REC domain structures; red circle indicates the location of the phosphoaccepting D56 residue. b). Analysis of apo-EL_LovR backbone chemical shifts with TALOS-N (151) identified several secondary structure elements (yellow: helices; blue: strands), although truncated compared to expected boundaries. S^2_{CS} analyses of the same chemical shifts predict significant dynamics on the ps-ns timescale throughout much of the protein. Red bars indicate residues without chemical shift assignments due to intermediate chemical exchange. c). Compared to apo-EL_LovR, the Mg^{2+} -bound state showed additional secondary structure elements and increased S^2_{CS} values, consistent with ligand-induced order. d). Addition of both Mg^{2+} and BeF_3^- leads to EL_LovR adopting the canonical $(\beta\alpha)_5$ topology of a REC domain, and an overall increase of S^2_{CS} to 0.8-0.9 values for most of the protein, indicating limited ns-ps timescale dynamics.

This parameter, which scales from 0 to 1 with increasing rigidity at any given backbone amide site, reveals that apo-EL_LovR is clearly unfolded, with few regions having $S^2 \sim 0.8-0.9$ values typically observed of well-folded protein. Addition of Mg^{2+} substantially elevates these values, particularly for the N-terminal half of the domain. However, we still observe large variations in S^2 along the sequence, with low values ($S^2 \sim 0.6$) occurring in regions that usually adopt the stable $\alpha 4$ helix and $\beta 5$ strand. Indeed, only when LovR was incubated with both Mg^{2+} and BeF_3^- did we observe full ordering of the protein with $S^2 \sim 0.8-0.9$ values and all expected secondary structures present (Figure 4.6b).

To further assess the stability and dynamics of the fully-structured Mg^{2+} and BeF_3^- bound state of EL_LovR, we used a combination of 2H exchange and ^{15}N relaxation measurements. While 2H exchange measurements of the unfolded apo- and Mg^{2+} -bound species exchanged too quickly within the 20' deadtime and duration of the first $^{15}N/^1H$ HSQC spectrum to accurately quantitate exchange rates, we measured 2H protection factors of 10^5-10^6 for residues in secondary structure elements through most of the Mg^{2+} / BeF_3^- loaded state (Figure 4.7). Intriguingly, this did not include residues in the $\alpha 4-\beta 5-\alpha 5$ region that normally interacts with downstream effectors, as these exchanged too quickly to measure (Figure 4.7). Complementary measurements of backbone dynamics via ^{15}N R_1 and R_2 relaxation rates paralleled these results (Figure 4.7b and c). Through most of the N-terminal portion of Mg^{2+} / BeF_3^- loaded EL_LovR, we observe uniform values of both relaxation parameters through secondary structure elements, consistent with minimal dynamics aside from overall tumbling.

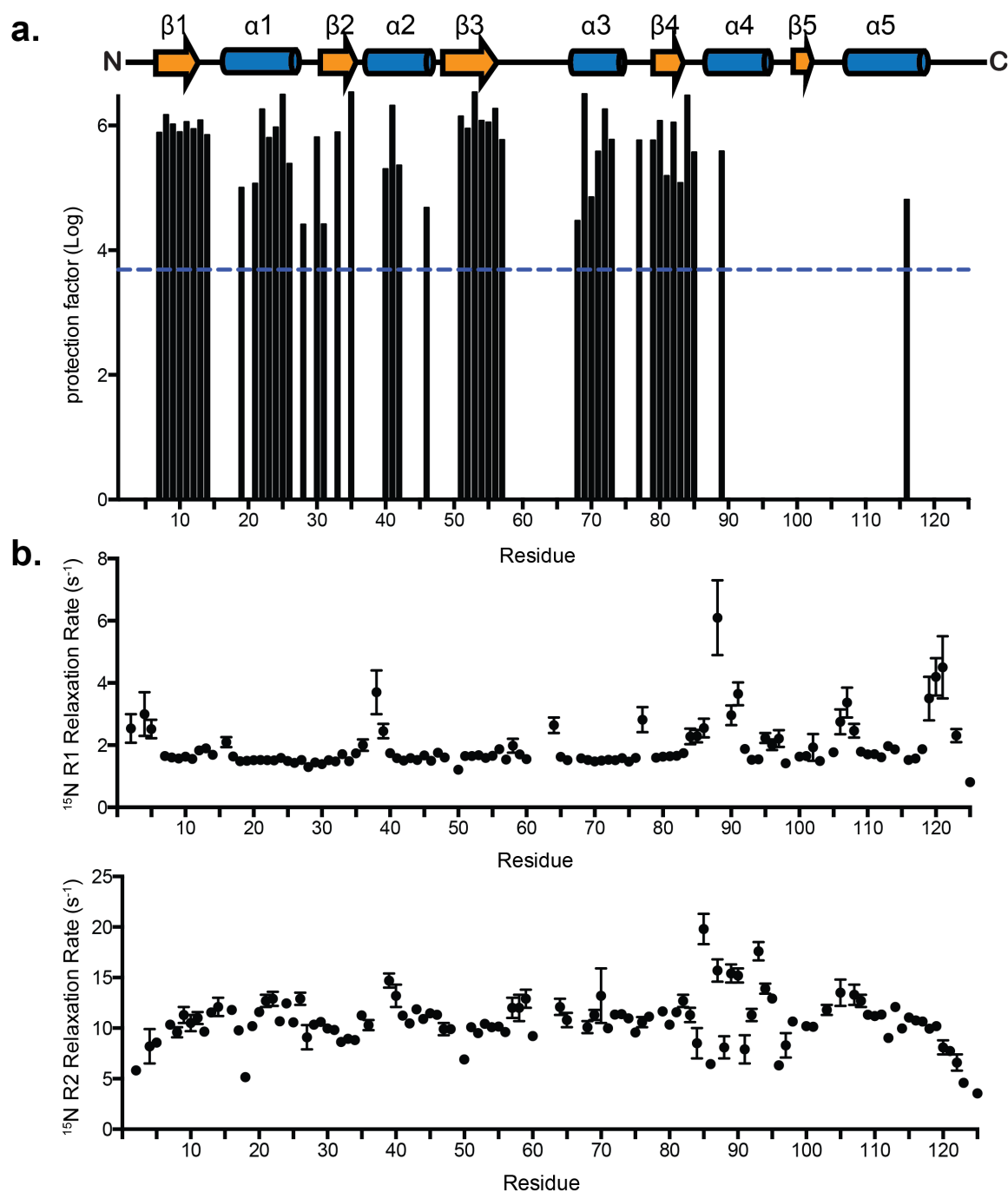


Figure 4.7 C-terminal region of EL_LovR ($\alpha 4/\beta 5/\alpha 5$) exhibit conformational exchange.

a) Protection factor measured in deuterium exchange experiments. The rate in which proton atoms in amide groups found in secondary structure elements exchange with deuterons was much slower when compared to atoms exposed to solvent. b) Spin lattice relaxation (R1) and spin-spin relaxation (R2) experiments show greater degree of conformational exchange at the C-terminus of EL_LovR

In contrast, we saw significant variability of both R_1 and R_2 values at several helical or strand sites in the $\alpha 4$ - $\beta 5$ - $\alpha 5$ region, implicating greater flexibility in these regions on the ms (R_2) and ns-ps (R_1 , R_2) timescales. Taken together, these data clearly establish a progression of increasing structure in EL_LovR by addition of Mg^{2+} and BeF_3^- ligands; the resulting fully-activated mimic state appears to contain all of the expected structural elements of a REC domain while remaining dynamic in an important region that is typically functionally important for dimerization and regulation of effector domains (2).

4.2.3 Solution structure of EL_LovR

Based on these observations, we sought to determine the NMR solution structure of activated EL_LovR to gain more insight into the structural features driving the ligand-induced folding process. Using standard solution NMR methods, we solved the structure of Mg^{2+} / BeF_3^- loaded EL_LovR with high precision (Figure 4.8a, Table 4.1), confirming that it adopts the canonical $(\beta\alpha)_5$ REC domain fold (3). Examination of the structure shows that the phosphoaccepting D56 is located at the end of $\beta 3$, adjacent to T83 on the subsequent $\beta 4$ strand. Furthermore, residues predicted to bind Mg^{2+} (E12, D13 and E14) are found in the loop region 1 (between $\beta 1$ and $\alpha 1$), positioning them within ~ 5 Å of the oxygen atom of D56. Interestingly, V100 occupies the predicted position of the conserved Phe/Tyr residues normally involved in the activation of REC domains (103,111). Additionally, the sidechain of a lysine residue (K103) also predicted to stabilize the active state of REC domains is oriented in close proximity to D56. All of these residues form a tight signaling network that runs from the N-terminal region of

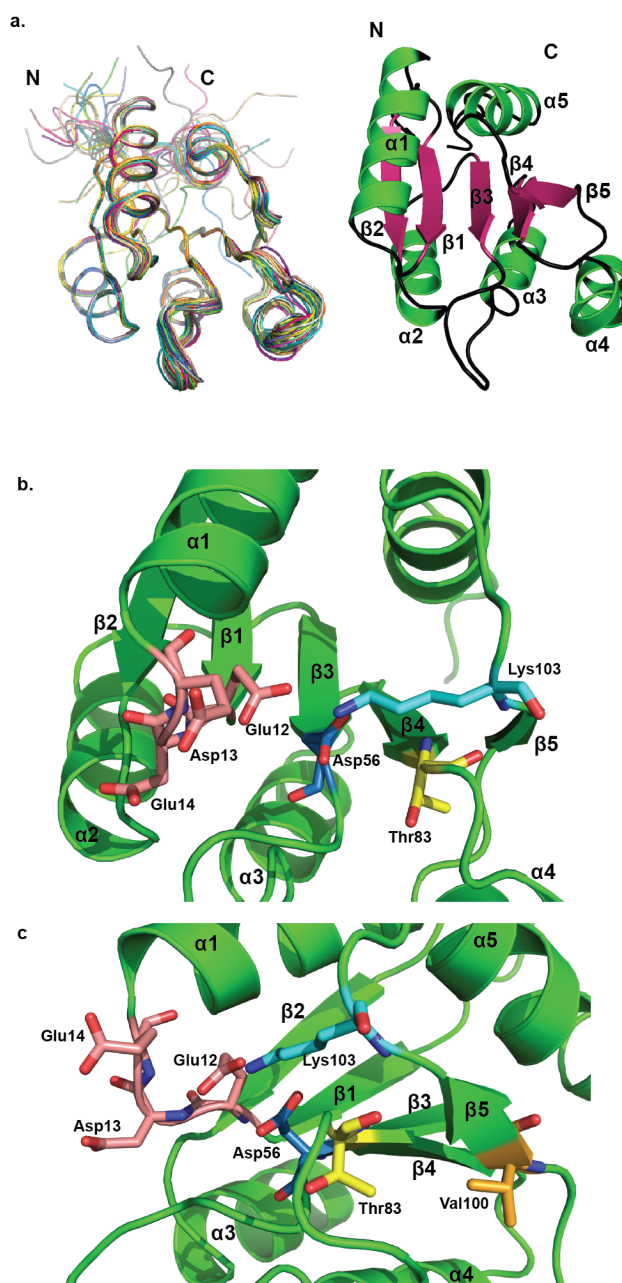


Figure 4.8 NMR solution structure of EL_LovR + Mg^{2+} + BeF_3^- .

a). Ensemble of twenty solution structure models of activated EL_LovR, as calculated by ARIA 2.2 (152) and ribbon diagram of lowest-energy structure. b). The EL_LovR active site is diagrammed, with key residues highlighted. Acidic residues involved in coordinating Mg^{2+} (E12, D13, E14) are indicated in pink; the phosphoaccepting D56 (blue) is positioned at the end of $\beta 3$ in close proximity to T83 (yellow), with the sidechain of the conserved K103 residue (cyan) oriented towards the active site to stabilize the active state. c). The $\alpha 4$ - $\beta 5$ - $\alpha 5$ region of EL_LovR, showing the locations of the D56 – T84 – V100 signaling pathway, where V100 occupies the position of the conserved tyrosine involved in “Y-T coupling” found in many REC domains (103,123).

NOE distance restraints	
Unambiguous	1766
Ambiguous	845
Hydrogen bond restraints	50
Dihedral angle restraints	178
Mean rmsd from experimental restraints	
NOE, Å	0.03 ± 0.001
Dihedral angles, °	0.4 ± 0.05
Average no. of	
NOE violations >0.5 Å	0.0
NOE violations >0.3 Å	0.5 ± 0.5
Dihedral violations >5°	0.0
Mean rmsd from idealized covalent geometry	
Bond lengths, Å	0.004 ± 0.0001
Bond angles, °	0.5 ± 0.01
Impropers, °	1.4 ± 0.06
Geometric analysis of residues 8-118	
rmsd from the mean	
Backbone atoms, Å	0.5 ± 0.1
All heavy atoms, Å	1.1 ± 0.1
Ramachandran analysis (PROCHECK)	
Most-favored region, %	91.2
Additionally allowed region, %	8.5
Generously allowed region, %	0.1
Disfavored region, %	0.2

Table 4.1 Statistics for EL_LovR solution structure determination.

EL_LovR (D12, E13, E14, D56) all the way to the C-terminus (T83, K103) allowing the protein to properly signal upon phosphorylation (109,110). In summary, our biophysical characterization of EL_LovR conclusively establishes that it has minimal structure in the apo form, progressively folds with the addition of Mg^{2+} and BeF_3^- , culminating in a properly-structured REC domain upon full activation.

4.2.4 Conserved residues involved in Mg^{+2} binding have a key role in structural changes of EL_LovR

With the presence of four closely-spaced acidic residues predicted for Mg^{2+} binding (E12, D13, E14 and D56), we hypothesized that repulsion among these negatively-charged residues in the EL_LovR active site would destabilize the protein in the absence of Mg^{2+} or another divalent cation, as previously observed for CheY (209). To test this possibility, we mutated these four acidic residues in EL_LovR to alanine, and examined the resulting effects on protein structure in the absence and presence of Mg^{2+} . For all four mutant proteins (E12A, D13A, E14A, D56A), we observed a lack of chemical shift changes upon adding $MgCl_2$, demonstrating that removal of these negatively-charged residues affected Mg^{2+} binding (Figure 4.9). While two of the mutant proteins, E12A and E14A, appear to be comparably unfolded as wildtype based on amide proton chemical shift dispersion (Figure 4.9), several qualities of the $^{15}N/^1H$ HSQC spectra of two other mutants (D13A and D56A) suggested that they no longer required Mg^{2+} to fold. SEC-MALS analysis of both point mutants and a D13A/D56A double mutant show shifts to later elution

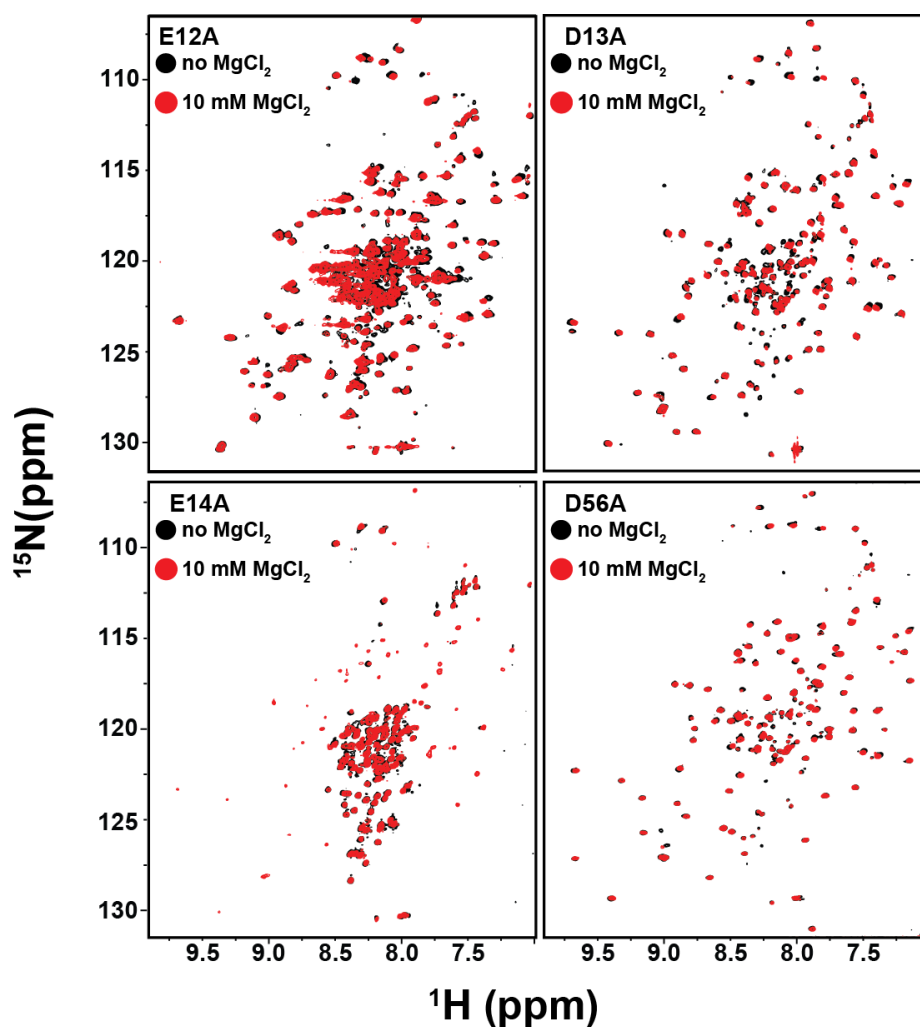


Figure 4.9 Structural effects of point mutations to the acidic Mg^{2+} -binding residues of EL_LovR.

$^{15}N/^{1}H$ HSQC spectra of EL_LovR E12A, D13A, E14A and D56A are shown in the absence of Mg^{2+} (black) or presence of 10 mM $MgCl_2$ (red). For all four cases, the minimal Mg^{2+} -induced chemical shift changes indicate these residues are all required for Mg^{2+} coordination. Additionally, the improved 1H chemical shift dispersion and uniform peak intensities of D13A and D56A (compared to the other mutants or wildtype protein, Fig. 4.4) indicate that these proteins have become folded without requiring ligand binding.

volumes on Superdex S200 gel filtration while the protein remains monomeric (Figure 4.10).

These shifts, reminiscent of changes observed upon phosphorylation in wildtype EL_LovR, are consistent with increased folding of the protein, underscoring the importance of the cluster of negatively-charged residues in destabilizing EL_LovR without ligand.

4.2.5 EL_LovR has a short-lived phosphorylated state

Genetic analyses of the *C. crescentus* LovR homolog of EL_LovR strongly suggest that it functions as a phosphate sink in stress response pathways in that organism (36,132), leading us to hypothesize a similar role for EL_LovR. We tested this possibility with a series of *in vitro* dephosphorylation assays, using the EL368 kinase to initially generate EL_LovR~P. Once this was completed, we added a non-hydrolyzable ATP analogue AMP-PNP to stop further incorporation of phosphate into the RR and allow solely dephosphorylation to occur. We observed the expected time-dependence of residual EL_LovR~P after AMP-PNP addition, with EL_LovR completely dephosphorylated after approximately 25 min (Figure 4.11). Fitting the time dependence of this process to a single exponential decay, we calculated the rate constant of dephosphorylation to be $k = 0.265 \text{ min}^{-1}$ (approximately a 2.5 min half-life) roughly comparable to CheY, a well-known phosphate sink (210). Coupled with our prior demonstration of EL_LovR promoting dephosphorylation of the EL_PhyR response regulator *in vitro* (63), these observations suggest that EL_LovR functions as a phosphate sink within *E. litoralis* stress response pathways.

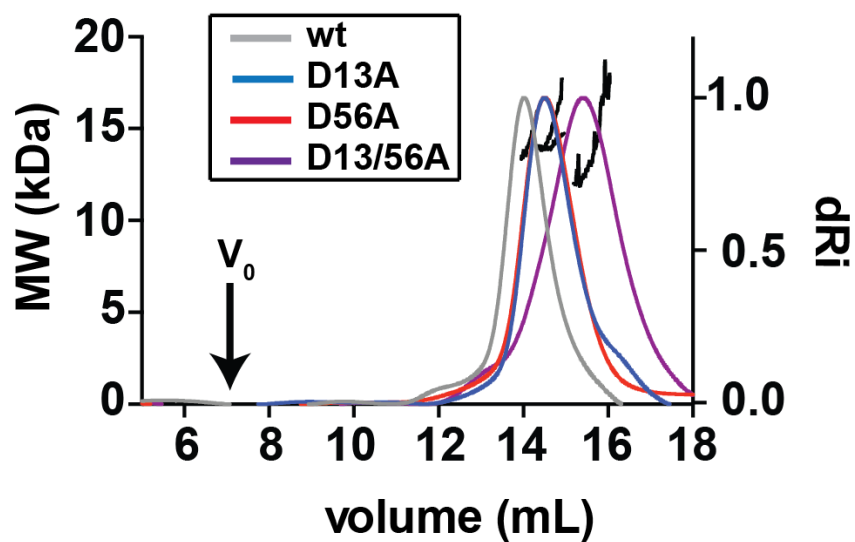


Figure 4.10 Mutation of conserved D13/D56 to alanine allows EL_LovR to fold in the absence of phosphate and Mg^{2+} .

SEC-MALS show that mutation of phosphoaccepting Asp (D56) and Mg^{2+} binding Asp (D13) to Ala induced a change in the structure toward the folded state.

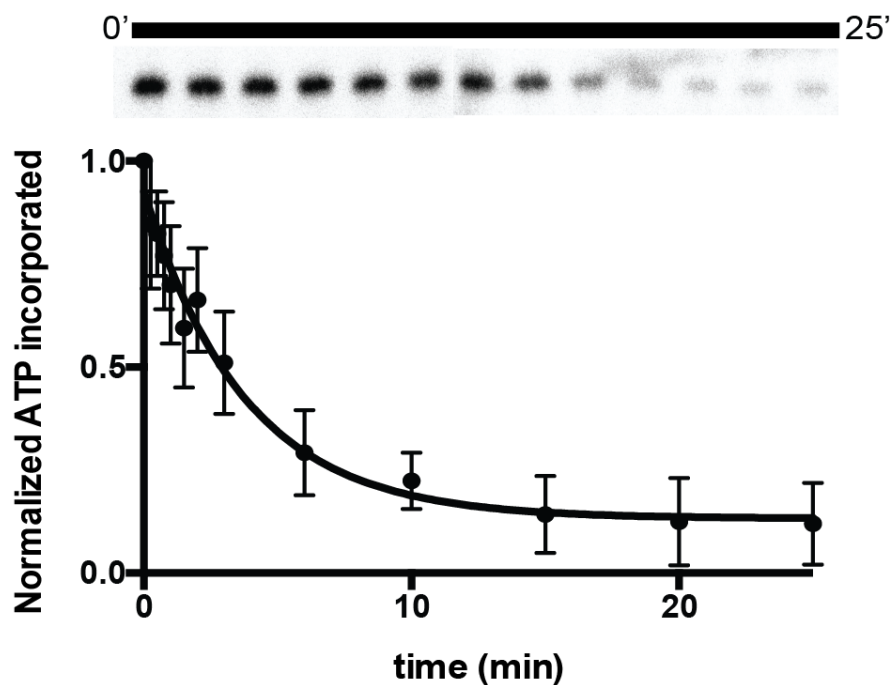


Figure 4.11 EL_LovR~P is short-lived *in vitro*.

EL_LovR was phosphorylated by EL368 for 10 min before treatment with 5 mM AMP-PNP to allow the monitoring of phosphate loss over the next 25 min. Normalized levels of incorporated ATP were plotted and fit with a first-order exponential decay to determine the dephosphorylation rate of EL_LovR~P ($k=0.265 \text{ min}^{-1}$). Error bars indicate the standard deviation of 3 independent experiments.

4.3 Discussion

REC domains are found almost in all TCS studied to date. They harbor the phospho-accepting aspartate and function as a switch to regulate a wide variety of functions that is dictated by the effector domain (86,211-213). Understanding how these molecular switches function upon phosphorylation has been of interest for many years. Special attention has been given toward few well-known RRs. Crystallographic and NMR studies have been performed on these proteins giving insight at what happens when the REC domain is phosphorylated by phosphate mimics (94,115-117,202,214). The mechanism of activation on RRs has been extensively described (97). Upon phosphorylation the phosphate group interacts with the hydroxyl group of a Ser/Thr located at β 4 strand. Subsequently, in what is known as the Y-T coupling, an aromatic residue in the β 5 strand rotates to fill the pocket previously occupied by the Ser/Thr residue (111). However, recent studies show evidence against the widely accepted Y-T coupling as a mechanism of activation (123). Mutation of the conserved Tyr to a Leu on NtrC did not impair its ability to be phosphorylated. This led to the hypothesis that the aromatic residue is important for downstream interactions (123). Other residues also play an important role in activation, for example a Lys at the β -strand 5 makes contacts to the phosphate and stabilizes the active state and negative charged residues (Asp/Glu) at the loop region 1 between β -strand 1 and α -helix 1 help coordinate a metal ion. Together all of this residues induce conformational changes at the α 4- β 5- α 5 interface, a region commonly used by REC domains to regulate function and protein-protein interactions (207).

To gain more insights as to how REC domain switch from an inactive to an active conformation many studies were focused on structural changes of REC domains upon phosphorylation. Many studies suggest that in solution REC domains are found in a preexisting equilibrium between inactive and active conformations (117,215-217). Biochemical and biophysical characterization revealed that EL_LovR, unlike other well studied RRs, exhibit significant conformational changes that are consistent of a protein going from a disordered to a folded state upon phosphorylation. NMR studies of the activated state of EL_LovR show that it adopts the conserved REC domain fold. Backbone chemical shift analysis shows that there is high probability of secondary structure throughout the protein. However, hydrogen-exchange and relaxation experiments suggested that the C-terminal region encompassing the α 4- β 5- α 5 interface is undergoing some degree of conformational exchange. This is comparable to a recently described SDRR, Sma0114 (203,204). NMR solution structure of this RR contains a disordered α 4 helix in the inactive and active state.

To characterize the conformational changes EL_LovR undergoes upon phosphorylation, SEC-MALS, limited proteolysis and ^{15}N - ^1H HSQC analyses were performed. EL_LovR has three distinct conformational states. When the protein is in solution without Mg^{2+} or phosphate it appears to be disordered with poor secondary structure elements present. Literature search of X-ray crystal structures and NMR structures of other RRs show that the REC domains remains folded in the inactive (94,107,108), active state (116,117,202) and even in the absence of Mg^{2+} (95,105). Recently a solution NMR structure of Sma0114, a SDRR found in *S. meliloti*, was solved which contains a disordered α 4-helix region in both the inactive and active state

(203,204). This provides evidence that there are other RRs that have not been characterized and have different features that diverge from classical REC domains. We believe that the significant conformational changes of EL_LovR fall in this category of REC domains with unusual structural features. For instance RRs that contain substitutions in the active site (close to the phosphoaccepting Asp) and conserved regions (for example, the β 4- α 5- β 5 interface) are prime candidates to have unusual characteristics that diverge from classical RRs.

Upon Mg^{2+} binding secondary structure elements at the N-terminal region, mainly β 1- α 1- β 2- α 2- β 3, of the molecule are stabilized. We hypothesize that stabilization of the N-terminus of EL_LovR upon Mg^{2+} binding plays an important role in priming the protein for phosphorylation by the HK, because the residues that makes contact to the kinase and dictate specificity are found in the α 1 helix of REC domains (218). Metal binding is very important for the phosphorylation of the REC. It is known that a set of negatively charged residues (Asp/Glu) in the loop region between α 1-helix and β 1-strand are required for efficient coordination of the phosphate group in the active site (104). Additionally, it has been shown that REC domains are capable of binding various metals like magnesium, calcium and manganese using these negatively charged residues (105,106). For example, in the bacterial chemotaxis protein CheY, Mg^{2+} induces slight conformational changes involving reorientation of the side-chain of D57, D13 and K109 to form hydrogen bonds in the active site (105). We believe that Mg^{2+} has a stabilizing effect to the structure of EL_LovR. ^{15}N - 1H HSQC, and backbone chemical shift assignment of EL_LovR incubated with 10 mM $MgCl_2$ showed high probability for secondary structure elements at the N-terminal half of the protein in contrast to

the apo-state (Figure 4.6). This region encompasses the α 1-helix, which determines specificity to the HK (196). This region contains the residues that coordinate Mg^{2+} (E12, D13 and E14) as mutation to alanine abolished chemical shift changes induced by the metal. Further examination of mutants that generated a well dispersed spectra (D13A, D56A and double mutant) by SEC-MALS show that removing some of these negatively charged residues allow the protein to become structured in the absence of Mg^{2+} (Figure 4.10). Based on these observations we suggest that the stabilizing effects generated by Mg^{2+} at the N-terminal half of EL_LovR primes the protein for efficient recognition by the HK and phosphotransfer.

RRs are capable of catalyzing the dephosphorylation reaction while others rely on accessory proteins to accelerate this reaction (219). Usually this reaction involves an asparagine or glutamine residue to coordinate a water molecule in the active site resulting in the hydrolysis of the phospho-Asp (219). Phosphatase assay of EL_LovR shows that it has a half-life of approximately 2 min. Closer examination of the sequence in the active site shows that an asparagine residue (N58) is in close proximity to D56. We believe that this residue is able to coordinate a water molecule and catalyze the dephosphorylation reaction of EL_LovR. Dephosphorylation assays of EL_LovR_(N58K) shows that the protein remains phosphorylated for at least 15 min (data not shown) when compared to wildtype protein. Additionally, the protein can only be phosphorylated by EL368 and not by small phosphodonors, like carbamoyl phosphate. This suggests that the longer sidechain of the lysine residue is blocking access to the small phosphodonors and water molecules prolonging the phosphorylated state of the protein, and obstacle that the HK can overcome possibly through conformational changes. Similar

results have been observed in mutational studies in CheY (210). Mutation of two residues N59 and E89 had an impact in the dephosphorylation rate of CheY.

Since SDRRs contain only a REC domain, sequence analysis to predict its physiological role is not productive. This led us to explore the implications of EL_LovR *in vivo*. *E. litoralis* is not a genetically tractable organism, but EL_LovR shares high similarity (>50%) to LovR, described in *C. crescentus*. This microorganism has been studied as a model of cell cycle regulation and cell differentiation and can be genetically manipulated with ease (220). When *C. crescentus* is under osmotic stress, a HK (PhyK) is activated and phosphorylates the cognate RR (PhyR) (132,221). Activation of this TCS results in activation of sigma T (SigT)-regulated genes. Among this genes are, *lovK* and *lovR* a light regulated TCS involved in cell attachment and negative regulation of stress response (132,174). Evidence suggests that LovR in combination with LovK act as a phosphatase to PhyR~P resulting in inactivation of genes that are regulated by SigT (132). Bioinformatics analysis shows that *E. litoralis* also contains homologous genes suggesting that these proteins might be functionally redundant. Initial *in vitro* experiments show that co-incubation of EL368 and EL_LovR induce dephosphorylation of EL_PhyR~P, giving indications that indeed this proteins act in a similar fashion to their counterparts in *C. crescentus* (63).

Taken together these studies provide evidence of a SDRR that has structural features that differ from characterized RRs. Its ability to undergo a unfolded to folded transition is an example of a new type of conformational changes a RR exhibit, which could have implications on the regulatory role of this protein.

Chapter 5 Functional analysis of EL_LovR: Using *C. crescentus* as a model

5.1 Introduction

Bacteria have different strategies to cope with changes in the environment. Two of the most common strategies used by bacteria are the use of sigma factors and TCSs. Sigma factors are a RNA polymerase subunit which allows for the recognition and initiation of transcription (222). Bacteria contain a housekeeping sigma factor responsible for the transcription of essential genes (223) and most contain additional alternative sigma factors used for the transcription of genes required for adaptive responses. Among the different classes of alternative sigma factors that can be found in a bacterial cell, the ECF sigma factors (SigT in *C. crescentus*) play an critical role in environmental adaptation (166). Often, the activity of this type of sigma factor is negatively regulated by an anti-sigma factor protein (NepR), which prevents association to the RNA polymerase (224,225). Another way bacteria can achieve changes in gene expression is through TCS pathways. As noted above an HK phosphorylates a RR in response to specific changes in the environment. The RR is usually a transcriptional regulator, which upon phosphorylation gets recruited to a promoter region and activates gene transcription.

Recently, a RR has been identified that incorporates both the TCS regulation and sigma factor mimicry to activate gene transcription called PhyR (166). PhyR contains an N-terminal

ECF sigma factor like (SL) domain and a C-terminal REC domain, which is phosphorylated by the cognate HK (PhyK). Additionally, bioinformatic analyses have shown that PhyR is conserved in α -proteobacteria (124,166). For example, in the α -proteobacteria *Methylobacterium extorquens* and *C. crescentus*, PhyR is responsible for the activation of many stress related genes (124,167,182). Biochemical and genetic studies have shown that SigT is negatively regulated by the anti-sigma factor NepR (Figure 5.1) (166). Upon stress (e.g. temperature shifts, oxidative stress, desiccation), the sensor HK PhyK phosphorylates PhyR, allowing the SL domain to bind NepR, resulting in activating gene transcription by SigT (166,182,221). In the α -proteobacteria *C. crescentus* and *E. litoralis*, the PhyK/PhyR TCS can be found with a similar genetic organization and high sequence identity (57%) for PhyR (Figure 5.2) (63). In *C. crescentus*, microarray data showed that upon osmotic stress SigT upregulates two genes involved in a blue light regulated TCS (*lovK/lovR*) (132). Genetic analysis demonstrated that LovK/LovR is responsible for light-regulated cell attachment and dephosphorylation of PhyR (36,132). More specifically, overexpression of LovK/LovR proteins resulted in repression of SigT activity (132).

Similarly to *C. crescentus*, *E. litoralis* contains such blue light regulated TCS (63).

Bioinformatics analyses suggest that the light regulated HK (EL362) and RR (EL_LovR) is SigT dependent (63). Furthermore, dephosphorylation assays showed that another light regulated HK (EL368) and EL_LovR dephosphorylate EL_PhyR *in vitro* (Figure 3.9) (63). One of the challenges in studying the *in vivo* implications of EL368/EL_LovR is that *E. litoralis* is not a genetically tractable organism. Given the fact that *E. litoralis* and *C. crescentus* proteins share

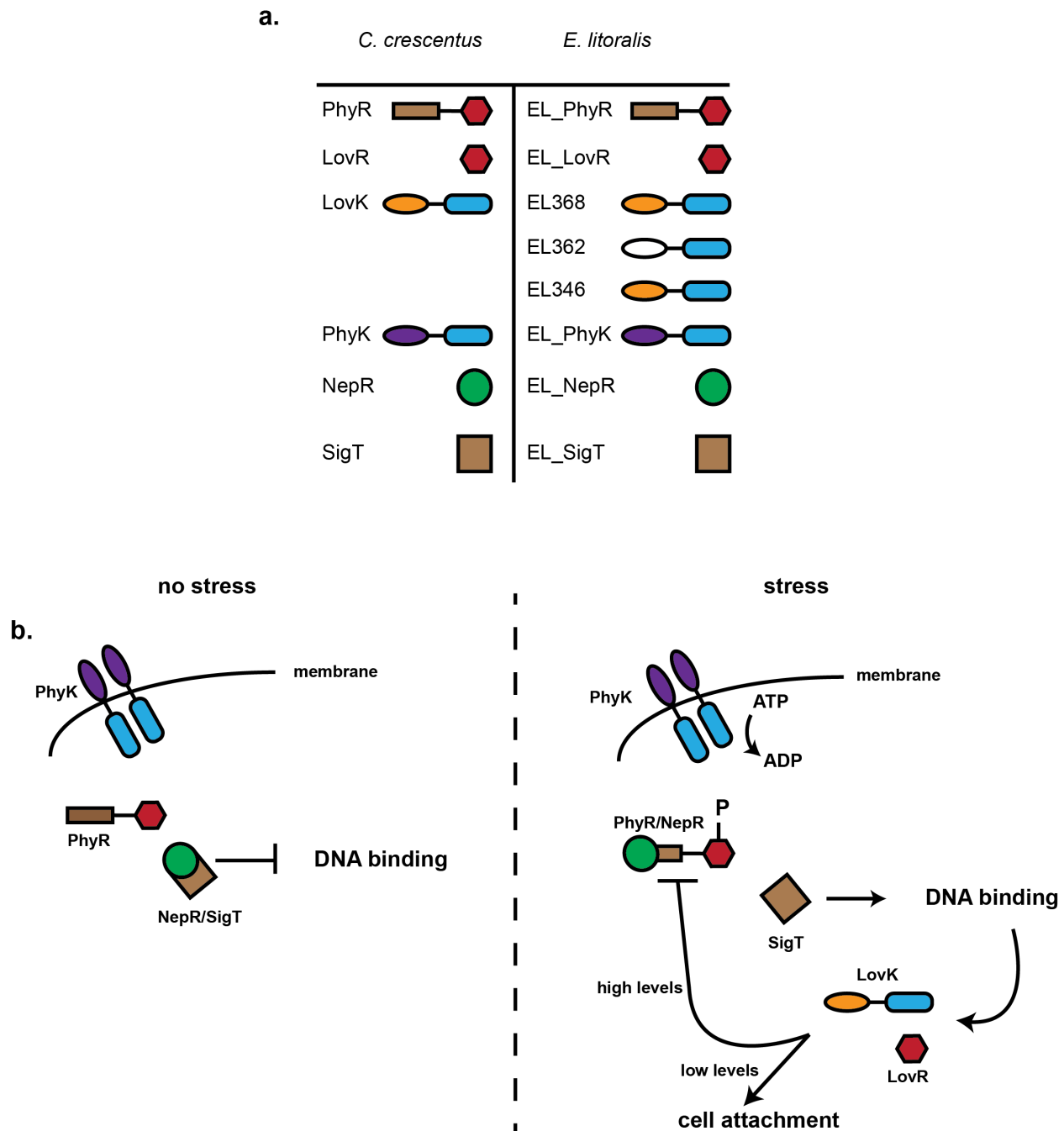


Figure 5.1 *C. crescentus* and *E. litoralis* TCS components.

a) Schematic representation of the light regulated TCS and stress TCS proteins of *C. crescentus* compared to the *E. litoralis* homologues. b) Proposed model of SigT regulation, modified from Foreman *et.al.* (132).

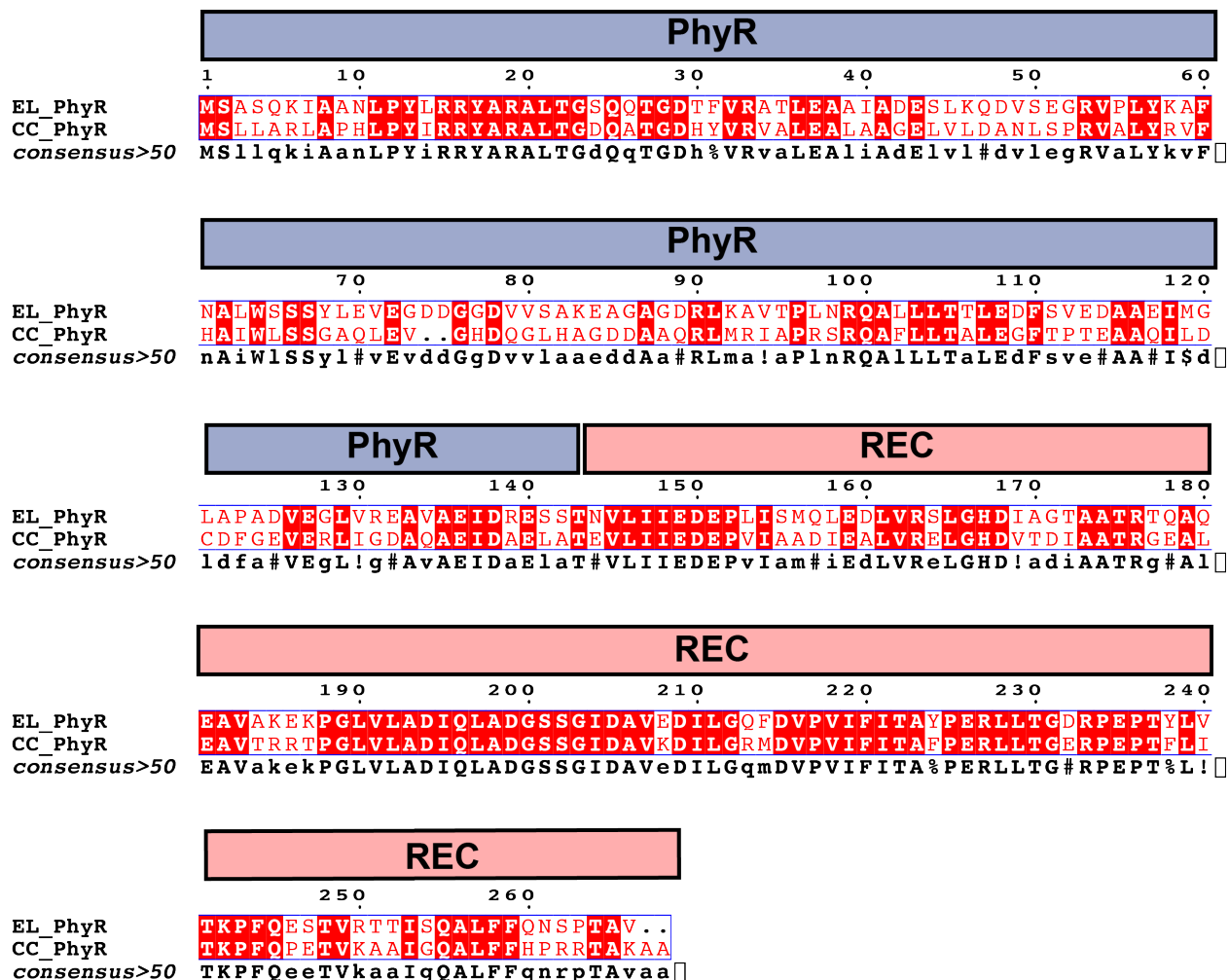


Figure 5.2 Sequence alignments of EL_PhyR and PhyR.

Sequence comparison between EL_PhyR and PhyR show high sequence conservation (57%).

high sequence similarity EL368/EL_LovR and EL_PhyR was ectopically expressed in the context of *C. crescentus*, to test for the ability of these proteins to repress SigT mediated gene transcription.

5.2 Results

5.2.1 Functional analysis of *E. litoralis* light regulated TCS

As described in chapter 3, biochemical and biophysical studies have shown that *E. litoralis* contains three LOV-HKs (EL346, EL362 and EL368) (63). These studies have shown that the kinase activities of EL368 and EL346 are enhanced upon blue light exposure. In contrast, EL362 contains a naturally occurring point mutation (glycine to arginine) in the core of the LOV domain that prevents chromophore binding. As a result, EL362 does not exhibit light dependent enhancement of kinase activity (63). Bioinformatics analysis also showed that EL362 forms an operon with the SDRR (EL_LovR), which is the typical organization of cognate TCS pairs. Finally, phosphotransfer profiling showed that all three LOV-HKs are able to phosphorylate EL_LovR, while EL_PhyR is only phosphorylated by EL368 and EL346 (63). This presented a complicated many-to-many signaling network, where three HKs target two RRs (63,101).

Like in *E. litoralis*, a light regulated TCS with similar features was identified in *C. crescentus*. Through genetic analysis, it was demonstrated that light enhances cell attachment (36). Additionally, it was shown that both the kinase (LovK) and the cognate RR (LovR), are

required for negative regulation of SigT (132). When *C. crescentus* is under stress (e.g. osmotic stress, oxidative stress) PhyK gets activated. This reaction leads to phosphorylation of the REC domain of PhyR allowing the sigma like domain binding to the anti-sigma factor NepR and activating SigT. The sigma factor recruits the RNA polymerase to stress related gene (e.g. LovK and LovR). LovK and LovR can sense light or redox state to regulate cell attachment (36). However, Foreman *et.al.* (132) have shown through genetic analysis that overexpression of LovK/LovR can dephosphorylate PhyR, which results in inhibition of SigT activity by NepR (Figure 5.1). These observations, together with the biochemical and biophysical data obtained from *E. litoralis* TCS, led us to propose that EL368, EL_LovR and EL_PhyR have similar roles to their homologues in *C. crescentus*.

5.2.2 EL368 and EL_LovR have specific phosphatase activity to EL_PhyR

To test the ability of *E. litoralis* TCS to functionally complement *C. crescentus* TCS, EL368/EL_LovR/EL_PhyR were ectopically expressed in a *C. crescentus* strain bearing a *lacZ* transcriptional fusion with the SigT consensus promoter. Genes encoding EL368 and EL_LovR proteins were cloned into a suicide vector containing vanillate or xylose inducible promoter (153), and electroporated into *C. crescentus* strains harboring a deletion of *lovK/lovR* genes. These cells were grown in 2 mL of minimal M2X media containing 0.15% xylose and 0.5 mM vanillate as sole carbon source for 1 hr. To induce osmotic stress, 150 mM sucrose (130 μ L) was added to the media and cells were grown for four hours in parallel to unstressed

cells (130 μ L water). After 4 hr, 200 μ L of cells were collected and added 50 μ L of chloroform to permeabilize the cells. Z-buffer was added to a final volume of 800 μ L (cells + Z-buffer) and mixed. Finally, 200 μ L of ONPG substrate was added and mixed thoroughly. The reaction time was recorded until a medium yellow color developed. The absorbance A_{420} of 1 mL of reaction was determined and miller units calculated as described in chapter 2.

C. crescentus strains harboring a *lacZ* transcriptional fusion with SigT promoter elements exhibited osmotic stress dependent activity (Figure 5.3). Deletion of LovK/LovR resulted in wild-type levels of *lacZ* activity, suggesting that phosphorylated PhyR levels did not decrease (Figure 5.3). Alternatively, *lacZ* activity was repressed in a *C. crescentus* strain overexpressing LovK/LovR (LovK⁺⁺/LovR⁺⁺) (Figure 5.3). Based on this observations we hypothesized that overexpressing EL368/EL_LovR will result in a similar phenotype. β -galactosidase activity of a *C. crescentus* strain overexpressing (*EL368/EL_lovR*) showed wild type levels of *lacZ* activity (Figure 5.3). This suggested that EL368/EL_LovR failed at dephosphorylating PhyR. To test this possibility, *in vitro* dephosphorylation assays of PhyR were performed in the presence of EL368/EL_LovR or LovR. Phosphate levels of PhyR did not decrease when EL_LovR or LovR were added to the reaction (Figure 5.4b, Figure 5.4c). This suggested that the phosphatase activity of EL368/EL_LovR is specific to EL_PhyR.

5.2.3 EL_PhyR can restore SigT dependent transcription to wild type levels

PhyR is a response regulator with an N-terminal sigma like (SL) domain and a

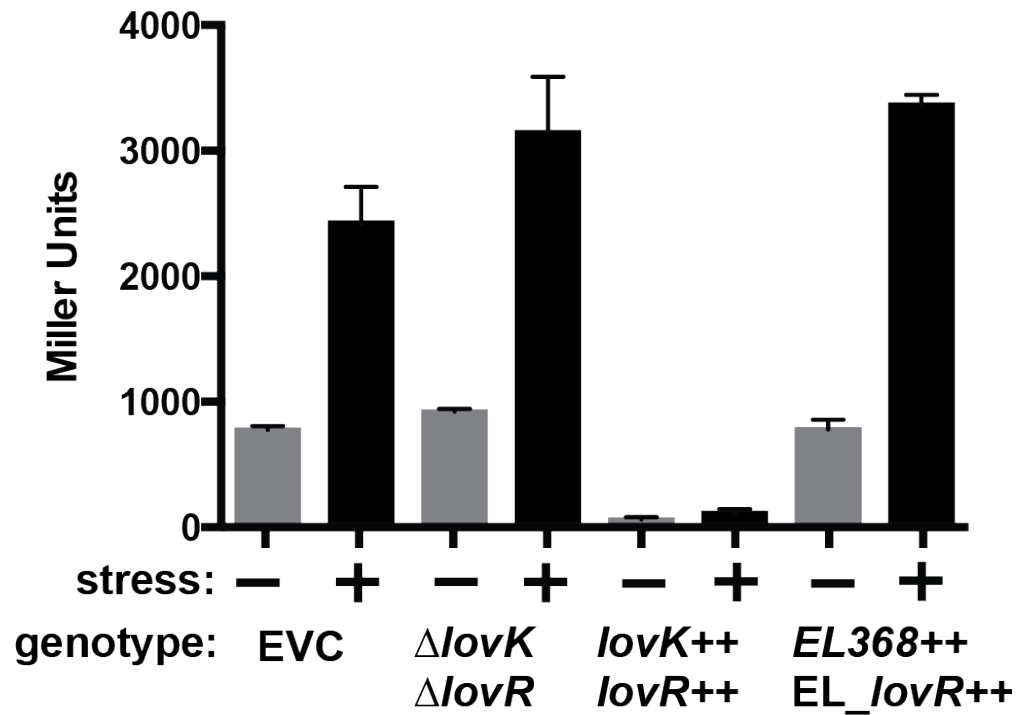


Figure 5.3 Overexpression of EL368/EL_LovR in *C. crescentus* containing P_{sigT} -lacZ transcriptional fusion results in wild type levels of SigT activity.

Overexpression of EL368 and EL_LovR did not have comparable expression to overexpression of LovK/LovR in *C. crescentus*. This suggests a failure of the HK and RR to interact with PhyR.

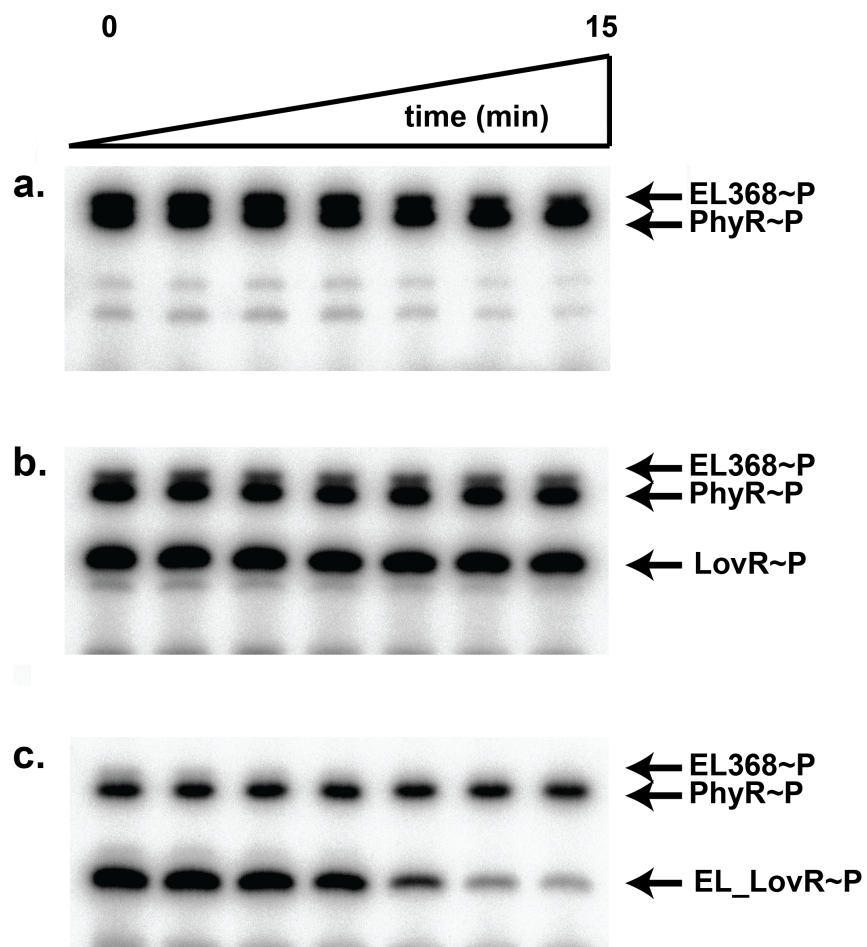


Figure 5.4 The presence of LovR or EL_LovR failed to induce phosphate loss of PhyR.

a) EL368 is able to phosphorylate PhyR. Addition of LovR (b) or EL_LovR (c) did not induce phosphatase activity towards PhyR. This suggests the phosphatase activity of EL368 is specific to EL_PhyR (63).

C-terminal REC domain, as shown by crystal structures of the full-length protein and the isolated SL domain in complex with the SigT inhibitor NepR (182,221). Additionally, biochemical characterization of PhyR has shown that upon phosphorylation of PhyR, the SL domain sequesters NepR allowing SigT to activate stress related gene transcription (166).

Bioinformatic analysis has shown that PhyR has high sequence similarity (57%) to EL_PhyR, suggesting that it might have a similar role in activating gene transcription of stress related genes in *E. litoralis*. To test this hypothesis, EL_ *phyR* was cloned in a suicide vector containing a xylose inducible promoter and electroporated into a *C. crescentus* strain with *phyR* deletion. Reporter assays showed that EL_PhyR was able to modestly increased *lacZ* activity when compared to wild type cells. This suggested one of three possible scenarios: 1) EL_PhyR was not able to effectively bind NepR, 2) EL_PhyR levels were low or 3) endogenous HK (LovK and PhyK) did not efficiently phosphorylate the protein.

To examine these possibilities, EL_PhyR and NepR were purified and subjected to SEC-MALS to test for interaction (Figure 5.5). The data indicates that phosphorylated EL_PhyR (~33.4 kDa) is able to bind NepR (~7.7 kDa), eluting at ~17 mL with a molecular weight ~44.4 kDa for the complex. This indicates that upon phosphorylation, EL_PhyR in *C. crescentus* should be sufficient for interaction and potential activation of SigT. To address the possibility of low levels of EL_PhyR in the cell, the gene was cloned in a different construct bearing a vanillate-inducible promoter. β -galactosidase assays of a *C. crescentus* strain harboring EL_ *phyR* under a vanillate inducible promoter restored SigT activity to wild type levels (Figure 5.6). Suggesting that the vanillate-inducible promoter is more robust when

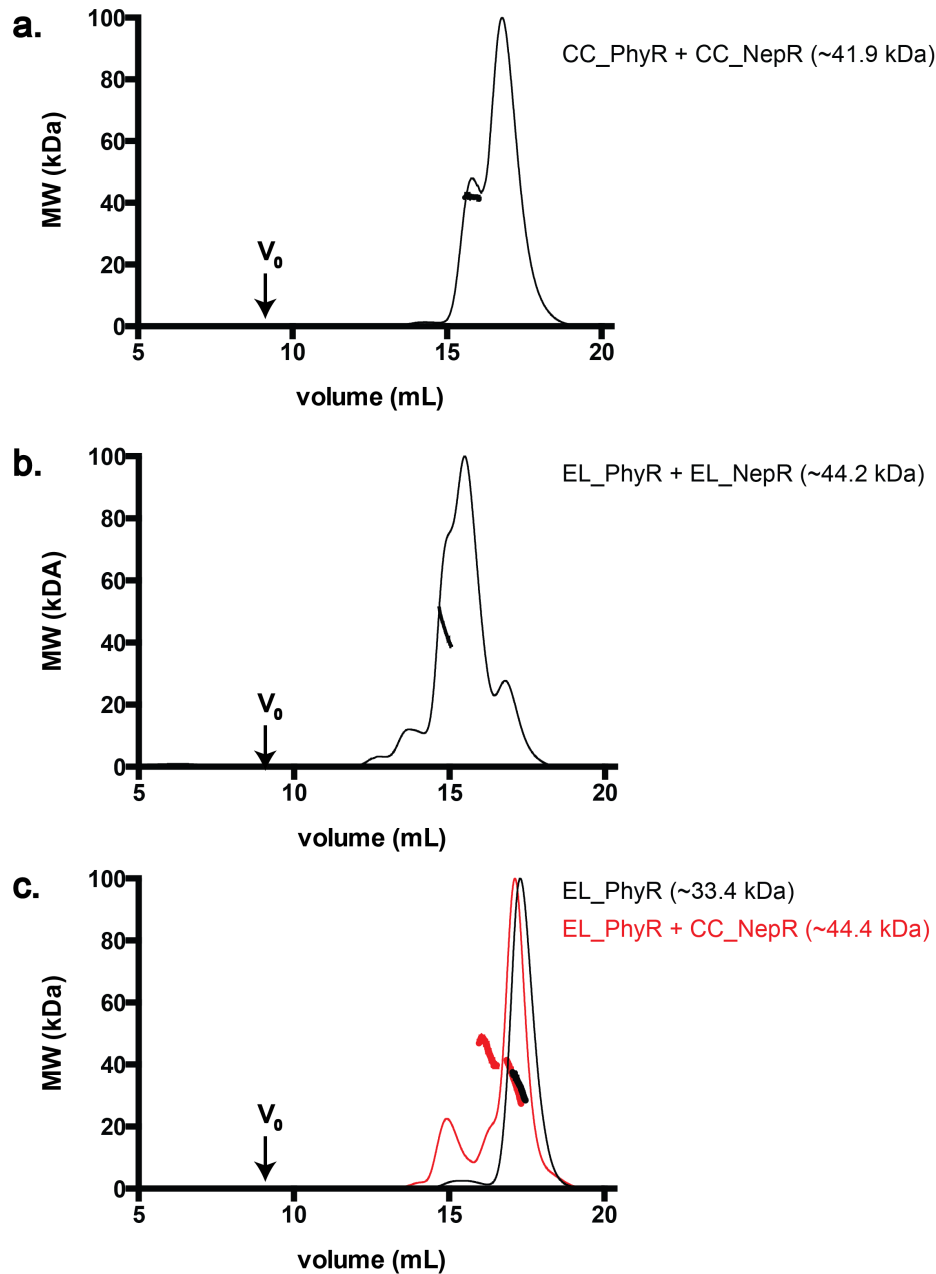


Figure 5.5 EL_PhyR can form a complex with NepR upon phosphorylation.

a) Phosphorylated PhyR (~34.9 kDa) is able to form a complex with CC_NepR (~7.7 kDa) with a molecular weight of ~41.9 kDa. b) EL_NepR (~6.1 kDa) can form a complex with phosphorylated EL_PhyR (~33.4 kDa) with a molecular weight of ~44.2 kDa. c) Phosphorylation of EL_PhyR (~33.4 kDa) is able to interact with CC_NepR (7.7 kDa) forming a 44.4 kDa complex.

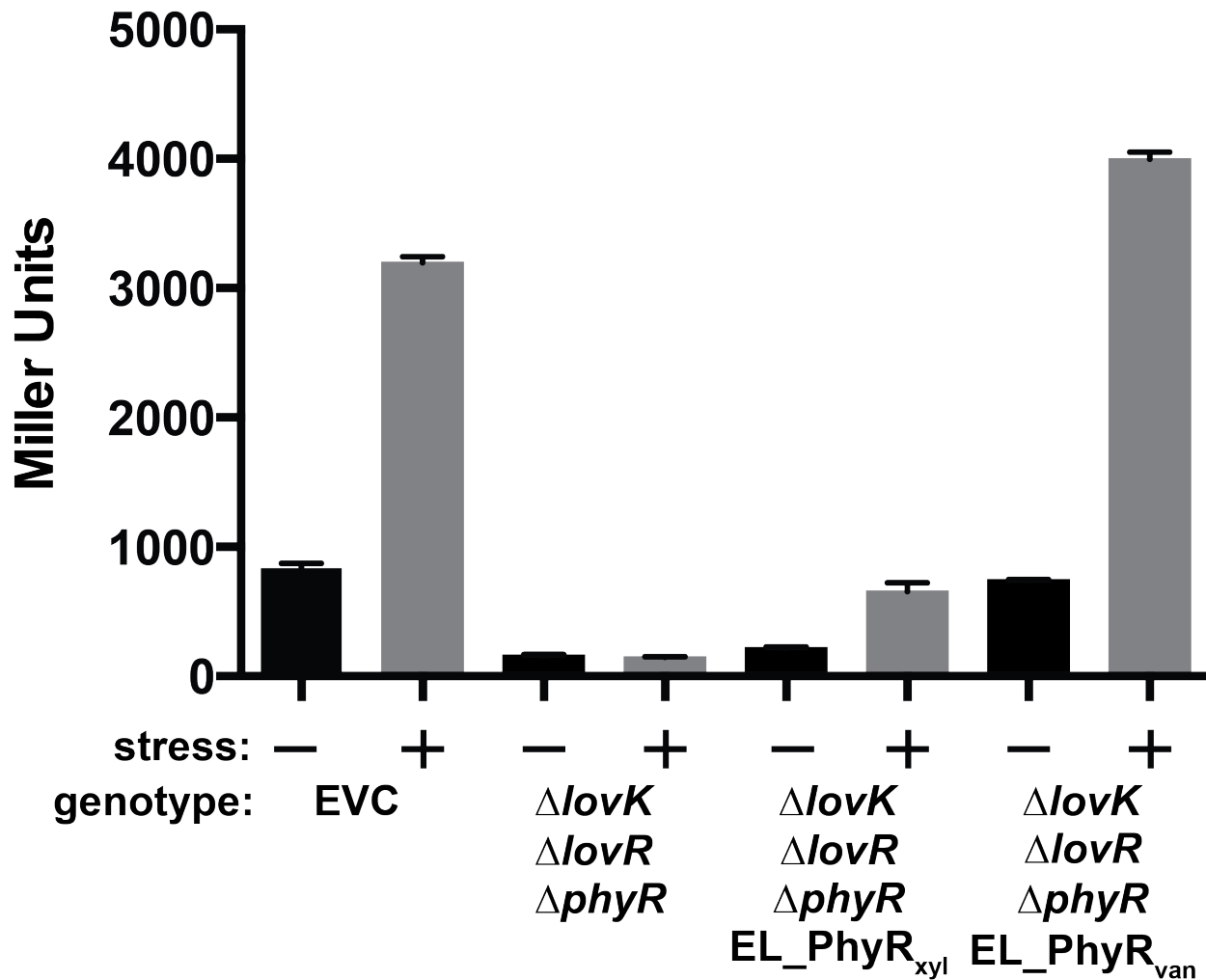


Figure 5.6 EL_PhyR expression under control of a vanillate-inducible promoter is able to restore SigT activity to wild type levels.

Overexpression of EL_{phyR} in *C. crescentus* strain bearing a deletion in *lovK/lovR* and *PhyR* gene is able to restore SigT activity under osmotic stress. Suggesting that EL_PhyR is functionally redundant to PhyR.

compared to the xylose-inducible promoter. These data demonstrated that EL_PhyR is capable of being phosphorylated by endogenous HK (PhyK) and activate SigT under osmotic stress.

5.2.4 EL368/EL_LovR/EL_PhyR results in hyper-activation of sigT dependent transcription

Expression of EL368 and EL_LovR in *C. crescentus* resulted in wild type levels of SigT activation. Additionally, in chapter 3 it was shown that EL368/EL_LovR acts as a phosphatase specifically to EL_PhyR (Figure 3.9). In light of these observations, a triple mutant *C. crescentus* strain with deletions of *lovK*, *lovR* and *phyR* was complemented with *E. litoralis* homologues under vanillate-inducible promoter. β -galactosidase assay of this strain under osmotic stress resulted in overall increased *lacZ* activity (Figure 5.7). These results suggested that increased levels of phosphorylated EL_PhyR resulted in *higher activation* of SigT-regulated transcription in the absence of osmotic stress, possibly due to high levels of EL368 present in the cell.

5.3 Discussion

Functional characterization of protein signaling networks in an organism that is not genetically tractable can be challenging. One way to circumvent this problem is the expression of proteins in a different organism that contains a homologous system (226,227). *E. litoralis* is not a genetically tractable microorganism (V. Ocasio, G. Rivera-Cancel, unpublished data),

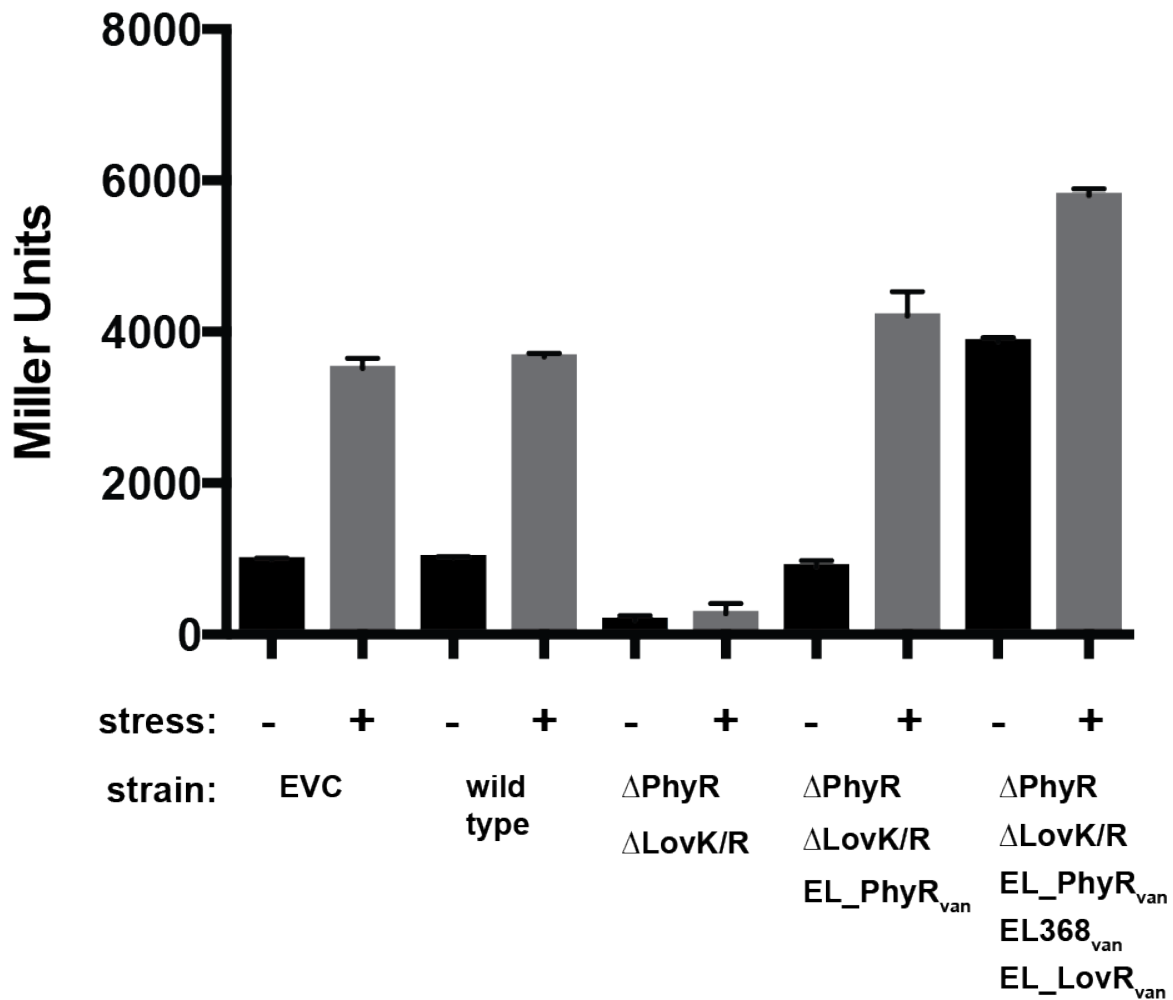


Figure 5.7 Overexpression of EL_368, EL_lovR, EL_phyR results in hyper activation of SigT activity.

Overexpression of *E. litoralis* proteins results in high SigT activity in the absence of osmotic stress. Upon addition of 150 mM sucrose, SigT activity increases even further. This suggests that high levels of EL368 and endogenous levels of CC_PhyK phosphorylate EL_PhyR, resulting in higher activity for SigT.

which makes *in vivo* functional analysis very challenging. To understand how the light regulated TCS from *E. litoralis* works, we tested the *in vivo* implications of expressing EL368, EL_LovR and EL_PhyR in the context of *C. crescentus* strains with deletions in the LovK/LovR TCS. Previous work has demonstrated that *E. litoralis* provides three soluble LOV-HKs, which respond to blue light and two cognate RRs, making this an excellent system for *in vitro* characterization (63). In contrast, *C. crescentus* is a microorganism that can be genetically manipulated with ease (220), which allows for *in vivo* functional analysis. But despite the ease of genetic manipulation, the *C. crescentus* LOV-HK and cognate RR proteins are not well behaved *in vitro* (V. Ocasio, F. Correa, unpublished results, S. Crosson, personal communication). For instance, multiple attempts to show *in vitro* phosphorylation of LovR by LovK have been unsuccessful. For this reason, we combined *C. crescentus* genetics and the biochemical and biophysical data provided by the *E. litoralis* TCS to test the function of these proteins within *C. crescentus* context.

It has been shown that EL368/EL_LovR induces dephosphorylation of EL_PhyR *in vitro* (63). Similarly, in *C. crescentus*, transcriptional reporter assays demonstrated that LovK/CC_LovR work together to dephosphorylate PhyR, resulting in negative regulation of SigT (132). Based on this evidence, we sought to ectopically express EL368/EL_LovR/EL_PhyR in a *C. crescentus* strain bearing a *sigT* transcriptional reporter, to test if these proteins are functionally redundant to LovK/LovR/PhyR. These experiments showed that EL_PhyR could functionally complement PhyR, increasing SigT dependent transcription under osmotic stress. This indicated that PhyK could phosphorylate EL_PhyR and

activate SigT dependent gene transcription. Additionally, SEC-MALS data confirm that phosphorylated EL_PhyR is capable of interacting with CC_NepR, as shown by the shift in elution volume and a molecular weight that corresponds to the complex ~44.4 kDa.

In contrast, addition of EL368/EL_LovR alone was not sufficient to negatively regulate SigT dependent transcription. Although, *in vitro* phosphorylation assays demonstrated that EL368 is capable of phosphorylating PhyR, it cannot act as a phosphatase in the presence of EL_LovR or LovR (Figure 5.3). This implies that EL368 is a bifunctional kinase that has specific phosphatase activity towards EL_PhyR. HKs with phosphatase activity have been described previously. For example, the osmosensor protein EnvZ is known to act as a kinase and a phosphatase to the cognate RR OmpR (228,229). Additionally, other HKs that exhibit both kinase and phosphatase activity toward their cognate RRs are CpxA and CheA (230,231).

Because EL368 has specific phosphatase activity to EL_PhyR, *C. crescentus* was complemented with EL368/EL_LovR/EL_PhyR, to test for specific dephosphorylation of EL_PhyR *in vivo*. Transcriptional reporter assays performed under osmotic stress resulted in higher SigT dependent transcription when compared to wild type. This result indicates that there are increased levels of phosphorylated EL_PhyR in the absence of osmotic stress, which could explain the increased SigT activity in the absence of osmotic stress. Overexpression of EL368 in combination with endogenous levels of PhyK could be responsible for the “hyper phosphorylation” of EL_PhyR *in vivo* in the absence of osmotic stress (Figure 5.7). This suggests that careful control and regulation of EL368 or EL_PhyR levels might be required to observed negative regulation of SigT activity.

5.4 Conclusion

In conclusion, this work provides preliminary data on the *in vivo* implications of EL368/EL_LovR/EL_PhyR. Transcriptional reporter assays have shown that EL_PhyR can functionally complement PhyR, by activating SigT upon osmotic stress. Additionally, dephosphorylation assays showed that EL368 is a bifunctional kinase, with specific phosphatase activity towards EL_PhyR. Further biochemical and genetic analysis will not only help understand the mechanism of dephosphorylation of EL_PhyR by EL368, but improve our knowledge on the complex crosstalk and regulation of TCS.

Chapter 6 Conclusions

It has been over two decades since TCS were initially described (1), with considerable amount of information about how these systems affect bacteria. However, there are still open questions about activation and regulation of TCS. For instance, the molecular mechanisms of HK activation by the sensor domains is not fully understood. Identification of activating environmental stimuli, membrane association and poor biochemical behavior has been one of the main reasons that has hampered the characterization of such systems. It is clear that in the near future many of these questions will be answered as more full-length structures of HKs become available. The work presented here aims at answering some of the questions by using a light regulated TCS from the marine α -proteobacterium *E. litoralis*. This bacterium contains three soluble HKs with a LOV domain as the sensor domain (EL346, EL362 and EL368). This work takes advantage of existing knowledge on PAS and LOV domains to understand the interaction between the sensor domain and the kinase core (159,232,233). It has been previously shown that that EL368 and EL346 exhibit light dependent kinase activity, giving us a valuable tool to study how an environmental stimulus activates an HK. Additionally, biochemical characterization of EL362 showed that a naturally occurring point mutation (G150R) in the LOV domain, prevented chromophore binding (63). This resulted in the HK not exhibiting light dependent kinase activity. Reverting the point mutation restored chromophore binding and light dependent kinase activity.

Full-length structures of HKs have been very scarce. The membrane bound natures of many HKs have impeded structural characterization. Structural biology in this area, as in others, has relied on the “divide and conquer” strategy, where structures of fragments have been solved and complemented with genetic and biochemical evidence to support the findings. Structures of the entire cytoplasmic region of HKs have been solved, revealing details of how the CA domain is able to contact the DHp domain for the autophosphorylation reaction (78,79). Recently, a crystal structure of full-length EL346 was solved by Rivera-Cancel *et.al.*, 2014 (submitted). EL346 is a monomeric HK that consists of a N-terminal LOV domain a DHpL (DHp like) domain and a CA domain. Mutational analysis have revealed that key residues between the LOV and DHpL domain, as well as the DHpL and CA domain are important for the light dependent activation. This is an example of how the light regulated TCS found in *E. litoralis* are helping to answer many existing question of HK regulation and activation.

RRs execute specific functions in the cell, and like the HKs, have been extensively studied for the past two decades. Early studies on the nitrogen assimilation pathway and bacterial chemotaxis in *E. coli* have shown that these proteins are essential and versatile (1,16). Additionally, it has been demonstrated that in some microorganisms like *S. typhimurium*, *B. abortus* and *S. aureus*, TCS play a critical role in the infectious process with typically a RR activating transcription of virulence genes (4,53,234). Even though a wealth of information is known about RRs, there are still open questions about the activation of these signaling molecules. For instance, structural work, coupled to mutational and biochemical analysis of a few REC domains of RRs (e.g. NtrC, CheY) has shed some light at what residues are critical for

phosphorylation and activation (95,97,116,117). These studies have shown that REC domains are in often equilibria between two folded states, inactive and active conformations.

Additionally, as more structures of full-length RRs have been solved, it has been suggested that the activation of the REC domain is greatly influenced by the output domain. For example, work done by Barbieri *et.al.* (235) showed that the rates of RR phosphorylation are affected by the size and type of domain interface between REC and output domain. Phosphorylation with small phosphodonors (i.e. acetyl phosphate) of RRs with substantial domain interface exhibited slow phosphorylation rates. In contrast, increased phosphorylation rates were observed in RRs with small domain interface and isolated REC domain constructs. In contrast, phosphorylation rates of full-length RR and isolated REC domain using the cognate HK, did not exhibit any difference. This suggested that the interface between REC and output domain restricts the conformational dynamics of the REC domain, stabilizing the inactive conformation and preventing phosphorylation by small phosphodonors. More recently, Corrêa *et. al.* (manuscript in preparation) has shown that the removal of the SL domain of *E. litoralis* EL_PhyR allows the REC domain to adopt an active-like conformation. This agrees with previous observations that the interaction between REC and output domains stabilizes the inactive conformation of the REC domain until phosphorylation by the HK.

This work aims to provide more information on RR activation upon a known environmental stimulus (blue light). Previous work identified two cognate RR that are targeted by the light regulated TCS in *E. litoralis* (63). EL_PhyR is an anti-anti sigma factor RR identified to play an important role in stress response in α -proteobacteria. The second RR identified by

phosphotransfer profiling was EL_LovR, a SDRR. Biochemical and biophysical analysis suggested that this RR might play a similar role to LovR in *C. crescentus*. In this work I was able to solve a high resolution NMR structure of EL_LovR in the active state. Additionally, I observed that EL_LovR differs in the conformational changes a RR undergoes upon activation. It was determined by four independent methods that EL_LovR is in a partially disordered state when inactive and quickly becomes folded upon Mg^{2+} binding and phosphorylation. Furthermore, EL_LovR exhibits three distinct states *in vitro*, 1) mostly disordered state in the absence of Mg^{2+} , 2) partially disordered state in the presence of Mg^{2+} and 3) folded state in the presence of $Mg^{2+} + BeF_3^-$ or phosphate. This differs substantially from the two state equilibrium model, previously described for the activation of many RRs (117). Finally, mutations of residues predicted to bind Mg^{2+} altered the folding state of EL_LovR, suggesting that these residues (E12, D13, E14 and D56) play an important role in the phosphorylation mediated folding of EL_LovR. Similarly, in the α -proteobacterium *S. meliloti*, the solution structure of the SDRR Sma0114 in the active and inactive state was determined (203,204). Even though Sma0114 adopts the $(\beta\alpha)_5$ fold of REC domains, the $\alpha 4$ region is disordered in the inactive and active state. This example and the work presented here with EL_LovR illustrate that there are many more RRs to be described that may not follow the established model of activation.

The physiological role of the light regulated TCS in *E. litoralis* has not been determined. Through comparison of a homologous light regulated TCS in *C. crescentus*, it has been proposed that EL346/EL368/EL362 and EL_PhyR/EL_LovR have a role in the stress response pathway.

Initial *in vitro* dephosphorylation assays show that EL_PhyR is dephosphorylated in the presence of EL368 and EL_LovR. A similar observation was suggested in transcriptional reporter assays in *C. crescentus* (132), where overexpression of LovK/LovR dephosphorylates PhyR resulting in negative regulation of the stress response sigma factor SigT. All of these observations are supported by genetic analysis of *C. crescentus* strains harboring deletions in one or more components of the stress response pathway. These observations, in combination with the dephosphorylation of EL_PhyR *in vitro*, led to the hypothesis that the light regulated TCS in *E. litoralis* has a similar role. *E. litoralis* is not a genetically tractable organism, making the *in vivo* functional characterization a very challenging task. However, bioinformatic analysis shows that the genetic organization of the TCS and stress response pathway is very similar to *C. crescentus*. This would allow us to harness the genetic tools provided by *C. crescentus* and the *in vitro* data obtained from *E. litoralis* to test the physiological role of these proteins.

Overexpression of EL368/EL_LovR/EL_PhyR in *C. crescentus* strains harboring a transcriptional reporter of *sigT* was performed. With these assays it was demonstrated that upon osmotic stress, EL_PhyR is able to activate the stress response pathway in *C. crescentus*. This represents the first *in vivo* evidence of the physiological role of EL_PhyR. Based on these results, it is expected that upon stress response EL_PhyR will activate the stress response pathway in *E. litoralis*. Work is still ongoing in testing the physiological role of EL368 and EL_LovR. Transcriptional reporter assays of *C. crescentus* strains harboring overexpression constructs of EL368/EL_LovR/EL_PhyR exhibited increased SigT activity in the absence of osmotic stress. These data indicates increased levels of phosphorylated EL_PhyR in the

absence of osmotic stress, likely due to high levels of EL368 present in the cell. Additional experiments modulating the concentration of the inducer to regulate protein levels in the cell will help determine if EL368 and EL_LovR can dephosphorylate EL_PhyR *in vivo*.

The work presented here provides extensive *in vitro* biochemical and biophysical characterization of a light regulated TCS in the marine α -proteobacteria *E. litoralis*. We showed that one of the LOV-HKs (EL362) contain a natural point mutation (G150R) that prevents chromophore binding. Additionally, it was demonstrated that the cognate RR (EL_LovR) undergoes a phosphorylation mediated folding event. Solution NMR structure of EL_LovR shows the protein adopts the canonical REC domain fold in the active state. Additional NMR experiments will help gather more details on EL_LovR extensive conformational changes. Finally, initial transcriptional reporter assays done in *C. crescentus* were aimed at demonstrating for the first time the physiological role of EL368/EL_LovR/EL_PhyR *in vivo* in the context of *C. crescentus* biology. Taken together, this work expands the knowledge on HK activation and the kinds of conformational changes RR undergo upon phosphorylation.

REFERENCES

1. Nixon, B. T., Ronson, C. W., and Ausubel, F. M. (1986) Two-component regulatory systems responsive to environmental stimuli share strongly conserved domains with the nitrogen assimilation regulatory genes *ntrB* and *ntrC*. *Proc Natl Acad Sci U S A* **83**, 7850-7854
2. Gao, R., Mack, T. R., and Stock, A. M. (2007) Bacterial response regulators: versatile regulatory strategies from common domains. *Trends Biochem Sci* **32**, 225-234
3. Gao, R., and Stock, A. M. (2009) Biological insights from structures of two-component proteins. *Annu Rev Microbiol* **63**, 133-154
4. Novick, R. P. (2003) Autoinduction and signal transduction in the regulation of staphylococcal virulence. *Mol Microbiol* **48**, 1429-1449
5. Mitrophanov, A. Y., and Groisman, E. A. (2008) Signal integration in bacterial two-component regulatory systems. *Genes Dev* **22**, 2601-2611
6. Purcell, E. B., Boutte, C. C., and Crosson, S. (2008) Two-component signaling systems and cell cycle control in *Caulobacter crescentus*. *Adv Exp Med Biol* **631**, 122-130
7. Hazelbauer, G. L., and Lai, W. C. (2010) Bacterial chemoreceptors: providing enhanced features to two-component signaling. *Curr Opin Microbiol* **13**, 124-132
8. Mizuno, T. (1997) Compilation of all genes encoding two-component phosphotransfer signal transducers in the genome of *Escherichia coli*. *DNA Res* **4**, 161-168

9. Galperin, M. Y. (2004) Bacterial signal transduction network in a genomic perspective. *Environ Microbiol* **6**, 552-567
10. Schultz, J., Milpetz, F., Bork, P., and Ponting, C. P. (1998) SMART, a simple modular architecture research tool: identification of signaling domains. *Proc Natl Acad Sci U S A* **95**, 5857-5864
11. Letunic, I., Doerks, T., and Bork, P. (2012) SMART 7: recent updates to the protein domain annotation resource. *Nucleic Acids Res* **40**, D302-305
12. Galperin, M. Y. (2010) Diversity of structure and function of response regulator output domains. *Curr Opin Microbiol* **13**, 150-159
13. Ninfa, A. J., and Magasanik, B. (1986) Covalent modification of the glnG product, NRI, by the glnL product, NRII, regulates the transcription of the glnALG operon in *Escherichia coli*. *Proc Natl Acad Sci U S A* **83**, 5909-5913
14. Sperandio, V., Mellies, J. L., Nguyen, W., Shin, S., and Kaper, J. B. (1999) Quorum sensing controls expression of the type III secretion gene transcription and protein secretion in enterohemorrhagic and enteropathogenic *Escherichia coli*. *Proc Natl Acad Sci U S A* **96**, 15196-15201
15. Sperandio, V., Torres, A. G., and Kaper, J. B. (2002) Quorum sensing *Escherichia coli* regulators B and C (QseBC): a novel two-component regulatory system involved in the regulation of flagella and motility by quorum sensing in *E. coli*. *Mol Microbiol* **43**, 809-821
16. Kuo, S. C., and Koshland, D. E., Jr. (1987) Roles of cheY and cheZ gene products in

- controlling flagellar rotation in bacterial chemotaxis of *Escherichia coli*. *J Bacteriol* **169**, 1307-1314
17. Borkovich, K. A., Kaplan, N., Hess, J. F., and Simon, M. I. (1989) Transmembrane signal transduction in bacterial chemotaxis involves ligand-dependent activation of phosphate group transfer. *Proc Natl Acad Sci U S A* **86**, 1208-1212
 18. Novick, R. P., Ross, H. F., Projan, S. J., Kornblum, J., Kreiswirth, B., and Moghazeh, S. (1993) Synthesis of staphylococcal virulence factors is controlled by a regulatory RNA molecule. *EMBO J* **12**, 3967-3975
 19. Lina, G., Jarraud, S., Ji, G., Greenland, T., Pedraza, A., Etienne, J., Novick, R. P., and Vandenesch, F. (1998) Transmembrane topology and histidine protein kinase activity of AgrC, the agr signal receptor in *Staphylococcus aureus*. *Mol Microbiol* **28**, 655-662
 20. Trach, K., Burbulys, D., Strauch, M., Wu, J. J., Dhillon, N., Jonas, R., Hanstein, C., Kallio, P., Perego, M., Bird, T., and et al. (1991) Control of the initiation of sporulation in *Bacillus subtilis* by a phosphorelay. *Res Microbiol* **142**, 815-823
 21. Wanner, B. L. (1993) Gene regulation by phosphate in enteric bacteria. *J Cell Biochem* **51**, 47-54
 22. Wosten, M. M., Kox, L. F., Chamnongpol, S., Soncini, F. C., and Groisman, E. A. (2000) A signal transduction system that responds to extracellular iron. *Cell* **103**, 113-125
 23. Stock, A. M., Robinson, V. L., and Goudreau, P. N. (2000) Two-component signal transduction. *Annu Rev Biochem* **69**, 183-215
 24. Cheung, J., and Hendrickson, W. A. (2010) Sensor domains of two-component regulatory

- systems. *Curr Opin Microbiol* **13**, 116-123
25. Pappalardo, L., Janausch, I. G., Vijayan, V., Zientz, E., Junker, J., Peti, W., Zweckstetter, M., Uden, G., and Griesinger, C. (2003) The NMR structure of the sensory domain of the membranous two-component fumarate sensor (histidine protein kinase) DcuS of *Escherichia coli*. *J Biol Chem* **278**, 39185-39188
 26. Reinelt, S., Hofmann, E., Gerharz, T., Bott, M., and Madden, D. R. (2003) The structure of the periplasmic ligand-binding domain of the sensor kinase CitA reveals the first extracellular PAS domain. *J Biol Chem* **278**, 39189-39196
 27. Cheung, J., Bingman, C. A., Reyngold, M., Hendrickson, W. A., and Waldburger, C. D. (2008) Crystal structure of a functional dimer of the PhoQ sensor domain. *J Biol Chem* **283**, 13762-13770
 28. Zhou, Y. F., Nan, B., Nan, J., Ma, Q., Panjekar, S., Liang, Y. H., Wang, Y., and Su, X. D. (2008) C4-dicarboxylates sensing mechanism revealed by the crystal structures of DctB sensor domain. *J Mol Biol* **383**, 49-61
 29. Moglich, A., Ayers, R. A., and Moffat, K. (2009) Structure and signaling mechanism of Per-ARNT-Sim domains. *Structure* **17**, 1282-1294
 30. Mascher, T., Helmann, J. D., and Uden, G. (2006) Stimulus perception in bacterial signal-transducing histidine kinases. *Microbiol Mol Biol Rev* **70**, 910-938
 31. Yamada, S., and Shiro, Y. (2008) Structural basis of the signal transduction in the two-component system. *Adv Exp Med Biol* **631**, 22-39
 32. Albanesi, D., Martin, M., Trajtenberg, F., Mansilla, M. C., Haouz, A., Alzari, P. M., de

- Mendoza, D., and Buschiazzo, A. (2009) Structural plasticity and catalysis regulation of a thermosensor histidine kinase. *Proc Natl Acad Sci U S A* **106**, 16185-16190
33. Martin, M., Albanesi, D., Alzari, P. M., and de Mendoza, D. (2009) Functional in vitro assembly of the integral membrane bacterial thermosensor DesK. *Protein Expr Purif* **66**, 39-45
34. Miyatake, H., Mukai, M., Park, S. Y., Adachi, S., Tamura, K., Nakamura, H., Nakamura, K., Tsuchiya, T., Iizuka, T., and Shiro, Y. (2000) Sensory mechanism of oxygen sensor FixL from *Rhizobium meliloti*: crystallographic, mutagenesis and resonance Raman spectroscopic studies. *J Mol Biol* **301**, 415-431
35. Mullner, M., Hammel, O., Mienert, B., Schlag, S., Bill, E., and Uden, G. (2008) A PAS domain with an oxygen labile [4Fe-4S](2+) cluster in the oxygen sensor kinase NreB of *Staphylococcus carnosus*. *Biochemistry* **47**, 13921-13932
36. Purcell, E. B., Siegal-Gaskins, D., Rawling, D. C., Fiebig, A., and Crosson, S. (2007) A photosensory two-component system regulates bacterial cell attachment. *Proc Natl Acad Sci U S A* **104**, 18241-18246
37. Hoffman, E. C., Reyes, H., Chu, F. F., Sander, F., Conley, L. H., Brooks, B. A., and Hankinson, O. (1991) Cloning of a factor required for activity of the Ah (dioxin) receptor. *Science* **252**, 954-958
38. Nambu, J. R., Lewis, J. O., Wharton, K. A., Jr., and Crews, S. T. (1991) The *Drosophila* single-minded gene encodes a helix-loop-helix protein that acts as a master regulator of CNS midline development. *Cell* **67**, 1157-1167

39. Taylor, B. L., and Zhulin, I. B. (1999) PAS domains: internal sensors of oxygen, redox potential, and light. *Microbiol Mol Biol Rev* **63**, 479-506
40. Christie, J. M., Salomon, M., Nozue, K., Wada, M., and Briggs, W. R. (1999) LOV (light, oxygen, or voltage) domains of the blue-light photoreceptor phototropin (nph1): binding sites for the chromophore flavin mononucleotide. *Proc Natl Acad Sci U S A* **96**, 8779-8783
41. Pellequer, J. L., Wager-Smith, K. A., Kay, S. A., and Getzoff, E. D. (1998) Photoactive yellow protein: a structural prototype for the three-dimensional fold of the PAS domain superfamily. *Proc Natl Acad Sci U S A* **95**, 5884-5890
42. Neiditch, M. B., Federle, M. J., Miller, S. T., Bassler, B. L., and Hughson, F. M. (2005) Regulation of LuxPQ receptor activity by the quorum-sensing signal autoinducer-2. *Mol Cell* **18**, 507-518
43. Finn, R. D., Mistry, J., Schuster-Bockler, B., Griffiths-Jones, S., Hollich, V., Lassmann, T., Moxon, S., Marshall, M., Khanna, A., Durbin, R., Eddy, S. R., Sonnhammer, E. L., and Bateman, A. (2006) Pfam: clans, web tools and services. *Nucleic Acids Res* **34**, D247-251
44. Punta, M., Coggill, P. C., Eberhardt, R. Y., Mistry, J., Tate, J., Boursnell, C., Pang, N., Forslund, K., Ceric, G., Clements, J., Heger, A., Holm, L., Sonnhammer, E. L., Eddy, S. R., Bateman, A., and Finn, R. D. (2012) The Pfam protein families database. *Nucleic Acids Res* **40**, D290-301
45. Zoltowski, B. D., Schwerdtfeger, C., Widom, J., Loros, J. J., Bilwes, A. M., Dunlap, J. C.,

- and Crane, B. R. (2007) Conformational switching in the fungal light sensor Vivid. *Science* **316**, 1054-1057
46. Crosson, S., Rajagopal, S., and Moffat, K. (2003) The LOV domain family: photoresponsive signaling modules coupled to diverse output domains. *Biochemistry* **42**, 2-10
47. Huala, E., Oeller, P. W., Liscum, E., Han, I. S., Larsen, E., and Briggs, W. R. (1997) Arabidopsis NPH1: a protein kinase with a putative redox-sensing domain. *Science* **278**, 2120-2123
48. Christie, J. M., Reymond, P., Powell, G. K., Bernasconi, P., Raibekas, A. A., Liscum, E., and Briggs, W. R. (1998) Arabidopsis NPH1: a flavoprotein with the properties of a photoreceptor for phototropism. *Science* **282**, 1698-1701
49. Jarillo, J. A., Gabrys, H., Capel, J., Alonso, J. M., Ecker, J. R., and Cashmore, A. R. (2001) Phototropin-related NPL1 controls chloroplast relocation induced by blue light. *Nature* **410**, 952-954
50. Kagawa, T., Sakai, T., Suetsugu, N., Oikawa, K., Ishiguro, S., Kato, T., Tabata, S., Okada, K., and Wada, M. (2001) Arabidopsis NPL1: a phototropin homolog controlling the chloroplast high-light avoidance response. *Science* **291**, 2138-2141
51. Kinoshita, T., Doi, M., Suetsugu, N., Kagawa, T., Wada, M., and Shimazaki, K. (2001) Phot1 and phot2 mediate blue light regulation of stomatal opening. *Nature* **414**, 656-660
52. Salomon, M., Christie, J. M., Knieb, E., Lempert, U., and Briggs, W. R. (2000) Photochemical and mutational analysis of the FMN-binding domains of the plant blue

- light receptor, phototropin. *Biochemistry* **39**, 9401-9410
53. Swartz, T. E., Tseng, T. S., Frederickson, M. A., Paris, G., Comerci, D. J., Rajashekara, G., Kim, J. G., Mudgett, M. B., Splitter, G. A., Ugalde, R. A., Goldbaum, F. A., Briggs, W. R., and Bogomolni, R. A. (2007) Blue-light-activated histidine kinases: two-component sensors in bacteria. *Science* **317**, 1090-1093
 54. Idnurm, A., and Crosson, S. (2009) The photobiology of microbial pathogenesis. *PLoS Pathog* **5**, e1000470
 55. Rivera-Cancel, G., Motta-Mena, L. B., and Gardner, K. H. (2012) Identification of natural and artificial DNA substrates for light-activated LOV-HTH transcription factor EL222. *Biochemistry* **51**, 10024-10034
 56. Zoltowski, B. D., Motta-Mena, L. B., and Gardner, K. H. (2013) Blue light-induced dimerization of a bacterial LOV-HTH DNA-binding protein. *Biochemistry* **52**, 6653-6661
 57. Motta-Mena, L. B., Reade, A., Mallory, M. J., Glantz, S., Weiner, O. D., Lynch, K. W., and Gardner, K. H. (2014) An optogenetic gene expression system with rapid activation and deactivation kinetics. *Nat Chem Biol* **10**, 196-202
 58. Jurk, M., Dorn, M., and Schmieder, P. (2011) Blue flickers of hope: secondary structure, dynamics, and putative dimerization interface of the blue-light receptor YtvA from *Bacillus subtilis*. *Biochemistry* **50**, 8163-8171
 59. Chan, R. H., Lewis, J. W., and Bogomolni, R. A. (2013) Photocycle of the LOV-STAS protein from the pathogen *Listeria monocytogenes*. *Photochem Photobiol* **89**, 361-369
 60. Vaidya, A. T., Chen, C. H., Dunlap, J. C., Loros, J. J., and Crane, B. R. (2011) Structure

- of a light-activated LOV protein dimer that regulates transcription. *Sci Signal* **4**, ra50
61. Schleicher, E., Kowalczyk, R. M., Kay, C. W., Hegemann, P., Bacher, A., Fischer, M., Bittl, R., Richter, G., and Weber, S. (2004) On the reaction mechanism of adduct formation in LOV domains of the plant blue-light receptor phototropin. *J Am Chem Soc* **126**, 11067-11076
 62. Miller, S. M., Massey, V., Ballou, D., Williams, C. H., Jr., Distefano, M. D., Moore, M. J., and Walsh, C. T. (1990) Use of a site-directed triple mutant to trap intermediates: demonstration that the flavin C(4a)-thiol adduct and reduced flavin are kinetically competent intermediates in mercuric ion reductase. *Biochemistry* **29**, 2831-2841
 63. Correa, F., Ko, W. H., Ocasio, V., Bogomolni, R. A., and Gardner, K. H. (2013) Blue Light Regulated Two-Component Systems: Enzymatic and Functional Analyses of Light-Oxygen-Voltage (LOV)-Histidine Kinases and Downstream Response Regulators. *Biochemistry*
 64. Parkinson, J. S., and Kofoid, E. C. (1992) Communication modules in bacterial signaling proteins. *Annu Rev Genet* **26**, 71-112
 65. Grebe, T. W., and Stock, J. B. (1999) The histidine protein kinase superfamily. *Adv Microb Physiol* **41**, 139-227
 66. Barakat, M., Ortet, P., Jourlin-Castelli, C., Ansaldi, M., Mejean, V., and Whitworth, D. E. (2009) P2CS: a two-component system resource for prokaryotic signal transduction research. *BMC Genomics* **10**, 315
 67. Barakat, M., Ortet, P., and Whitworth, D. E. (2011) P2CS: a database of prokaryotic

- two-component systems. *Nucleic Acids Res* **39**, D771-776
68. Bilwes, A. M., Alex, L. A., Crane, B. R., and Simon, M. I. (1999) Structure of CheA, a signal-transducing histidine kinase. *Cell* **96**, 131-141
69. McEvoy, M. M., Hausrath, A. C., Randolph, G. B., Remington, S. J., and Dahlquist, F. W. (1998) Two binding modes reveal flexibility in kinase/response regulator interactions in the bacterial chemotaxis pathway. *Proc Natl Acad Sci U S A* **95**, 7333-7338
70. Welch, M., Chinardet, N., Mourey, L., Birck, C., and Samama, J. P. (1998) Structure of the CheY-binding domain of histidine kinase CheA in complex with CheY. *Nat Struct Biol* **5**, 25-29
71. Bilwes, A. M., Quezada, C. M., Croal, L. R., Crane, B. R., and Simon, M. I. (2001) Nucleotide binding by the histidine kinase CheA. *Nat Struct Biol* **8**, 353-360
72. Mourey, L., Da Re, S., Pedelacq, J. D., Tolstykh, T., Faurie, C., Guillet, V., Stock, J. B., and Samama, J. P. (2001) Crystal structure of the CheA histidine phosphotransfer domain that mediates response regulator phosphorylation in bacterial chemotaxis. *J Biol Chem* **276**, 31074-31082
73. Park, S. Y., Borbat, P. P., Gonzalez-Bonet, G., Bhatnagar, J., Pollard, A. M., Freed, J. H., Bilwes, A. M., and Crane, B. R. (2006) Reconstruction of the chemotaxis receptor-kinase assembly. *Nat Struct Mol Biol* **13**, 400-407
74. Karniol, B., and Vierstra, R. D. (2004) The HWE histidine kinases, a new family of bacterial two-component sensor kinases with potentially diverse roles in environmental signaling. *J Bacteriol* **186**, 445-453

75. Casino, P., Rubio, V., and Marina, A. (2009) Structural insight into partner specificity and phosphoryl transfer in two-component signal transduction. *Cell* **139**, 325-336
76. Tanaka, T., Saha, S. K., Tomomori, C., Ishima, R., Liu, D., Tong, K. I., Park, H., Dutta, R., Qin, L., Swindells, M. B., Yamazaki, T., Ono, A. M., Kainosho, M., Inouye, M., and Ikura, M. (1998) NMR structure of the histidine kinase domain of the E. coli osmosensor EnvZ. *Nature* **396**, 88-92
77. Dutta, R., and Inouye, M. (2000) GHKL, an emergent ATPase/kinase superfamily. *Trends Biochem Sci* **25**, 24-28
78. Marina, A., Waldburger, C. D., and Hendrickson, W. A. (2005) Structure of the entire cytoplasmic portion of a sensor histidine-kinase protein. *EMBO J* **24**, 4247-4259
79. Bick, M. J., Lamour, V., Rajashankar, K. R., Gordiyenko, Y., Robinson, C. V., and Darst, S. A. (2009) How to switch off a histidine kinase: crystal structure of *Geobacillus stearothermophilus* KinB with the inhibitor Sda. *J Mol Biol* **386**, 163-177
80. Burkholder, W. F., Kurtser, I., and Grossman, A. D. (2001) Replication initiation proteins regulate a developmental checkpoint in *Bacillus subtilis*. *Cell* **104**, 269-279
81. Diensthuber, R. P., Bommer, M., Gleichmann, T., and Moglich, A. (2013) Full-length structure of a sensor histidine kinase pinpoints coaxial coiled coils as signal transducers and modulators. *Structure* **21**, 1127-1136
82. Mechaly, A. E., Sassoon, N., Betton, J. M., and Alzari, P. M. (2014) Segmental helical motions and dynamical asymmetry modulate histidine kinase autophosphorylation. *PLoS Biol* **12**, e1001776

83. Wang, C., Sang, J., Wang, J., Su, M., Downey, J. S., Wu, Q., Wang, S., Cai, Y., Xu, X., Wu, J., Senadheera, D. B., Cvitkovitch, D. G., Chen, L., Goodman, S. D., and Han, A. (2013) Mechanistic insights revealed by the crystal structure of a histidine kinase with signal transducer and sensor domains. *PLoS Biol* **11**, e1001493
84. Moglich, A., Ayers, R. A., and Moffat, K. (2009) Design and signaling mechanism of light-regulated histidine kinases. *J Mol Biol* **385**, 1433-1444
85. Vetter, I. R., and Wittinghofer, A. (2001) The guanine nucleotide-binding switch in three dimensions. *Science* **294**, 1299-1304
86. Jenal, U., and Galperin, M. Y. (2009) Single domain response regulators: molecular switches with emerging roles in cell organization and dynamics. *Curr Opin Microbiol* **12**, 152-160
87. Bourret, R. B., Hess, J. F., Borkovich, K. A., Pakula, A. A., and Simon, M. I. (1989) Protein phosphorylation in chemotaxis and two-component regulatory systems of bacteria. *J Biol Chem* **264**, 7085-7088
88. Lemon, K. P., Kurtser, I., Wu, J., and Grossman, A. D. (2000) Control of initiation of sporulation by replication initiation genes in *Bacillus subtilis*. *J Bacteriol* **182**, 2989-2991
89. Varughese, K. I. (2005) Conformational changes of Spo0F along the phosphotransfer pathway. *J Bacteriol* **187**, 8221-8227
90. Jacobs, C., Hung, D., and Shapiro, L. (2001) Dynamic localization of a cytoplasmic signal transduction response regulator controls morphogenesis during the *Caulobacter* cell cycle. *Proc Natl Acad Sci U S A* **98**, 4095-4100

91. Hung, D. Y., and Shapiro, L. (2002) A signal transduction protein cues proteolytic events critical to *Caulobacter* cell cycle progression. *Proc Natl Acad Sci U S A* **99**, 13160-13165
92. Volz, K. (1993) Structural conservation in the CheY superfamily. *Biochemistry* **32**, 11741-11753
93. Berman, H. M., Westbrook, J., Feng, Z., Gilliland, G., Bhat, T. N., Weissig, H., Shindyalov, I. N., and Bourne, P. E. (2000) The Protein Data Bank. *Nucleic Acids Res* **28**, 235-242
94. Volz, K., and Matsumura, P. (1991) Crystal structure of *Escherichia coli* CheY refined at 1.7-Å resolution. *J Biol Chem* **266**, 15511-15519
95. Stock, A. M., Martinez-Hackert, E., Rasmussen, B. F., West, A. H., Stock, J. B., Ringe, D., and Petsko, G. A. (1993) Structure of the Mg(2+)-bound form of CheY and mechanism of phosphoryl transfer in bacterial chemotaxis. *Biochemistry* **32**, 13375-13380
96. Needham, J. V., Chen, T. Y., and Falke, J. J. (1993) Novel ion specificity of a carboxylate cluster Mg(II) binding site: strong charge selectivity and weak size selectivity. *Biochemistry* **32**, 3363-3367
97. Bourret, R. B. (2010) Receiver domain structure and function in response regulator proteins. *Curr Opin Microbiol* **13**, 142-149
98. Bahn, Y. S., Kojima, K., Cox, G. M., and Heitman, J. (2006) A unique fungal two-component system regulates stress responses, drug sensitivity, sexual development, and virulence of *Cryptococcus neoformans*. *Mol Biol Cell* **17**, 3122-3135

99. Veerabagu, M., Elgass, K., Kirchler, T., Huppenberger, P., Harter, K., Chaban, C., and Mira-Rodado, V. (2012) The Arabidopsis B-type response regulator 18 homomerizes and positively regulates cytokinin responses. *Plant J* **72**, 721-731
100. Gotoh, Y., Eguchi, Y., Watanabe, T., Okamoto, S., Doi, A., and Utsumi, R. (2010) Two-component signal transduction as potential drug targets in pathogenic bacteria. *Curr Opin Microbiol* **13**, 232-239
101. Laub, M. T., and Goulian, M. (2007) Specificity in two-component signal transduction pathways. *Annu Rev Genet* **41**, 121-145
102. Lukat, G. S., McCleary, W. R., Stock, A. M., and Stock, J. B. (1992) Phosphorylation of bacterial response regulator proteins by low molecular weight phospho-donors. *Proc Natl Acad Sci U S A* **89**, 718-722
103. Cho, H. S., Lee, S. Y., Yan, D., Pan, X., Parkinson, J. S., Kustu, S., Wemmer, D. E., and Pelton, J. G. (2000) NMR structure of activated CheY. *J Mol Biol* **297**, 543-551
104. Lukat, G. S., Stock, A. M., and Stock, J. B. (1990) Divalent metal ion binding to the CheY protein and its significance to phosphotransfer in bacterial chemotaxis. *Biochemistry* **29**, 5436-5442
105. Bellsollell, L., Prieto, J., Serrano, L., and Coll, M. (1994) Magnesium binding to the bacterial chemotaxis protein CheY results in large conformational changes involving its functional surface. *J Mol Biol* **238**, 489-495
106. Kojetin, D. J., Thompson, R. J., Benson, L. M., Naylor, S., Waterman, J., Davies, K. G., Opperman, C. H., Stephenson, K., Hoch, J. A., and Cavanagh, J. (2005) Structural

- analysis of divalent metals binding to the *Bacillus subtilis* response regulator Spo0F: the possibility for in vitro metalloregulation in the initiation of sporulation. *BioMetals* **18**, 449-466
107. Volkman, B. F., Nohaile, M. J., Amy, N. K., Kustu, S., and Wemmer, D. E. (1995) Three-dimensional solution structure of the N-terminal receiver domain of NTRC. *Biochemistry* **34**, 1413-1424
108. Feher, V. A., Zapf, J. W., Hoch, J. A., Whiteley, J. M., McIntosh, L. P., Rance, M., Skelton, N. J., Dahlquist, F. W., and Cavanagh, J. (1997) High-resolution NMR structure and backbone dynamics of the *Bacillus subtilis* response regulator, Spo0F: implications for phosphorylation and molecular recognition. *Biochemistry* **36**, 10015-10025
109. Appleby, J. L., and Bourret, R. B. (1998) Proposed signal transduction role for conserved CheY residue Thr87, a member of the response regulator active-site quintet. *J Bacteriol* **180**, 3563-3569
110. Lukat, G. S., Lee, B. H., Mottonen, J. M., Stock, A. M., and Stock, J. B. (1991) Roles of the highly conserved aspartate and lysine residues in the response regulator of bacterial chemotaxis. *J Biol Chem* **266**, 8348-8354
111. Stock, A. M., and Guhaniyogi, J. (2006) A new perspective on response regulator activation. *J Bacteriol* **188**, 7328-7330
112. Lee, S. Y., Cho, H. S., Pelton, J. G., Yan, D., Berry, E. A., and Wemmer, D. E. (2001) Crystal structure of activated CheY. Comparison with other activated receiver domains. *J Biol Chem* **276**, 16425-16431

113. Loria, J. P., Berlow, R. B., and Watt, E. D. (2008) Characterization of enzyme motions by solution NMR relaxation dispersion. *Acc Chem Res* **41**, 214-221
114. Kleckner, I. R., and Foster, M. P. (2011) An introduction to NMR-based approaches for measuring protein dynamics. *Biochim Biophys Acta* **1814**, 942-968
115. McDonald, L. R., Boyer, J. A., and Lee, A. L. (2012) Segmental motions, not a two-state concerted switch, underlie allostery in CheY. *Structure* **20**, 1363-1373
116. Kern, D., Volkman, B. F., Luginbuhl, P., Nohaile, M. J., Kustu, S., and Wemmer, D. E. (1999) Structure of a transiently phosphorylated switch in bacterial signal transduction. *Nature* **402**, 894-898
117. Volkman, B. F., Lipson, D., Wemmer, D. E., and Kern, D. (2001) Two-state allosteric behavior in a single-domain signaling protein. *Science* **291**, 2429-2433
118. Gardino, A. K., and Kern, D. (2007) Functional dynamics of response regulators using NMR relaxation techniques. *Methods Enzymol* **423**, 149-165
119. Yan, D., Cho, H. S., Hastings, C. A., Igo, M. M., Lee, S. Y., Pelton, J. G., Stewart, V., Wemmer, D. E., and Kustu, S. (1999) Beryllofluoride mimics phosphorylation of NtrC and other bacterial response regulators. *Proc Natl Acad Sci U S A* **96**, 14789-14794
120. Hastings, C. A., Lee, S. Y., Cho, H. S., Yan, D., Kustu, S., and Wemmer, D. E. (2003) High-resolution solution structure of the beryllofluoride-activated NtrC receiver domain. *Biochemistry* **42**, 9081-9090
121. Wemmer, D. E., and Kern, D. (2005) Beryllofluoride binding mimics phosphorylation of aspartate in response regulators. *J Bacteriol* **187**, 8229-8230

122. Nohaile, M., Kern, D., Wemmer, D., Stedman, K., and Kustu, S. (1997) Structural and functional analyses of activating amino acid substitutions in the receiver domain of NtrC: evidence for an activating surface. *J Mol Biol* **273**, 299-316
123. Villali, J., Pontiggia, F., Clarkson, M. W., Hagan, M. F., and Kern, D. (2014) Evidence Against the "Y-T Coupling" Mechanism of Activation in the Response Regulator NtrC. *J Mol Biol*
124. Galperin, M. Y. (2006) Structural classification of bacterial response regulators: diversity of output domains and domain combinations. *J Bacteriol* **188**, 4169-4182
125. Lee, S. Y., Cho, H. S., Pelton, J. G., Yan, D., Henderson, R. K., King, D. S., Huang, L., Kustu, S., Berry, E. A., and Wemmer, D. E. (2001) Crystal structure of an activated response regulator bound to its target. *Nat Struct Biol* **8**, 52-56
126. Sourjik, V., and Schmitt, R. (1998) Phosphotransfer between CheA, CheY1, and CheY2 in the chemotaxis signal transduction chain of *Rhizobium meliloti*. *Biochemistry* **37**, 2327-2335
127. Paul, R., Jaeger, T., Abel, S., Wiederkehr, I., Folcher, M., Biondi, E. G., Laub, M. T., and Jenal, U. (2008) Allosteric regulation of histidine kinases by their cognate response regulator determines cell fate. *Cell* **133**, 452-461
128. Shu, C. J., and Zhulin, I. B. (2002) ANTAR: an RNA-binding domain in transcription antitermination regulatory proteins. *Trends Biochem Sci* **27**, 3-5
129. Fraser, J. S., Merlie, J. P., Jr., Echols, N., Weisfield, S. R., Mignot, T., Wemmer, D. E., Zusman, D. R., and Alber, T. (2007) An atypical receiver domain controls the dynamic

- polar localization of the *Myxococcus xanthus* social motility protein FrzS. *Mol Microbiol* **65**, 319-332
130. Ruiz, D., Salinas, P., Lopez-Redondo, M. L., Cayuela, M. L., Marina, A., and Contreras, A. (2008) Phosphorylation-independent activation of the atypical response regulator NblR. *Microbiology* **154**, 3002-3015
131. Espinosa, J., Lopez-Redondo, M. L., Miguel-Romero, L., Neira, J. L., Marina, A., and Contreras, A. (2012) Insights into the mechanism of activation of the phosphorylation-independent response regulator NblR. Role of residues Cys69 and Cys96. *Biochim Biophys Acta* **1819**, 382-390
132. Foreman, R., Fiebig, A., and Crosson, S. (2012) The LovK-LovR two-component system is a regulator of the general stress pathway in *Caulobacter crescentus*. *J Bacteriol* **194**, 3038-3049
133. Lourenco, R. F., Kohler, C., and Gomes, S. L. (2011) A two-component system, an anti-sigma factor and two paralogous ECF sigma factors are involved in the control of general stress response in *Caulobacter crescentus*. *Mol Microbiol* **80**, 1598-1612
134. Koblizek, M., Beja, O., Bidigare, R. R., Christensen, S., Benitez-Nelson, B., Vetriani, C., Kolber, M. K., Falkowski, P. G., and Kolber, Z. S. (2003) Isolation and characterization of *Erythro bacter* sp. strains from the upper ocean. *Arch Microbiol* **180**, 327-338
135. Oh, H. M., Giovannoni, S. J., Ferriera, S., Johnson, J., and Cho, J. C. (2009) Complete genome sequence of *Erythro bacter litoralis* HTCC2594. *J Bacteriol* **191**, 2419-2420
136. Koblizek, M., Janouskovec, J., Obornik, M., Johnson, J. H., Ferriera, S., and Falkowski,

- P. G. (2011) Genome sequence of the marine photoheterotrophic bacterium *Erythrobacter* sp. strain NAP1. *J Bacteriol* **193**, 5881-5882
137. Liu, G. Y. (2009) Molecular pathogenesis of *Staphylococcus aureus* infection. *Pediatr Res* **65**, 71R-77R
138. Migliori, G. B., Dheda, K., Centis, R., Mwaba, P., Bates, M., O'Grady, J., Hoelscher, M., and Zumla, A. (2010) Review of multidrug-resistant and extensively drug-resistant TB: global perspectives with a focus on sub-Saharan Africa. *Trop Med Int Health* **15**, 1052-1066
139. Ohnishi, M., Golparian, D., Shimuta, K., Saika, T., Hoshina, S., Iwasaku, K., Nakayama, S., Kitawaki, J., and Unemo, M. (2011) Is *Neisseria gonorrhoeae* initiating a future era of untreatable gonorrhea?: detailed characterization of the first strain with high-level resistance to ceftriaxone. *Antimicrob Agents Chemother* **55**, 3538-3545
140. Barrett, J. F., Goldschmidt, R. M., Lawrence, L. E., Foleno, B., Chen, R., Demers, J. P., Johnson, S., Kanojia, R., Fernandez, J., Bernstein, J., Licata, L., Donetz, A., Huang, S., Hlasta, D. J., Macielag, M. J., Ohemeng, K., Frechette, R., Frosco, M. B., Klaubert, D. H., Whiteley, J. M., Wang, L., and Hoch, J. A. (1998) Antibacterial agents that inhibit two-component signal transduction systems. *Proc Natl Acad Sci U S A* **95**, 5317-5322
141. Tang, Y. T., Gao, R., Havranek, J. J., Groisman, E. A., Stock, A. M., and Marshall, G. R. (2012) Inhibition of bacterial virulence: drug-like molecules targeting the *Salmonella enterica* PhoP response regulator. *Chem Biol Drug Des* **79**, 1007-1017
142. Sheffield, P., Garrard, S., and Derewenda, Z. (1999) Overcoming expression and

- purification problems of RhoGDI using a family of "parallel" expression vectors. *Protein Expr Purif* **15**, 34-39
143. Amezcua, C. A., Harper, S. M., Rutter, J., and Gardner, K. H. (2002) Structure and interactions of PAS kinase N-terminal PAS domain: model for intramolecular kinase regulation. *Structure* **10**, 1349-1361
144. Blommel, P. G., and Fox, B. G. (2007) A combined approach to improving large-scale production of tobacco etch virus protease. *Protein Expr Purif* **55**, 53-68
145. Bradford, M. M. (1976) A rapid and sensitive method for the quantitation of microgram quantities of protein utilizing the principle of protein-dye binding. *Anal Biochem* **72**, 248-254
146. Delaglio, F., Grzesiek, S., Vuister, G. W., Zhu, G., Pfeifer, J., and Bax, A. (1995) NMRPipe: a multidimensional spectral processing system based on UNIX pipes. *J Biomol NMR* **6**, 277-293
147. Johnson, B. A., and Blevins, R. A. (1994) NMR View: A computer program for the visualization and analysis of NMR data. *J Biomol NMR* **4**, 603-614
148. Yamazaki T., L. W., Arrowsmith C.H., Muhandiram D.R., and Kay, L.E. (1994) A Suite of Triple Resonance NMR Experiments for the Backbone Assignment of 15N , 13C , 2H Labeled Proteins with High Sensitivity. *J Am Chem Soc* **116**, 11655-11666
149. Pascal, S. M., Muhandiram, D. R., Yamazaki, T., Formankay, J. D., and Kay, L. E. (1994) Simultaneous Acquisition of N-15-Edited and C-13-Edited Noe Spectra of Proteins Dissolved in H₂O. *Journal of Magnetic Resonance Series B* **103**, 197-201

150. Bai, Y., Milne, J. S., Mayne, L., and Englander, S. W. (1993) Primary structure effects on peptide group hydrogen exchange. *Proteins* **17**, 75-86
151. Shen, Y., and Bax, A. (2013) Protein backbone and sidechain torsion angles predicted from NMR chemical shifts using artificial neural networks. *J Biomol NMR* **56**, 227-241
152. Rieping, W., Habeck, M., Bardiaux, B., Bernard, A., Malliavin, T. E., and Nilges, M. (2007) ARIA2: automated NOE assignment and data integration in NMR structure calculation. *Bioinformatics* **23**, 381-382
153. Thanbichler, M., Iniesta, A. A., and Shapiro, L. (2007) A comprehensive set of plasmids for vanillate- and xylose-inducible gene expression in *Caulobacter crescentus*. *Nucleic Acids Res* **35**, e137
154. Capra, E. J., and Laub, M. T. (2012) Evolution of two-component signal transduction systems. *Annu Rev Microbiol* **66**, 325-347
155. Herrou, J., and Crosson, S. (2011) Function, structure and mechanism of bacterial photosensory LOV proteins. *Nat Rev Microbiol* **9**, 713-723
156. Losi, A., and Gartner, W. (2012) The evolution of flavin-binding photoreceptors: an ancient chromophore serving trendy blue-light sensors. *Annu Rev Plant Biol* **63**, 49-72
157. Henry, J. T., and Crosson, S. (2011) Ligand-binding PAS domains in a genomic, cellular, and structural context. *Annu Rev Microbiol* **65**, 261-286
158. Zoltowski, B. D., Vaccaro, B., and Crane, B. R. (2009) Mechanism-based tuning of a LOV domain photoreceptor. *Nat Chem Biol* **5**, 827-834
159. Harper, S. M., Christie, J. M., and Gardner, K. H. (2004) Disruption of the LOV-Jalpha

- helix interaction activates phototropin kinase activity. *Biochemistry* **43**, 16184-16192
160. Harper, S. M., Neil, L. C., Day, I. J., Hore, P. J., and Gardner, K. H. (2004) Conformational changes in a photosensory LOV domain monitored by time-resolved NMR spectroscopy. *J Am Chem Soc* **126**, 3390-3391
161. Cao, Z., Buttani, V., Losi, A., and Gartner, W. (2008) A blue light inducible two-component signal transduction system in the plant pathogen *Pseudomonas syringae* pv. tomato. *Biophys J* **94**, 897-905
162. Losi, A. (2004) The bacterial counterparts of plant phototropins. *Photochem Photobiol Sci* **3**, 566-574
163. Kraiselburd, I., Alet, A. I., Tondo, M. L., Petrocelli, S., Daurelio, L. D., Monzon, J., Ruiz, O. A., Losi, A., and Orellano, E. G. (2012) A LOV Protein Modulates the Physiological Attributes of *Xanthomonas axonopodis* pv. citri Relevant for Host Plant Colonization. *PLoS One* **7**, e38226
164. Pathak, G. P., Losi, A., and Gartner, W. (2012) Metagenome-based screening reveals worldwide distribution of LOV-domain proteins. *Photochem Photobiol* **88**, 107-118
165. Bonomi, H. R., Posadas, D. M., Paris, G., Carrica, M. D., Frederickson, M., Pietrasanta, L. I., Bogomolni, R. A., Zorreguieta, A., and Goldbaum, F. A. (2012) Light regulates attachment, exopolysaccharide production, and nodulation in *Rhizobium leguminosarum* through a LOV-histidine kinase photoreceptor. *Proc Natl Acad Sci U S A* **109**, 12135-12140
166. Francez-Charlot, A., Frunzke, J., Reichen, C., Ebnetter, J. Z., Gourion, B., and Vorholt, J.

- A. (2009) Sigma factor mimicry involved in regulation of general stress response. *Proc Natl Acad Sci U S A* **106**, 3467-3472
167. Gourion, B., Francez-Charlot, A., and Vorholt, J. A. (2008) PhyR is involved in the general stress response of *Methylobacterium extorquens* AM1. *J Bacteriol* **190**, 1027-1035
168. Surette, M. G., Levit, M., Liu, Y., Lukat, G., Ninfa, E. G., Ninfa, A., and Stock, J. B. (1996) Dimerization is required for the activity of the protein histidine kinase CheA that mediates signal transduction in bacterial chemotaxis. *J Biol Chem* **271**, 939-945
169. Kenney, L. J. (1997) Kinase activity of EnvZ, an osmoregulatory signal transducing protein of *Escherichia coli*. *Arch Biochem Biophys* **346**, 303-311
170. Sousa, E. H., Gonzalez, G., and Gilles-Gonzalez, M. A. (2005) Oxygen blocks the reaction of the FixL-FixJ complex with ATP but does not influence binding of FixJ or ATP to FixL. *Biochemistry* **44**, 15359-15365
171. Tawa, P., and Stewart, R. C. (1994) Kinetics of CheA autophosphorylation and dephosphorylation reactions. *Biochemistry* **33**, 7917-7924
172. Yang, Y., and Inouye, M. (1991) Intermolecular complementation between two defective mutant signal-transducing receptors of *Escherichia coli*. *Proc Natl Acad Sci U S A* **88**, 11057-11061
173. Ninfa, E. G., Atkinson, M. R., Kamberov, E. S., and Ninfa, A. J. (1993) Mechanism of autophosphorylation of *Escherichia coli* nitrogen regulator II (NRII or NtrB): trans-phosphorylation between subunits. *J Bacteriol* **175**, 7024-7032

174. Purcell, E. B., McDonald, C. A., Palfey, B. A., and Crosson, S. (2010) An analysis of the solution structure and signaling mechanism of LovK, a sensor histidine kinase integrating light and redox signals. *Biochemistry* **49**, 6761-6770
175. Cole, C., Barber, J. D., and Barton, G. J. (2008) The Jpred 3 secondary structure prediction server. *Nucleic Acids Res* **36**, W197-201
176. Harper, S. M., Neil, L. C., and Gardner, K. H. (2003) Structural basis of a phototropin light switch. *Science* **301**, 1541-1544
177. Jentzsch, K., Wirtz, A., Circolone, F., Drepper, T., Losi, A., Gartner, W., Jaeger, K. E., and Krauss, U. (2009) Mutual exchange of kinetic properties by extended mutagenesis in two short LOV domain proteins from *Pseudomonas putida*. *Biochemistry* **48**, 10321-10333
178. Whitworth, D. E., and Cock, P. J. (2009) Evolution of prokaryotic two-component systems: insights from comparative genomics. *Amino Acids* **37**, 459-466
179. Laub, M. T., Biondi, E. G., and Skerker, J. M. (2007) Phosphotransfer profiling: systematic mapping of two-component signal transduction pathways and phosphorelays. *Methods Enzymol* **423**, 531-548
180. Bateman, A., Coin, L., Durbin, R., Finn, R. D., Hollich, V., Griffiths-Jones, S., Khanna, A., Marshall, M., Moxon, S., Sonnhammer, E. L., Studholme, D. J., Yeats, C., and Eddy, S. R. (2004) The Pfam protein families database. *Nucleic Acids Res* **32**, D138-141
181. Gourion, B., Rossignol, M., and Vorholt, J. A. (2006) A proteomic study of *Methylobacterium extorquens* reveals a response regulator essential for epiphytic growth.

- Proc Natl Acad Sci U S A* **103**, 13186-13191
182. Herrou, J., Rotskoff, G., Luo, Y., Roux, B., and Crosson, S. (2012) Structural basis of a protein partner switch that regulates the general stress response of alpha-proteobacteria. *Proc Natl Acad Sci U S A* **109**, E1415-1423
183. Campagne, S., Damberger, F. F., Kaczmarczyk, A., Francez-Charlot, A., Allain, F. H., and Vorholt, J. A. (2012) Structural basis for sigma factor mimicry in the general stress response of Alphaproteobacteria. *Proc Natl Acad Sci U S A* **109**, E1405-1414
184. Delgado, J., Forst, S., Harlocker, S., and Inouye, M. (1993) Identification of a phosphorylation site and functional analysis of conserved aspartic acid residues of OmpR, a transcriptional activator for ompF and ompC in Escherichia coli. *Mol Microbiol* **10**, 1037-1047
185. Altschul, S. F., Gish, W., Miller, W., Myers, E. W., and Lipman, D. J. (1990) Basic local alignment search tool. *J Mol Biol* **215**, 403-410
186. Christie, J. M., Hitomi, K., Arvai, A. S., Hartfield, K. A., Mettlen, M., Pratt, A. J., Tainer, J. A., and Getzoff, E. D. (2012) Structural tuning of the fluorescent protein iLOV for improved photostability. *J Biol Chem* **287**, 22295-22304
187. Nash, A. I., McNulty, R., Shillito, M. E., Swartz, T. E., Bogomolni, R. A., Luecke, H., and Gardner, K. H. (2011) Structural basis of photosensitivity in a bacterial light-oxygen-voltage/helix-turn-helix (LOV-HTH) DNA-binding protein. *Proc Natl Acad Sci U S A* **108**, 9449-9454
188. Zoltowski, B. D., and Crane, B. R. (2008) Light activation of the LOV protein vivid

- generates a rapidly exchanging dimer. *Biochemistry* **47**, 7012-7019
189. Jurk, M., Dorn, M., Kikhney, A., Svergun, D., Gartner, W., and Schmieder, P. (2010) The switch that does not flip: the blue-light receptor YtvA from *Bacillus subtilis* adopts an elongated dimer conformation independent of the activation state as revealed by a combined AUC and SAXS study. *J Mol Biol* **403**, 78-87
190. Moglich, A., Ayers, R. A., and Moffat, K. (2009) Design and signaling mechanism of light-regulated histidine kinases. *J Mol Biol* **385**, 1433-1444
191. Moglich, A., Ayers, R. A., and Moffat, K. (2010) Addition at the molecular level: signal integration in designed Per-ARNT-Sim receptor proteins. *J Mol Biol* **400**, 477-486
192. Diensthuber, R. P., Bommer, M., Gleichmann, T., and Moglich, A. (2013) Full-Length Structure of a Sensor Histidine Kinase Pinpoints Coaxial Coiled Coils as Signal Transducers and Modulators. *Structure* **in press**
193. Lupas, A., Van Dyke, M., and Stock, J. (1991) Predicting coiled coils from protein sequences. *Science* **252**, 1162-1164
194. van der Horst, M. A., Key, J., and Hellingwerf, K. J. (2007) Photosensing in chemotrophic, non-phototrophic bacteria: let there be light sensing too. *Trends Microbiol* **15**, 554-562
195. Avila-Perez, M., Hellingwerf, K. J., and Kort, R. (2006) Blue light activates the sigmaB-dependent stress response of *Bacillus subtilis* via YtvA. *J Bacteriol* **188**, 6411-6414
196. Skerker, J. M., Perchuk, B. S., Siryaporn, A., Lubin, E. A., Ashenberg, O., Goulian, M.,

- and Laub, M. T. (2008) Rewiring the specificity of two-component signal transduction systems. *Cell* **133**, 1043-1054
197. Yamada, S., Sugimoto, H., Kobayashi, M., Ohno, A., Nakamura, H., and Shiro, Y. (2009) Structure of PAS-linked histidine kinase and the response regulator complex. *Structure* **17**, 1333-1344
198. Szurmant, H., Bobay, B. G., White, R. A., Sullivan, D. M., Thompson, R. J., Hwa, T., Hoch, J. A., and Cavanagh, J. (2008) Co-evolving motions at protein-protein interfaces of two-component signaling systems identified by covariance analysis. *Biochemistry* **47**, 7782-7784
199. Corpet, F. (1988) Multiple sequence alignment with hierarchical clustering. *Nucleic Acids Res* **16**, 10881-10890
200. Bourret, R. B., and Silversmith, R. E. (2010) Two-component signal transduction. *Curr Opin Microbiol* **13**, 113-115
201. Bren, A., and Eisenbach, M. (1998) The N terminus of the flagellar switch protein, FliM, is the binding domain for the chemotactic response regulator, CheY. *J Mol Biol* **278**, 507-514
202. Gardino, A. K., Volkman, B. F., Cho, H. S., Lee, S. Y., Wemmer, D. E., and Kern, D. (2003) The NMR solution structure of BeF₃(-)-activated Spo0F reveals the conformational switch in a phosphorelay system. *J Mol Biol* **331**, 245-254
203. Sheftic, S. R., White, E., Gage, D. J., and Alexandrescu, A. T. (2014) NMR Structure of the HWE Kinase Associated Response Regulator Sma0114 in Its Activated State.

- Biochemistry* **53**, 311-322
204. Sheftic, S. R., Garcia, P. P., Robinson, V. L., Gage, D. J., and Alexandrescu, A. T. (2011) NMR assignments for the *Sinorhizobium meliloti* response regulator Sma0114. *Biomol NMR Assign* **5**, 55-58
 205. Wyman, C., Rombel, I., North, A. K., Bustamante, C., and Kustu, S. (1997) Unusual oligomerization required for activity of NtrC, a bacterial enhancer-binding protein. *Science* **275**, 1658-1661
 206. Creager-Allen, R. L., Silversmith, R. E., and Bourret, R. B. (2013) A link between dimerization and autophosphorylation of the response regulator PhoB. *J Biol Chem* **288**, 21755-21769
 207. Gao, R., and Stock, A. M. (2010) Molecular strategies for phosphorylation-mediated regulation of response regulator activity. *Curr Opin Microbiol* **13**, 160-167
 208. Berjanskii, M. V., and Wishart, D. S. (2005) A simple method to predict protein flexibility using secondary chemical shifts. *J Am Chem Soc* **127**, 14970-14971
 209. Smith, J. G., Latiolais, J. A., Guanga, G. P., Citineni, S., Silversmith, R. E., and Bourret, R. B. (2003) Investigation of the role of electrostatic charge in activation of the *Escherichia coli* response regulator CheY. *J Bacteriol* **185**, 6385-6391
 210. Thomas, S. A., Brewster, J. A., and Bourret, R. B. (2008) Two variable active site residues modulate response regulator phosphoryl group stability. *Mol Microbiol* **69**, 453-465
 211. Garcia Vescovi, E., Sciara, M. I., and Castelli, M. E. (2010) Two component systems in

- the spatial program of bacteria. *Curr Opin Microbiol* **13**, 210-218
212. Menon, S., and Wang, S. (2011) Structure of the response regulator PhoP from *Mycobacterium tuberculosis* reveals a dimer through the receiver domain. *Biochemistry* **50**, 5948-5957
213. Metzger, L. C., Francez-Charlot, A., and Vorholt, J. A. (2013) Single-domain response regulator involved in the general stress response of *Methylobacterium extorquens*. *Microbiology* **159**, 1067-1076
214. McDonald, L. R., Whitley, M. J., Boyer, J. A., and Lee, A. L. (2013) Colocalization of fast and slow timescale dynamics in the allosteric signaling protein CheY. *J Mol Biol* **425**, 2372-2381
215. Birck, C., Mourey, L., Gouet, P., Fabry, B., Schumacher, J., Rousseau, P., Kahn, D., and Samama, J. P. (1999) Conformational changes induced by phosphorylation of the FixJ receiver domain. *Structure* **7**, 1505-1515
216. Feher, V. A., and Cavanagh, J. (1999) Millisecond-timescale motions contribute to the function of the bacterial response regulator protein Spo0F. *Nature* **400**, 289-293
217. Gardino, A. K., Villali, J., Kivenson, A., Lei, M., Liu, C. F., Steindel, P., Eisenmesser, E. Z., Labeikovsky, W., Wolf-Watz, M., Clarkson, M. W., and Kern, D. (2009) Transient non-native hydrogen bonds promote activation of a signaling protein. *Cell* **139**, 1109-1118
218. Podgornaia, A. I., and Laub, M. T. (2013) Determinants of specificity in two-component signal transduction. *Curr Opin Microbiol* **16**, 156-162

219. Silversmith, R. E. (2010) Auxiliary phosphatases in two-component signal transduction. *Curr Opin Microbiol* **13**, 177-183
220. Ely, B. (1991) Genetics of *Caulobacter crescentus*. *Methods Enzymol* **204**, 372-384
221. Herrou, J., Foreman, R., Fiebig, A., and Crosson, S. (2010) A structural model of anti-anti-sigma inhibition by a two-component receiver domain: the PhyR stress response regulator. *Mol Microbiol* **78**, 290-304
222. Browning, D. F., and Busby, S. J. (2004) The regulation of bacterial transcription initiation. *Nat Rev Microbiol* **2**, 57-65
223. Osterberg, S., del Peso-Santos, T., and Shingler, V. (2011) Regulation of alternative sigma factor use. *Annu Rev Microbiol* **65**, 37-55
224. Helmann, J. D. (1999) Anti-sigma factors. *Curr Opin Microbiol* **2**, 135-141
225. Campbell, E. A., Westblade, L. F., and Darst, S. A. (2008) Regulation of bacterial RNA polymerase sigma factor activity: a structural perspective. *Curr Opin Microbiol* **11**, 121-127
226. Pillutla, R. C., Sharer, J. D., Gulati, P. S., Wu, E., Yamashita, Y., Lerner, C. G., Inouye, M., and March, P. E. (1995) Cross-species complementation of the indispensable *Escherichia coli* era gene highlights amino acid regions essential for activity. *J Bacteriol* **177**, 2194-2196
227. Barker, C. S., and Samatey, F. A. (2012) Cross-complementation study of the flagellar type III export apparatus membrane protein FlhB. *PLoS One* **7**, e44030
228. Roberts, D. L., Bennett, D. W., and Forst, S. A. (1994) Identification of the site of

- phosphorylation on the osmosensor, EnvZ, of Escherichia coli. *J Biol Chem* **269**, 8728-8733
229. Zhu, Y., Qin, L., Yoshida, T., and Inouye, M. (2000) Phosphatase activity of histidine kinase EnvZ without kinase catalytic domain. *Proc Natl Acad Sci U S A* **97**, 7808-7813
230. Porter, S. L., Roberts, M. A., Manning, C. S., and Armitage, J. P. (2008) A bifunctional kinase-phosphatase in bacterial chemotaxis. *Proc Natl Acad Sci U S A* **105**, 18531-18536
231. Groban, E. S., Clarke, E. J., Salis, H. M., Miller, S. M., and Voigt, C. A. (2009) Kinetic buffering of cross talk between bacterial two-component sensors. *J Mol Biol* **390**, 380-393
232. Swartz, T. E., Corchnoy, S. B., Christie, J. M., Lewis, J. W., Szundi, I., Briggs, W. R., and Bogomolni, R. A. (2001) The photocycle of a flavin-binding domain of the blue light photoreceptor phototropin. *J Biol Chem* **276**, 36493-36500
233. Lee, J., Tomchick, D. R., Brautigam, C. A., Machius, M., Kort, R., Hellingwerf, K. J., and Gardner, K. H. (2008) Changes at the KinA PAS-A dimerization interface influence histidine kinase function. *Biochemistry* **47**, 4051-4064
234. Groisman, E. A. (2001) The pleiotropic two-component regulatory system PhoP-PhoQ. *J Bacteriol* **183**, 1835-1842
235. Barbieri, C. M., Mack, T. R., Robinson, V. L., Miller, M. T., and Stock, A. M. (2010) Regulation of response regulator autophosphorylation through interdomain contacts. *J Biol Chem* **285**, 32325-32335